

10-15-2019 11:15 AM

Progress Toward Durable Icephobic Materials

Matthew J. Coady, *The University of Western Ontario*

Supervisor: Ragogna, Paul J., *The University of Western Ontario*

A thesis submitted in partial fulfillment of the requirements for the Doctor of Philosophy degree in Chemistry

© Matthew J. Coady 2019

Follow this and additional works at: <https://ir.lib.uwo.ca/etd>

 Part of the [Inorganic Chemistry Commons](#), [Polymer Chemistry Commons](#), and the [Polymer Science Commons](#)

Recommended Citation

Coady, Matthew J., "Progress Toward Durable Icephobic Materials" (2019). *Electronic Thesis and Dissertation Repository*. 6590.
<https://ir.lib.uwo.ca/etd/6590>

This Dissertation/Thesis is brought to you for free and open access by Scholarship@Western. It has been accepted for inclusion in Electronic Thesis and Dissertation Repository by an authorized administrator of Scholarship@Western. For more information, please contact wlsadmin@uwo.ca.

Abstract

Ice accumulation is a major engineering challenge in many fields including aerospace, power generation, transportation, and infrastructure. A variety of solutions are being researched to address this challenge. Perhaps the most promising method of combating ice accumulation is by applying coatings with low values of interfacial ice adhesion strength, τ_{ice} . Icephobic materials are those with ice adhesion below 100 kPa, and it has been shown that passive delamination can occur on surfaces with τ_{ice} below 20 kPa. While various low adhesion surfaces have been prepared, durability concerns pervade applications where surfaces experience repeated icing or freeze-thaw cycles, mechanical abrasion, and particulate erosion. The present thesis explores methods of improving the durability of state-of-the-art icephobic materials in order to make them more suitable solutions to ‘the icing problem.’ Ice adhesion was measured using in-house load cell and centrifugation methods, allowing for the direct comparison of τ_{ice} values between the materials developed. Various ways of improving the durability of icephobic surfaces were identified, including the stabilization of slippery lubricant-infused porous surfaces (SLIPS) via polymer cross-linking at the interface, copolymerization of commercial poly(dimethylsiloxane) resins with acrylate / styrene monomers yielding highly cross-linked network copolymer coatings, and lowering ice adhesion on commercially available adhesive films by introducing areas of substrate-film detachment. A collaborative study of femtosecond laser micromachining done with McGill University is also included which showed the cross-link density dependence of threshold fluence, and the varied surface morphologies that could be accessed by these means. These studies show effective methods of influencing icephobic material durability using straightforward methodologies and will inspire new investigations toward creating more durable icephobic materials that can alleviate concerns with ice accumulation for people that live in cold climates. Our investigations and proposed work show that cutting-edge research in this field can be done at Western, making Canada a viable leader of global anti-icing research.

Keywords

icephobic materials, durable, radiation curing, ice, adhesion, accumulation, wind energy, turbines, interfacial, copolymer, network, cross-linking, laser micromachining, slippery surfaces, lubricated materials, siloxane, polymer coatings

Summary for Lay Audience

Ice accumulation occurs in many places in nature and in industry, threatening to destroy vital infrastructure such as roads and power transmission lines. The North American Ice Storm of 1998 is an example of the expense of extreme weather, causing \$5 Billion in damage in Canada over the course of six days and cost 35 Canadians their lives. Preventing large-scale damage to our infrastructure is of critical importance to protect lives, and to reduce the cost of maintenance paid by taxes.

Icephobic (*ice-fearing*) coatings are those that resist or prevent ice growth on their surfaces. To date, the best-performing materials are rubber-based and oil-containing coatings operating on a simple principle: rigid materials like ice do not adhere to flexible materials like rubber and oil. While there has been considerable success in applying well-known rubbers like silicones, challenges remain before these materials can be used on a large scale. Firstly, the materials must be made more durable. Icephobic materials, in particular those including oils, are prone to damage through abrasion, such as that experienced if sand or ice particles are blown across surfaces by high winds. Secondly, coatings must be applied to surfaces on a huge scale, such as on all powerlines within a city. To address these challenges, we hope to toughen these materials through different chemical modifications. These methods are presented in the present thesis: 1) Using cross-linking in silicone rubber coatings to retain oil in icephobic materials; 2) Inscribing special surface morphologies in rubber surfaces to reduce ice growth; 3) Making silicones more durable by incorporating plastic-like materials; 4) Decreasing ice adhesion strength on commercial adhesive tapes by changing how they adhere to their substrates.

The expected impact of this work is to inspire new investigations toward creating more durable icephobic materials that can alleviate concerns with ice accumulation for people that live in cold climates. Our investigations and proposed work show how cutting-edge research in this field can be done at Western, making Canada a viable leader of global anti-icing research.

Co-Authorship Statement

Chapter 2 has been adapted from the journal article “Icephobic Behavior of UV-Cured Polymer Networks: Improving SLIPS Durability”, published in *ACS Applied Materials and Interfaces*. Fabrication, testing, characterization (except AFM), and drafting of the article were done by Matthew J. Coady. Michael Wood, Kent E. Nielsen, Anne-Marie Kietzig, François Lagugné-Labarthet, and Paul J. Ragogna contributed to editing and content during the revision process. All AFM analysis was done by Gregory Q. Wallace.

Chapter 3 is a work of writing by Matthew J. Coady, based upon the journal article “Femtosecond laser micromachining of co-polymeric urethane materials”, written by Michael J. Wood with contributions from the co-authors. Figures indicated were used with permission of the authors. Experimental work for the original article pertaining to the preparation of materials was done by Matthew Coady, as was additional characterization by IR spectroscopy and thermal gravimetric analysis and differential scanning calorimetry.

Chapter 4 has been adapted from the journal article “Highly cross-linked UV-cured siloxane copolymer networks as icephobic coatings”, submitted to *Langmuir*. Preparation of the coatings, characterization other than nanoindentation and AFM, ice adhesion testing, and drafting of the article were done by Matthew Coady. Nuwansiri Getangama performed AFM analysis, and Aria Khalili performed nanoindentation for hardness measurements. Paul Ragogna and John de Bruyn reviewed and edited the manuscript prior to submission.

Chapter 5 contains experimental work, and writing by Matthew Coady, edited by Paul Ragogna. Sand erosion experiments described here were done by Cheryl Elsbernd and Ryan Marx at 3M Center, Minnesota.

Acknowledgments

I would like to thank those who helped me throughout my graduate career. Firstly, Prof. Paul Ragona for providing me the opportunity to pursue my doctorate in his group, and for his guidance over the years. Thank you as well to the researchers at 3M Canada who took time to review much of my work, and for providing insight toward new research directions. Thank you to all the co-authors with whom I have had the pleasure of working.

Ragona Group members present, and past have been instrumental to the completion of this document; thank you for your support. A special thanks to my undergraduate lab partner, Vanessa Béland, who later became my mentor when joining the Ragona group: a true scientist (but I have to say, I'm still better at math). Thanks as well to Brad Berven, who showed me the ropes of anti-icing research, and to Tim Stephens who I had the opportunity to mentor in the lab. You guys are the only ones who really appreciate what it's like to work in the Cold Weather Biome!

Thank you to all the support staff and faculty at Western, especially the crew in the Chemistry Electronics Shop and the Biotron, without whom measurements would have been impossible. Thanks to my supervisory committee for taking the time to review my thesis, and for your valuable input to my research.

Thank you to my friends and family. My friends have been a continuous influence (positive or otherwise) on me, my research, and my extra-curricular activities. My family have provided continuous support. Mom and Dad, you have always been there for me, and I appreciate everything that you've done to help me reach my goals. Alyssa and Bruno, thanks for being there for me when I needed it, even if you were unaware.

Lastly, thank you to my wife Lauren. Your dedication and focus are awe-inspiring, and you make me strive to be a better person. I'm sorry about the papers all over the apartment. Thank you!

Table of Contents

Abstract	ii
Summary for Lay Audience	iv
Co-Authorship Statement.....	v
Acknowledgments.....	vi
Table of Contents	vii
List of Tables	x
List of Figures	xi
List of Abbreviations	xvi
Preface.....	xviii
Chapter 1	1
1 Introduction	1
1.1 The Impetus of Icing Prevention.....	1
1.2 Adhesion: A Primer	2
1.3 Other Factors Influencing Ice Adhesion: The Interface	7
1.4 Strategies to Reduce Ice Accumulation	11
1.5 Passive Methods of Ice Abatement.....	12
1.6 Icephobic Materials.....	20
1.7 Remaining Challenges and Scope of Thesis	26
1.8 References Cited	27
Chapter 2.....	36
2 Icephobic behavior of UV-cured polymer networks incorporated into slippery lubricant-infused porous surfaces: Improving SLIPS durability	36
2.1 Introduction.....	36
2.2 Experimental	38
2.3 Results and Discussion	40

2.4	Conclusions	47
2.5	References Cited	47
Chapter 3		49
3	Fundamentals of Lasing Elastomeric Urethane Coatings to Prepare Icephobic Microstructures	49
3.1	Introduction	49
3.2	Experimental	50
3.3	Results and Discussion	52
3.4	Conclusions	60
3.5	References Cited	60
Chapter 4		65
4	Highly cross-linked UV-cured siloxane copolymer networks as icephobic coatings..	65
4.1	Introduction	65
4.2	Experimental	67
4.3	Results and Discussion	69
4.4	Conclusions	76
4.5	References Cited	76
Chapter 5		79
5	Creating Arrays of film/substrate detachments as a means of lowering ice adhesion strength	79
5.1	Introduction	79
5.2	Experimental	81
5.3	Results and Discussion	83
5.4	Conclusions	90
5.5	References Cited	91
Chapter 6		93
6	Summary, Conclusions and Future Work	93

6.1 Summary and Conclusions	93
6.2 Future Work	96
6.2.1 Method Development.....	96
6.2.1.1 Simulating Winter Weather in the Cold Weather Biome	96
6.2.1.2 Ice Adhesion and Interfacial Toughness	98
6.2.2 Material Development	100
6.2.2.1 Thermoplastic Elastomers / Vulcanizates	100
6.2.2.2 Graphene/Polymer Nanocomposites	101
6.3 References Cited	105
Appendices.....	107
Appendix A: Supporting Information for Chapter 2.....	107
Appendix B: Supporting Information for Chapter 3.....	112
Appendix C: Supporting Information for Chapter 4.....	113
Appendix D: Supporting Information for Chapter 5.....	122
Curriculum Vitae	125

List of Tables

Table 1.1: Application Areas of Ice Repellent Surfaces	2
Table 2.1: Ice adhesion and wetting data for SLIPS and selected surfaces	43
Table 3.1: Gel content and swelling of polymer networks. Adapted with permission.....	58
Table 4.1: Table of physical data measured for the prepared icephobic coatings.	71

List of Figures

Figure 1.1: Water contact angles (θ_c) on (<i>left</i>) a smooth hydrophobic surface, and (<i>right</i>) a smooth hydrophilic surface.....	4
Figure 1.2:Diagram depicting the cause of surface energy (left) before cleavage, and (right) after cleavage. Circles represent lattice points in a crystalline material; grey for bulk, beige for surface. '!' indicate unbalanced forces on lattice points	5
Figure 1.3: Illustration of changing adhesion with surface roughness for hydrophobic and hydrophilic materials. Roughness causes decreased water / ice adhesion on hydrophobic materials, and increased water / ice adhesion on hydrophilic materials.	6
Figure 1.4: Hydrogen bonding to a generic surface with polar groups present. Hydrogen bonds are shown as dashed lines.....	7
Figure 1.5: Depiction of interfacial cavitation. A force F_{app} applied to two connected bodies, one soft and one firm, will bring about deformations in the soft body.....	8
Figure 1.6:Illustration explaining the observation of interfacial slippage observed in an elastomer film adhered to a surface. (<i>left</i>) A polymer film on top of a rigid substrate, with no forces acting upon it. The polymer particles shown have no net force acting upon them, and therefore no slip is observed. (<i>right</i>) The polymer film is experiencing an extensive force as it is being peeled from the surface. A net force in the direction labelled ‘extension’ leads to a concomitant contraction and slippage of the polymer particles.....	10
Figure 1.7: Illustration of (<i>left</i>) advancing and (<i>right</i>) receding contact angles.	13
Figure 1.8:Illustration of the Cassie-Baxter (left) and Wenzel (right) wetting states. Both have very high apparent contact angles.	14
Figure 1.9: Illustration of homogeneous nucleation. Liquid particles collide randomly, until a nucleus of critical size forms, leading to the formation of a crystal.	16
Figure 1.10: Ice adhesion measured using (left) load cell and (right) centrifuge. Arrows indicate the direction of the being being measured.	18

Figure 1.11: Chemical structures of polymers used in anti-icing / deicing research.	22
Figure 1.12: Fabrication of a generic slippery lubricant-infused porous surface, showing the formation of a trapped fluid layer deeper than the microstructure.	24
Figure 1.13: Extension and concomitant contraction of viscoelastic polymer chains in response to stress on the ice/polymer interface (F_{app}). This contraction causes cleavage where the media meet due to interfacial slippage.....	26
Figure 2.1: Process diagram for the fabrication of UV-cured SLIPS	37
Figure 2.2: (<i>left</i>) SEM image of porous structure of anodized coupons. (<i>right</i>) FIB-etched cross-section of coupon edge used to measure approximate depth of porous oxide layer. Both images captured at 3.00 kV.....	41
Figure 2.3: Comparison of wetting contact angle PAAO (<i>left</i>), silylated PAAO (<i>mid</i>) and oil-infused PAAO SLIPS (<i>right</i>).	41
Figure 2.4: AFM height images of 5 μm by 5 μm area of a) oil-only, b) Ebecryl 1360 and c) Ebecryl 1360 plus oil	42
Figure 2.5: Deicing results for oil-only (red), oil+1360 (yellow) and oil+350 (blue) SLIPS samples. Solid lines indicate the mean values measured after n deicing cycles, while the shaded areas correspond to the standard error associated with those measurements.	43
Figure 2.6: EDX spectra of oil-only SLIPS. Top image taken of area where ice was not grown. Bottom image taken in a deiced area.	45
Figure 2.7: Oil+350 resin EDX and SEM results. (<i>Top left</i>) Spectrum before icing, with no aluminum seen at the surface. (<i>Bottom</i>) Spectra representing different areas observed by SEM after deicing, correlated to the SEM image (<i>top right</i>): a) where much of the silicon still resides in the surface, and b) where the coating has been completely removed.....	46
Figure 3.1: (<i>left</i>) Ice interlocking with structure surface. (<i>right</i>) Release of ice occurring when a pillared surface is flexible.	49
Figure 3.2: Chemical structures of comonomers for lasing study	53

Figure 3.3: Scanning electron micrographs of the microstructures induced on the surface of the studied co-polymer materials irradiated with a 275 nm laser beam. Taken from Wood <i>et al</i> with permission.....	54
Figure 3.4: Scanning electron micrographs of the microstructures induced on the surface of the studied co-polymer materials irradiated with a 550 nm laser beam. Taken from Wood <i>et al</i> with permission.	55
Figure 3.5: Experimentally determined ionization threshold fluences of UV-cured polymer materials, irradiated with (a) 275 nm, and (b) 550 nm fs-laser beam, presented as a function of the number of laser pulses. Error bars represent the 95% confidence interval. Note that in many cases the error bar is smaller than the data marker. Adapted from Wood <i>et al</i> with permission.	56
Figure 3.6: Absorbance of (a) 275 nm wavelength light by the pristine polymer substrates, (b) 550 nm wavelength light by the pristine polymer substrates, (c) 275 nm wavelength light by the polymer substrates after ablation, and (d) 550 nm wavelength light after ablation. Used with permission.	57
Figure 3.7: Experimentally determined incubation coefficients ξ of UV-cured polymer materials irradiated with (a) 275 nm, and (b) 550 nm fs-laser beam. Error bars represent the 95% confidence interval. Adapted with permission.	59
Figure 4.1: Illustration of the differing cross-link densities in cured polymer networks with no comonomer (A) and with comonomer included (B).	67
Figure 4.2: Initial ice adhesion data of the three series of prepared coatings compared to EB1360. Red, blue, and green columns denote 5, 10 and 25 wt% comonomer. Error bars are the standard error of the measurements ($n = 5$).	70
Figure 4.3: SEM images showing wrinkling on surfaces of EB1360:Styrene coatings: a) EB1360, b) 5 wt% Sty, c) 10% Sty, d) 25 wt% Sty.	72
Figure 4.4: a) average wrinkle width and b) root-mean square roughness of copolymer network coatings measured by AFM.	72

Figure 4.5: AFM height images showing wrinkles present in EB1360:Sty copolymer films.	73
Figure 4.6: Plots showing ice adhesion over time measure on prepared copolymer networks. Red, blue, and green data series represent 5, 10 and 25 wt% comonomer.	74
Figure 4.7: Plots showing durability of coatings to successive deicing tests. Samples visibly damaged from testing were removed from the complement as damage occurred. The average τ_{ice} values in blue were calculated from intact samples only, and the orange plot shows the number of samples with no visible damage.	75
Figure 5.1: Ice grown on a film (<i>left</i>) completely (normally) attached to the substrate, or (<i>right</i>) partially detached from the substrate.	80
Figure 5.2: Ice adhesion τ_{ice} measured on commercial adhesive films. The right column of each series denotes films detached from the substrate under the iced area. ($A_{ice} = 0.28 \text{ cm}^2$, $A_{det} = 1 \text{ cm}^2$).	81
Figure 5.3: Ice adhesion (τ_{ice}) on commercial films with varied area of detachment between the film and substrate ($A_{ice} = 1 \text{ cm}^2$).	83
Figure 5.4: a) Image of ECO 360 applied to underside of 1577CW film, b) Pattern of ice column positions generated by Inkscape, c) and d) Ice columns corresponding to the first six and four remaining positions on the generated pattern.	84
Figure 5.5: Plots of ice adhesion measured on arrays of varying detachment size for: a) Masking tape, b) PVC tape, c) Aluminum shielding tape, and d) Skived PTFE film.	85
Figure 5.6: Plots showing the change in relative sample masses for films with varying detachment size: a) masking tape, b) PVC tape, c) jacketing tape, and d) PTFE skived film.	86
Figure 5.7: Photos showing surface damage to a) normally attached PVC film, and films with b) 10 mm, c) 16 mm, and d) 20 mm detachments in the path of the abrasive wheels.	88
Figure 5.8: Plots showing Al_2O_3 required to break through a) PVC film and b) masking tape with different detachment sizes. Photos showing surface damage to a) normally attached	

PVC film, and films with b) 10 mm, c) 16 mm, and d) 20 mm detachments in the path of the Al_2O_3 particles.	89
Figure 6.1: Proposed construction of a rack containing an array of coated aluminum coupons at different angles relative to spraying apparatus (left, top view; right, side view).....	97
Figure 6.2: Plot of force per unit width ($x = 1\text{ cm}$) versus length (L) of iced areas. Force per unit width is constant after a critical length, L_{crit}	99
Figure 6.3: Experimental setup for measuring interfacial toughness using ice columns with a fixed width (x) and variable length (L).	99
Figure 6.4: Blending of acidic graphene suspension with polymers containing sodium bicarbonate for concurrent dispersion and quenching.	103
Figure 6.5: Blending of graphene suspension with ‘surrogate’ polymer containing basic phosphine functionalities, followed by blending with elastomer of interest.	104

List of Abbreviations

AFM	atomic force microscopy
ASTM	American Society for Testing and Materials
°C	degrees Celsius
CAD	Canadian dollars
CAH	contact angle hysteresis
cm	centimeters
CNT	classical nucleation theory
CWB	cold weather biome
DC	direct current
DIA	droplet impact apparatus
EDX	energy dispersive x-ray spectroscopy
F_{app}	applied force
F_c	centripetal force
f_θ	shape factor
g	gram
G	shear modulus
GPa	gigapascals
h	hours
J	joule
kPa	kilopascal
L	length
L_c	critical length
LMA	lauryl methacrylate
m	meter
mJ	millijoule
MAA	methacrylic acid
MMA	methyl methacrylate
mol	mole
n^*	critical nucleus size
PAAO	porous anodic aluminum oxide
PDMS	polydimethylsiloxane
PTFE	polytetrafluoroethylene
PVC	polyvinyl chloride
SEM	scanning electron microscopy
SHS	superhydrophobic surface
SLIPS	slippery lubricant-infused porous surface
Sty	styrene
T_g	glass transition temperature

TGA	thermal gravimetric analysis
TPa	terrapascals
TPE	thermoplastic elastomer
USD	U.S. dollars
UV	ultraviolet
W_a	work of adhesion
γ	surface free energy
Γ	interfacial toughness
ΔG_n^*	free energy of nucleation
ε	strain
θ_C	static contact angle
θ_A	advancing contact angle
θ_R	receding contact angle
ν_e	cross-link density
σ	stress

Preface

Developing ice repellent materials is an interesting challenge. My favourite part about this research (more accurately, performing this research in Canada) is that whoever I speak to feels connected: they have *had* to deal with ice in some way, at some point, and likely will again soon. What is not obvious is how complex a problem ice adhesion is, and how diverse the research in the field. It's an unusual problem and makes for a thesis that seems an awkward fit for chemistry. For this reason, I have included this short preface, and a list of references that I believe are must reads for those interested in the field. Enjoy!

-Matt

John Sayward's Special Report entitled "Seeking Low Ice Adhesion" should be the first writing you consult. It frames the problem of adhesion and discusses the nascence of the field in such an accessible and interesting way, you must read it. I only wish that I had found this work earlier during my graduate studies.

Lars-Olof Andersson's Licentiate Thesis entitled "Ice Accretion and Ice Adhesion to Polymer Materials" furthers some discussion presented by Sayward, and beautifully summarizes work in the field up to 1993.

"Design of anti-icing surfaces: smooth, textured or slippery?" is a review by Michael Kreder, Jack Alvarenga, Philseok Kim, and Joanna Aizenberg published in 2016. I think it effectively captures the climate of contemporary anti-icing research.

Kevin Golovin's works published while at the University of Michigan with Anish Tuteja are without a doubt the closest to a true solution to ice repellent surfaces with high durability the field has come so far. The low-level discussion in these papers will change the direction of research occurring in the field. In particular, the measurement methods described here will be critical to large-scale application of ice repellent materials.

Chapter 1

1 Introduction

1.1 The Impetus of Icing Prevention

Ice is a diverse material that can be observed in many forms in nature, ranging from clouds to glaciers. These forms can be beautiful to view from a distance, but where humans interact with ice, it is a nuisance and a safety hazard. Icy sidewalks cause slips and falls, black ice causes motorists to lose control of their vehicles, downed power lines interrupt electricity and heating, and pose an electrocution risk. The underlying cause of these hazards is a simple matter of ice adhering to and accumulating on surfaces. While the problem is simple in nature, there is no consistently effective method of preventing ice accumulation. Prevention and removal encompass complex engineering challenges that have been researched for over a century.¹ Interest in icing prevention was sparked in a variety of industries, often linked in some way to the military, for preventing ice build-up on marine vehicles, locks and dams, telecommunication lines and aircraft,² with one of the earliest mentions of ice prevention in the literature was the 1940s by early commercial airlines “[...] anxious to make flying a safe routine in every type of weather.”^{1,3} These concerns are responsible for the birth of ice prevention, and continue to inspire contemporary research in the field (**Table 1.1**).

The applications listed in **Table 1.1** suggest many ways that anti-icing can improve our lives on a daily basis, as well as the potential economic impact. The cost of repairs in recent history further underscores the importance of this issue. The total annual costs of ice and snow removal in Canada is difficult to estimate as it is handled by municipalities, but certainly reaches into billions of dollars CAD. A single snow and ice removal operation in Montréal costs the city \$15 million, with several removal operations required during one winter season.⁴ The snow/ice removal budget in Toronto is \$90 million;⁵ in Ottawa, \$75 million and this was exceeded by more than \$7 million in 2018.⁶ These costs only take in to account the removal of ice and snow, and not the costs associated with infrastructure maintenance like replacing downed power lines, or the hidden costs of road deicing in the

form of corrosion damage to bridges and vehicles.⁷ In addition to annual costs associated with infrastructure maintenance, the acute costs of extreme weather (e.g. ice storms) also come at a great cost to the economy. In 2013 the Toronto ice storm cost the city over \$100 Million CAD in repairs,⁸ which is a small evaluation compared to The Great Ice Storm of 1998, which cost thirty-five Canadians their lives, and an estimated “[...] \$5.4 Billion [USD] in insurance claims, utility repairs and lost productivity [...]”.⁹ This undoubtably highlights the economic and health concerns for citizens in cold climates created by ice accumulation. Methods of preventing ice accumulation must be developed in order to protect the lives and tax dollars of Canadian citizens, and others globally. In pursuit of this goal, one must first develop an understanding of why ice adhesion occurs and what factors influence it, as well as the materials and methods that encompass the state of the art in ice prevention.

Table 1.1: Application Areas of Ice Repellent Surfaces

Application Area	Examples
Aerospace	<ul style="list-style-type: none"> - Ice buildup on wings / fuselage increases drag - Prevents operation of mechanical parts (e.g. ailerons) - Blocks air flow to vital instruments (e.g. Pitot tubes)
Appliances	<ul style="list-style-type: none"> - Heat exchangers are less efficient when iced over - Storage decreased in heavily iced fridge, freezer
Communication	<ul style="list-style-type: none"> - Transmission lines can be damaged by weight of ice - Towers can collapse under the weight
Infrastructure	<ul style="list-style-type: none"> - Buildings, bridges damaged by weight of ice - Potholes created when ice grows in road cracks - Salt used for deicing damages steel, concrete
Marine	<ul style="list-style-type: none"> - Boats become unstable when ice grows on hull - Prevents operation of canal locks, moving parts - Can damage navigation instruments
Power Generation	<ul style="list-style-type: none"> - Wind turbines can collapse under the weight of ice - Solar panels less efficient / inoperable when coated
Vehicles	<ul style="list-style-type: none"> - Windshields must be deiced - Salt from roads corrodes body, frame, infrastructure

1.2 Adhesion: A Primer

Adhesion describes the attachment of a material to another, forming what is often called a joint or adhesive bond (not to be confused with chemical bonding). The forces holding a joint together vary from system to system, but typically they include interactions described by one or more of the following adhesion theories:¹⁰ (1) mechanical interlocking theory, where adhesives infiltrate surface asperities of a material; (2) electrostatic theory, involving electron transfer between adhesive and substrate due to dissimilar band structure; (3) diffusion theory, where molecules of the adhesive/substrate interdiffuse, (4) wetting theory, which proposes that adhesion occurs because of molecular contact between two materials and the surface forces that develop as a result of Van der Waals forces; (5) chemical bonding theory, which attributes adhesion to surface chemical forces, such as covalent or ionic bonding, or hydrogen bonding; and (6) weak boundary layer theory, which deals primarily with bond failure, identifies the cause of failure in some cases to be weak attachment of a surface layer to the bulk, such as some metal oxides to their metals. Ice adhesion is generally considered to result from a combination of mechanical interlocking, wetting, and chemical bonding. Interlocking occurs when water infiltrates, freezes and expands into surface asperities, wetting is the spreading and adhesion of liquid water to a surface, and hydrogen bonding describes the sharing of water hydrogen atoms with polar surface groups. The formation of an adhesive bond has other requirements, as well. One material must ‘wet’ the other material, which allows for close interaction of the chemical groups or surface asperities that cause bonding. Next, a material must ‘set’; that is undergo a change that allows it to remain adhered to the other material. Ice sets when it undergoes a transition from liquid to solid as it cools to $\sim 0^\circ\text{C}$ when it adheres to a solid. The set material must then undergo significant enough deformations as to allow for the release of any elastic stresses that could cause the joint to fail.¹¹ The most often discussed adhesion requirement related to ice adhesion is the surface wetting of the material.

Wetting is a measure of droplet spreading on a material and is a necessary condition for good adhesion.¹¹⁻¹² Consider observing water droplets collecting on different surfaces and variations in their behavior. Water on a leaf tends to form a rotund droplet, whereas water on metal tends to spread into an oblong droplet or puddle: metal is wetted by the

droplet, but the leaf is not, or is to a lesser extent. A material that shows good droplet spreading is often called hydrophilic and non-wetting surfaces are called hydrophobic. The degree to which a material is wetted is measured using contact angle (**Figure 1.1**).

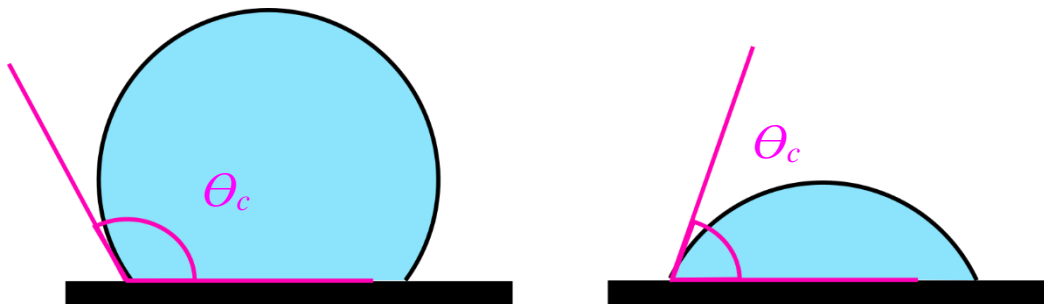


Figure 1.1: Water contact angles (θ_c) on (*left*) a smooth hydrophobic surface, and (*right*) a smooth hydrophilic surface.

A line tangent to the surface of the droplet creates angle θ_c when drawn to the droplet baseline. Lower values of θ_c indicate better or more complete wetting (hydrophilic, $0 \leq \theta_c \leq 90^\circ$) than higher values of θ_c (hydrophobic, $90 \leq \theta_c \leq 150^\circ$). Contact angles greater than 150° can be observed on superhydrophobic materials (**Section 1.5**). Droplets spread on surfaces when the forces of interaction between water and the surface overcome the cohesive forces holding the shape of the droplet. This occurs when the free energy of the surface is greater than the surface tension of the liquid (Note: for liquids, surface tension and surface energy are numerically the same). In any material, the surface possesses greater energy than the bulk. This surface free energy is the result of non-symmetric bonding of surface atoms or molecules at the surface (**Figure 1.2**) and is measured in Joules per meter squared (J/m^2).¹³

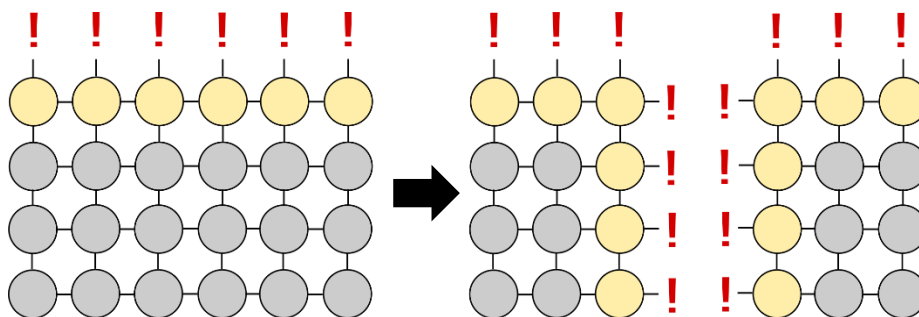


Figure 1.2:Diagram depicting the cause of surface energy (left) before cleavage, and (right) after cleavage. Circles represent lattice points in a crystalline material; grey for bulk, beige for surface. '!' indicate unbalanced forces on lattice points

Lattice points at the generic surface do not form bonds at the interface, leading to unbalanced forces (!) in the material, and therefore the surface possesses more energy than the coordinatively saturated bulk.¹⁴ When the material is cut, the energy required to do so is related to the energy needed to form new surfaces on each side of the cleavage. The relationship between surface wetting and surface energy is the Young's Equation:

$$\gamma_{SV} = \gamma_{SL} + \gamma_{LV} \cos \theta_c$$

Equation 1.1: Young's Equation

Where γ is the surface free energy, and S, V, and L denote solid, vapor and liquid. The equation shows the inverse relationship between the relative energies of the solid surface and the liquid, and θ_c . When the surface energy of a liquid is low relative to the solid it is on, θ_c will be small. Water has a γ of 72 mJ m⁻², meaning that on metals ($\gamma \sim 500\text{-}1500$ mJ m⁻²) and glass ($\gamma = 1200$ mJ m⁻²), θ_c will be small, and the surface will be wetted. On organic solids like polyethylene ($\gamma = 30$ mJ m⁻²) θ_c will be greater, meaning the surface is not wetted.¹⁵ The reason that metals and glass have higher surface energy than polymers comes from the greater strength of attractive interactions in the bulk, leading to greater unbalanced forces at the surface. Different wetting characteristics lead to different behavior when forming adhesive joints, which is why specialized adhesives are often required for lower-energy substrates like plastics. However, there are other properties affecting adhesion.

Surface roughness can influence how strongly two materials adhere, but according to adhesion theory simply knowing whether a surface is rough or smooth is not adequate to estimating ice adhesion on a material, and surface roughness should be considered only of secondary importance with respect to ice adhesion (**Figure 1.3**).¹

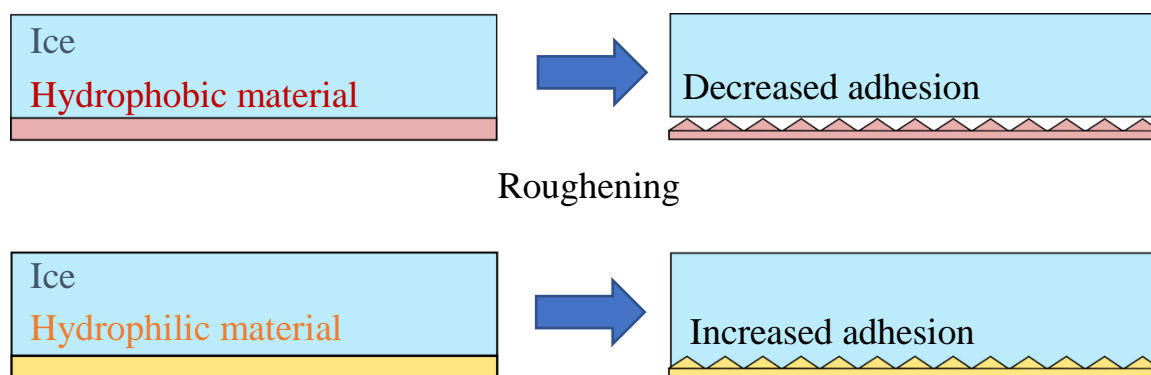


Figure 1.3: Illustration of changing adhesion with surface roughness for hydrophobic and hydrophilic materials. Roughness causes decreased water / ice adhesion on hydrophobic materials, and increased water / ice adhesion on hydrophilic materials.

Consider two materials that are similarly smooth. A hydrophobic material with low surface energy weakly interacts with water / ice, and therefore exhibits low adhesion. A hydrophilic material with higher surface energy strongly interacts with water/ice, and therefore has more complete wetting, and higher adhesion. Roughening both surfaces equally would have two different effects: adhesion to the hydrophobic surface would decrease, and adhesion to the hydrophilic one would increase. This has to do with changes in contact area between ice and the substrate. Weak surface interactions coupled with increased roughness yield a decrease in contact area, and therefore a decrease in adhesion. Conversely, stronger surface interactions coupled with increased roughness yield an increased contact area, and therefore improve adhesion. Both extremes of this scenario have been explored in the literature, and their relationship to anti-icing materials will be discussed in **Section 1.5**. By looking at adhesion through this classical lens, it sounds like creating ice repellent surfaces should be a relatively simple task: all that is required are materials with low surface energies, and tailored roughness to reach the minimum possible adhesion of ice to virtually any surface. Unfortunately, this is not the case. While surface wetting is important, there

are few links between surface energy and roughness, and obtaining ultralow ice adhesion. There are additional factors that influence ice adhesion that must be considered. Most importantly, characteristics of the ice/substrate interface are critical, rather than strictly properties of the coating materials.

1.3 Other Factors Influencing Ice Adhesion: The Interface

Ice adheres strongly to materials with high surface energy due to favourable wetting, and polar surfaces due to strong hydrogen bonding interactions. (**Figure 1.4**).

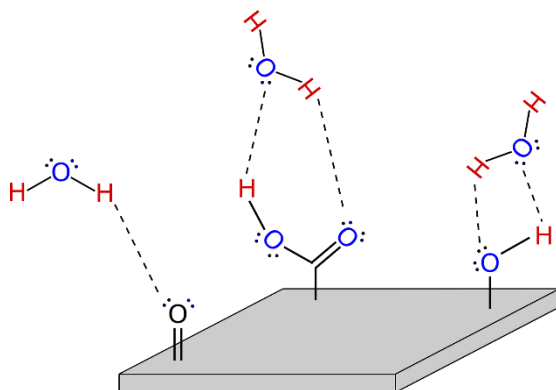


Figure 1.4: Hydrogen bonding to a generic surface with polar groups present. Hydrogen bonds are shown as dashed lines.

Surfaces with polar groups can strongly interact with water molecules through hydrogen bonding, contributing to strong wetting of the surface and formation of a strong adhesive bond and influencing adhesive strength in the solid phase. Ice is known to expand as it freezes, meaning that if water infiltrates scratches or cavities on a surface and freezes, the ice interlocks with these structures leading to strong mechanical adhesion. Sayward discusses how the toughness of the interface, rather than the strength can make ice very difficult to remove.¹ The contrasting effects of strength and toughness were more recently discussed by Golovin and coworkers, highlighting the importance of reducing the toughness of the interface.¹⁶ Strength and toughness are normally considered bulk properties of a material, relating to its ability to resist permanent deformation (strength), or to absorb energy in response to stress without fracture / crack propagation (toughness). These values can be extracted from stress-strain curves of the materials.

Interfacial strength and interfacial toughness are analogous to these characteristics but involve the interface of two materials. Interfacial strength describes resistance to deformation of an adhesive joint in response to stress, whereas interfacial toughness describes the ability of an interface to absorb energy in response to stress instead of fracturing. Toughness in particular is strongly related to the ice / material interface. The presence of a 'liquid-like' layer of water at ice/material interfaces has been studied, and the thickness of this layer influences ice adhesion.¹⁷ A thicker liquid-like layer can absorb more energy in response to stress, makes the bond between ice and a surface very tough. Properties of ice like this liquid-like layer, and the ice crystal structure are affected by variations in temperature, and the rate of freezing, meaning that ice may adhere differently to the same substrate under different conditions.¹⁸ The macroscopic structure of ice also has an effect on ice adhesion.¹⁹⁻²⁰ Rime ice and frost, both of which are milky-white mixtures of air and ice, tend to adhere more strongly to surfaces than glaze ice, which is smoother and clear. The reason relates again to toughness, which is higher in rime and frost because of voids in their structure. These voids prevent stress cracking in the material, reducing the probability of delamination occurring. These properties generally cannot be controlled through material design. Other interfacial effects that reduce adhesion may be influenced through the choice of materials and are therefore of great interest.

Interfacial cavitation is related to the relative stiffness of two attached materials, and the different ways in which they respond to an applied force (**Figure 1.5**).²¹

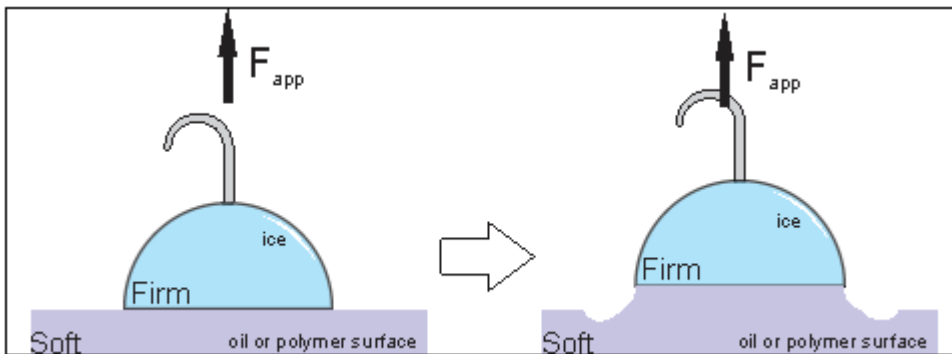


Figure 1.5: Depiction of interfacial cavitation. A force F_{app} applied to two connected bodies, one soft and one firm, will bring about deformations in the soft body.

Consider a rigid material like ice, attached to the surface of a softer material like rubber. If a force F_{app} is applied to the materials, the rubber material will deform, but ice will not. As the rubber continues to deform, ice is essentially peeled from its surface as cavities form at the interface until it becomes completely detached. Interfacial cavitation is typically observed at the interface of a viscous material and an elastic material and is closely related to the low ice adhesion occurring on viscoelastic materials like elastomers. Elastomers are often chosen for applications where they are above their glass transition temperature, T_g , where the material is in an amorphous state, the molecular chains in the polymer are mobile, and the material is soft and pliable. The shear force required to remove ice from an elastomer surface is related to both the thickness and the modulus of the material (Equation 1.2)^{16, 21-22} :

$$\tau = A \left(\frac{W_a G}{t} \right)^{1/2} \quad \text{Equation 1.2: Shear stress required to remove ice from a soft film}$$

Where τ is the shear stress required to remove the ice, A is an experimental constant, W_a is the work of adhesion of the ice, G is the shear modulus of the elastomer, and t is the thickness of the coating. Therefore, it is easier to remove ice from elastomeric coatings that have a lower shear modulus, and that are applied in thicker layers to the substrate. The use of elastomers as ice repellent materials is further discussed in **Section 1.6**.

Interfacial slippage is a phenomenon observed at the interface of ice and viscoelastic materials, specifically in systems where free chain polymers or lubricants have been incorporated into cross-linked polymer matrices.²³ Slippage in this instance describes a movement at the interface between two solids, where normally the conservation of momentum should dictate that no motion should occur. This occurs because when polymer chains in the system are sufficiently mobile at the interface that detachment can occur.¹⁶ Interfacial slippage has been observed in polymer melts,²⁴⁻²⁵ adhesives,²³ and rubbers,²⁴ and was recently applied to ice adhesion on polymer coatings by Golovin and coworkers (Section 1.6).¹⁶ Each case involves the interface of viscous and elastic materials. When a force is applied to an elastomer adhered to a rigid surface, slippage can occur at the

interface of the materials, which originates from contractive strain experienced by the material in response to the applied (extensive) force (**Figure 1.6**).²³



Figure 1.6: Illustration explaining the observation of interfacial slippage observed in an elastomer film adhered to a surface. (*left*) A polymer film on top of a rigid substrate, with no forces acting upon it. The polymer particles shown have no net force acting upon them, and therefore no slip is observed. (*right*) The polymer film is experiencing an extensive force as it is being peeled from the surface. A net force in the direction labelled ‘extension’ leads to a concomitant contraction and slippage of the polymer particles.

This observation is similar to how a piece of electrical tape gets narrower if stretched at the ends. The particles shown are therefore able to ‘slip’ along the surface with a non-zero velocity. This principle allows for the release of Command™ hooks from walls when the tab is pulled. When the release tab is pulled, the viscoelastic adhesive extends in the direction of the force, and the contraction causes separation between the adhesive and the wall.

The outlined interfacial phenomena and characteristics of the ice/material interface, coupled with the classical considerations of surface energy and topography, and must be tailored to achieve effective deicing. A variety of technologies have been explored to achieve decreased ice accretion. These properties have led to different strategies of reducing ice accumulation, resulting in significant progress over the last 10 years.²⁶

1.4 Strategies to Reduce Ice Accumulation

Researchers have made considerable progress in developing methods of reducing ice buildup by altering surface energy, topography, and interfacial characteristics of a variety of materials. These methods can broadly be separated into *anti-icing* and/or *deicing* approaches, which describe two distinct camps. Deicing refers to the removal of ice *after* it grows on a surface, examples of which are perhaps the most relatable. Scraping frost/ice off a car windshield, or melting it using the rear defroster, are examples of active deicing methods, where ‘active’ indicates that some energy input is required from the user for the method to work. Frankenstein (no relation) and Tuthill’s review of active methods outlines the many ways deicing has been attempted on large scales, primarily on marine locks,² including drilling, cutting, perforating using water jets and explosives, electrical resistive heating, mechanical breakage *via* electrical pulse, and applying a DC bias to resist ice buildup. A key point outlined by the authors is the impracticality of active deicing methods: a huge amount of energy is required for removal from structural surfaces like steel, due to the strong adhesive bonds between ice and high surface energy materials.²⁷⁻²⁸ This impracticality is exacerbated when accessing the iced structure is dangerous or if surfaces are remote, such as off-shore wind turbines. Furthermore, vigorous removal methods (e.g. smashing, exploding) can undermine the integrity of surfaces, making them prone to further ice accumulation, and device damage. Melting also presents a unique drawback, as water can traverse a structure and refreeze in a different position, which does not solve the problem of ice accumulation.

Anti-icing strategies refer to those that aiming to prevent ice growth from occurring on a surface. Returning to the prior example of using a vehicle’s rear defroster, one can imagine a scenario where the defroster was always left on, preventing water from freezing: an example of an active anti-icing strategy. Here, an input of energy is used proactively to prevent ice from growing, in contrast to the deicing method, where heating is used reactively. Although the goal has changed, this method should still be considered active, since there is a significant energy requirement associated with always having the heater on. Indeed, the energy costs associated with active types of both deicing and anti-icing are very high, whether in the form of electrical energy or human power. A *passive* method of either

anti-icing or deicing requires no input of energy from the user in which to work. In the case of anti-icing, this might mean that water is ejected from the surface before it freezes, keeping the surface consistently ice-free; in deicing, ice forming on a surface might delaminate in response to a gust of wind. Ideas of passive ice abatement have become increasingly discussed in recent literature, with some promising developments having occurred in the last ten years.²⁶

1.5 Passive Methods of Ice Abatement

Shenglin Jin *et al.* recently reviewed strategies of passive anti-icing.²⁹ The strategies discussed are: (1) timely removal of water droplets; (2) controlling ice formation (i.e. nucleation and spreading of ice on the surface); and (3) reducing the strength of ice adhesion. The first two approaches can be grouped together as anti-icing approaches as they seek to prevent ice from forming on the surface. Reducing ice adhesion strength deals with ice having already formed on the surface, and therefore describes passive deicing. Passive anti-icing strategies revolve around preventing water from freezing on a surface when the two come into contact. Anti-icing using water repellent surfaces is perhaps the most populated area of anti-icing research, and was the center of discussion in a recent review by Sojoudi and coworkers.²⁰ The enormous number of water repellent strategies to anti-icing is owed to the enormous amount of research dedicated to the related field of superhydrophobic surfaces (SHSs), which have been studied since the work of Adam, Wenzel, and Cassie and Baxter in the 1930s and 40s. Their work showed that ‘rough’ (i.e. textured) surfaces can support exceptional dewetting characteristics like water beading and rolling off these materials.³⁰⁻³¹ The extraordinary wetting characteristics of SHSs result from micro- / nanoscale surface texture that can be generated in a multitude of ways, including lithography,³² laser micromachining,³³ coating with particles,³⁴⁻³⁵ chemical etching,³⁶ and anodization.³⁷ Once roughness is produced, chemical modification can be performed to minimize the surface energy of a material, which yields very high contact angles ($> 150^\circ$) and low contact angle hysteresis (CAH, $< 10^\circ$), by which SHS are defined.

Contact angle hysteresis is the difference between the advancing (θ_A) and receding contact angles (θ_R) (**Figure 1.7**).

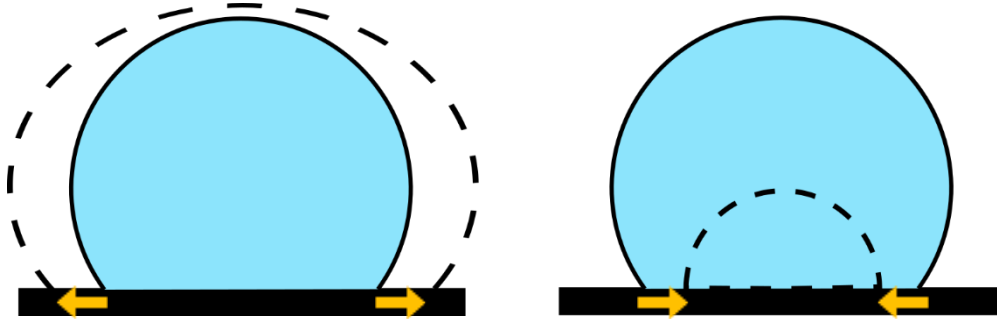


Figure 1.7: Illustration of (*left*) advancing and (*right*) receding contact angles.

Advancing contact angle θ_A is the contact angle measured while the base diameter is increasing (i.e. as water is added to the droplet) and tends to be a higher value than the static contact angle θ_C . Conversely, receding contact angle θ_R is measured as base diameter decreases (water is taken away from the droplet), and is lower than θ_C . These changes in contact angle are observed because of adhesion forces between the water droplet and the surface³⁸ The difference between θ_R and θ_A is contact angle hysteresis (CAH). CAH is the result of imperfections in surface topography causing increased droplet adhesion. This adhesion leads to differences between θ_R/θ_A and θ_C . It has been shown that under dynamic conditions CAH is a better measure of surface wettability than θ_c .³⁸ Small CAH means that surface wetting is consistent, and water can de-wet a surface reliably. Larger CAH means that droplets are adhering more strongly to a surface, leading to failed dewetting. Smaller CAH is therefore desirable for ‘water removal’-type anti-icing surfaces. Rapid dewetting phenomena such as rolling, bouncing, or jumping³⁹ off these surfaces are

facilitated by air trapped beneath droplets at the liquid-solid interface, called the Cassie-Baxter wetting state (**Figure 1.8**).

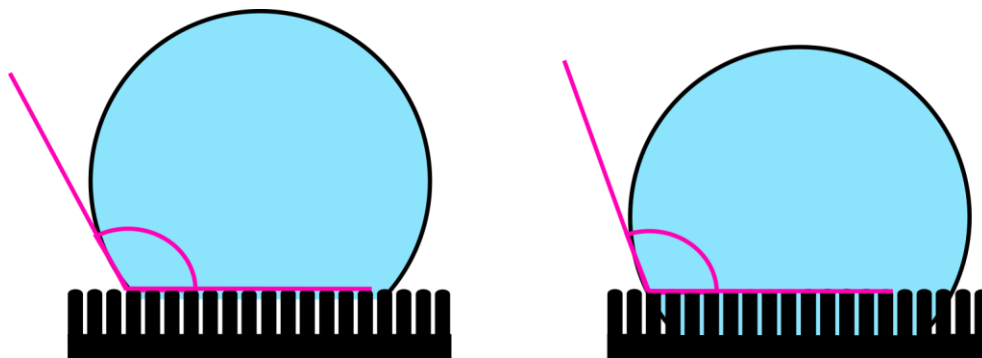


Figure 1.8: Illustration of the Cassie-Baxter (left) and Wenzel (right) wetting states. Both have very high apparent contact angles.

A Cassie-Baxter type state describes a situation where water sits on top of the microstructures, supported by a pocket of air, like the Leidenfrost effect observed when liquid N_2 is poured on a warmer surface. This pocket of air is supported by capillary pressure inside the unwetted microstructure, meaning this wetting state allows for high droplet mobility, and is the desirable mode of water contact in anti-icing by dewetting applications because water quickly leaves the surface before freezing. However, if a droplet overcomes the capillary pressure, for example by impacting the surface with sufficient velocity,⁴⁰⁻⁴¹ it can enter the Wenzel wetting state, the so-called Cassie-Wenzel transition.^{20, 42} The difference in these wetting states is important for discussing the applicability of SHS to anti-icing. A droplet “pinned” to the surface in this way is not mobile, and if cooled will freeze and interlock with the microstructure. This has been shown to be detrimental to their action as anti-icing surfaces, with the mechanical adhesion of ice and the surface structures leading to greater adhesion than that observed on smooth surfaces.⁴³

Superhydrophobic materials work as anti-icing agents in two ways. They facilitate rapid dewetting of surfaces before water has an opportunity to freeze, which has been shown to be effective even under freezing conditions.⁴⁴⁻⁴⁵ They also enforce a large contact angle, which minimizes the water-surface contact area. This both reduces how strongly ice

adheres,⁴⁶ and limits heat transfer between water and the surface, meaning that the rate of heterogeneous ice nucleation is suppressed.⁴⁷⁻⁴⁸ Despite some successful trials, anti-icing using textured superhydrophobic surfaces remains controversial.⁴⁹⁻⁵⁰ This is largely because of different environmental conditions greatly affects the performance of these surfaces.⁵¹ Infiltration of surface structures by condensing water vapor,^{18, 43, 52-53} or by droplets impacting at high velocity,⁵⁴ causes Wenzel type wetting, which when followed by freezing leads to anchoring of ice and damage of the microstructures. The concern of water infiltrating the pores is even a problem at low humidity, as Wang *et al.* demonstrated that droplets can increase the local humidity at the surface structures.⁵⁵ Contamination of surfaces by particulate matter, and damage by erosion or freezing/thawing, should also be considered a drawback of SHS-induced anti-icing. Particles on the surface provide sites for nucleation, meaning that dewetting capabilities are compromised, and all ice repelling ability is lost once the microstructures are damaged.⁵⁶ In addition to these drawbacks it is difficult to practically assess the effectiveness of SHSs as anti-icing materials: there are few metrics that directly relate surface wetting with surface icing. Metrics related to wetting, such as contact angle and its hysteresis give at best parallel trends⁵⁷ with ice growth, meaning there is no way of knowing how well a material will perform in a given environment without subjecting the material to that environment. This is challenging and time consuming, requiring winter weather, or the means to recreate it indoors. Without a method of directly comparing surfaces, rating their performance in anti-icing is not possible, and the goal of systematically improving anti-icing surfaces through experimentation becomes exceptionally difficult.

A second approach to passive anti-icing is ‘controlling ice growth’, the approaches to which are described as retarding either nucleation or propagation of ice on the surface.²⁹ Ice crystal formation, like the formation of many other crystal types, begins with nucleation.⁵⁸ In classical nucleation theory (CNT),⁵⁹ nucleation is a random process where

small crystalline groups of atoms, molecules, or particles come together through collision (Figure 1.9).

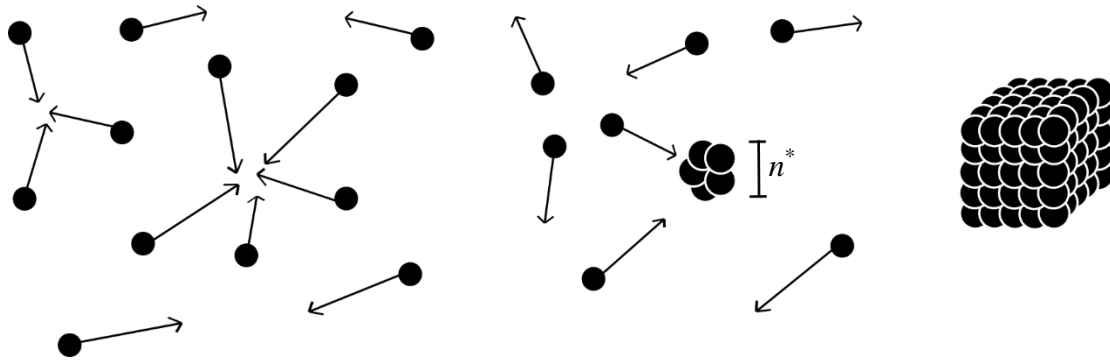


Figure 1.9: Illustration of homogeneous nucleation. Liquid particles collide randomly, until a nucleus of critical size forms, leading to the formation of a crystal.

Eventually, a group larger than a critical size n^* aggregates, allowing the system to overcome the energy barrier to crystal formation, ΔG_N^* . The time required for a collision to occur creating a nucleus greater than n^* is much greater than the time it takes for particles to add to a nucleus, so once a nucleus forms crystal growth accelerates. Nucleation from a pure liquid that relies on random collision of particles is called homogeneous nucleation, as all the molecules in the system are in the same phase until nucleation occurs. Typically, this is *not* how ice forms in nature. In fact, it has been shown that homogeneous nucleation of water may not occur until below -40°C .⁵⁸ The well-known water freezing point at $\sim 0^\circ\text{C}$ exists solely because of impurities in water, and a process called heterogeneous nucleation, whereby the presence of a “foreign phase”, such as a solid particle or a gas bubble, greatly lowers the barrier to nucleation. The relative Gibbs Free Energy of the processes follows the expression:

$$\Delta G_{N(hetero)}^* = \Delta G_{N(homo)}^* \cdot f(\theta) \quad \text{Equation 1.3: Relationship between the free energy barriers of heterogeneous and homogeneous nucleation}$$

Where $f(\theta) \leq 1$ and is called the shape factor and takes in to account interfacial energies between the crystal, liquid, and foreign phase. Despite being critically important in anti-icing applications, heterogeneous nucleation is not well understood. It is exceptionally challenging to study because of the nanoscale lengths and times associated with nucleation, and much of the work exploring heterogeneous ice nucleation is computational in nature, examining the effects of different surface topographies, hydrophilicities, and charges on ice nucleation rates. Early work in the field strongly suggested that ice nucleation was promoted by similarities in ice crystal lattice parameters to the lattice of the surfaces on which ice grows.⁶⁰ That is, that the structure of some surfaces ‘looks’ like ice, so it prefers to grow there. Recent computational studies by Fitzner *et al* support the notion that in some cases, a smaller lattice mismatch increases the rates of heterogeneous nucleation, but it is not a requirement for nucleation to occur.⁵⁸ While these and other computation studies mark huge accomplishments in our fundamental understanding of ice growth, there is still a considerable gap between learning about the causes of ice nucleation and applying them to surface/material design strategies. There are at least two practical measurement that can be made to evaluate materials’ anti-ice nucleation characteristics called freezing delay. Droplets placed on surfaces can be observed using high-speed photography, and the time measured until freezing may be recorded.⁶¹⁻⁶² This property has been explored on different surfaces, most of which are patterned SHS-type materials.⁶³ Freezing delays as long as 25 hours have been observed.⁶⁴ Sojoudi’s presents a comprehensive review of these methods, attributing freezing delay to insulating effects of air pockets in the Cassie-Baxter state reducing the contact area of water with surfaces, increasing the energy barrier to heterogeneous nucleation.²⁰

Propagation delay is a less studied property for ice growth on surfaces, where a surface prevents ice from spreading, and is typically measured in how far ice grows along a surface in a given timeframe as it is observed microscopically. Poulikakos and co-workers studied the effects of thermal conductivity on ice propagation, showing that more highly thermal conducting materials reduced ice propagation.⁶⁵ Jin and coworkers recently showed the effects of ions and hydration layer thickness.⁶⁶ In spite of major strides made developing an understanding of heterogeneous nucleation and freezing propagation, it is not likely that anti-nucleation/propagation surfaces will be applied in large-scale ice

prevention. Contaminants such as dust, sand, and ice particles (i.e. foreign phases) can provide nucleation sites for ice crystals to form on surfaces, or alternatively damage any surface structure designed to inhibit nucleation. Environmental conditions also present significant problems for these methodologies. Heydari and coworkers showed that beneficial effects of surfaces on demoting ice nucleation did not persist below the dew point, where water droplets condense on surfaces forming ice or frost.⁶⁷ Coupled with the comparative difficulty of creating surfaces that limit ice nucleation and propagation, it seems unlikely that this approach will see large-scale application. It is important to our fundamental understanding in other fields such as climate science that this type of work continue.

Recent discussion surrounding passive ice repellency has favoured reducing ice adhesion strength as the most promising avenue of development.²⁶ This quite literally means tailoring properties of materials to minimize the force required to remove ice once it forms on a surface, taking in to account all the preceding discussion of surface energy, surface topography, and interfacial characteristics. One of the greatest advantages of exploring these methods is the capability of directly measuring ice adhesion strength, typically expressed in kilopascals (kPa), which takes in to account both the force required to remove ice, and the area covered. Numerous methods have been developed to measure ice adhesion, the two most common being *via* load cell or centrifuge (**Figure 1.10**).

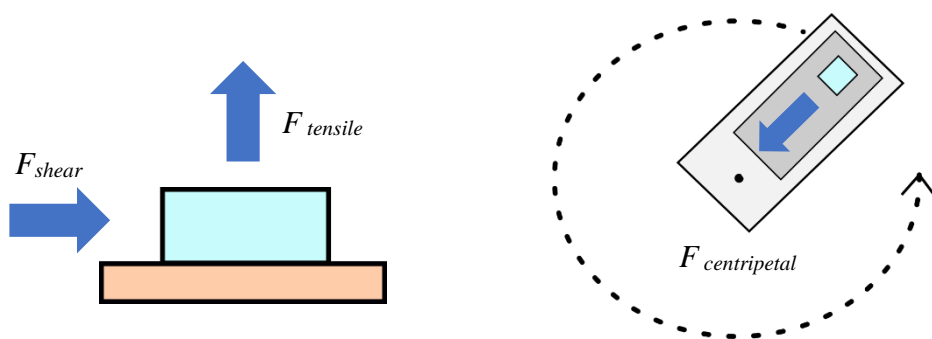


Figure 1.10: Ice adhesion measured using (left) load cell and (right) centrifuge. Arrows indicate the direction of the being being measured.

Shear force is typically used because it is associated with forces experience by ice on surfaces outdoors like gravity and wind shear, but has been criticized because of the

potential for unequal stress distribution in the ice, as the force is concentrated on whichever side of the column is in contact with the load cell.^{16, 18} Tensile strength on the other hand provides equal distribution of the stress but shows weaker correlation to deicing performance. Using a centrifuge to measure ice adhesion strength removes many of these concerns, because stress is distributed evenly across the ice-substrate interface, and the direction of force applied is in that of shear. The centripetal force experienced by the ice up to the time of detachment can be calculated in the maximum rotational speed of the arm is known by using the relation:

$$F_c = mr\left(\frac{2\pi}{T}\right)^2$$

Equation 1.4: Centripetal force equation for determining force of ice adhesion.

Where m is the mass of ice, r is the radius of the centrifuge arm rotation, and T is the period of rotation. Makkonen provides a good overview of methods for measuring ice adhesion, drawbacks of these methods, and how to minimize experimental error in measurements.¹⁸ There are a number of challenges associated with measuring ice adhesion. Reproducibly measuring ice adhesion is challenging because of small differences in surface characteristics which may cause greater changes in adhesion of the ice through the generation of stress within the ice itself. Ice should be frozen slowly to avoid this, but there will always be some variability. Relative standard deviation associated with these measurements is often ~15%. All of the factors influencing ice adhesion discussed in the preceding sections might reasonably cause variance in adhesion strength as well, causing these high relative standard deviations. Adhesion measured using different methods (e.g. one reference using centrifuge vs another using a load cell) cannot be directly compared because of differences in force distribution. These differences in stress distribution can lead to peak forces 5 to 10 times greater than the normal values of adhesion measured on a material, also contributing to variation in ice adhesion values.⁶⁸⁻⁷⁰ Furthermore, while centrifuge methods and load cell methods are the most common, there is no standardized testing method, which means that comparing results from different literary sources is unreliable.⁷¹ Other methods like using pistons or compressed gas to measure ice adhesion have been used.¹⁸ There remains strong support for developing materials with low ice adhesion in spite of these limitations. It has been shown that materials tested using the same

method can be rated in performance, and these ratings correlates strongly to behaviour under environmental conditions. This allows for systematic improvements to be made to passively deicing materials. In addition, low ice adhesion materials such as polymer coatings offer high durability compared with textured materials (e.g. durability measured by sand / water erosion, tape adhesion testing, pencil hardness, and abrasion). Lastly there is a philosophical argument that captures why passive deicing is a more appropriate means of reducing ice buildup. Consider the adage “prepare for the worst, and hope for the best,” where the worst-case scenario is ice forming on a surface. The primary goal of this research should be in weakening ice adhesion, because ice will form eventually and unfailingly on *any* surface, particularly in harsh winter conditions.^{20, 26} While discouraging surface wetting is important and should be considered at least of secondary importance, only by reducing ice adhesion can one reliably ensure ice will not continue to accumulate on a surface under environmental conditions.

1.6 Icephobic Materials

Icephobicity has been defined differently depending on the situation in which icing is being prevented. The review by Sojoudi *et al.* outlines various definitions of icephobicity, mostly relating to anti-icing methods and textured materials.⁷² One definition suggests that surfaces which repel incoming water droplets below freezing or prevent freezing of static droplets on the surfaces.^{65, 73} Icephobicity in a different context refers to prevention of frost formation, or resistance to the Cassie-to-Wenzel transition. Reducing ice adhesion strength has shown to be a highly practical method of preventing large amounts of ice from growing on structural surfaces. Ice adhesion strength can be measured directly, and so materials can be classified based upon these measured values. Materials are classified as icephobic if ice adheres with a strength less than 100 kPa.^{16, 20, 73} This is approximately one-tenth the adhesion strength exhibited by structural materials like metals, glass, wood, and concrete, which often exceeds 1000 kPa.^{18, 26} A decrease in ice adhesion strength of this magnitude indicates that removal from the surface becomes much easier, but in pursuit of passive deicing, ice adhesion must be lowered to an even greater extent. Dou *et al* showed in wind tunnel studies that ice adhesion strength around 20 kPa allowed for deicing to occur because of wind or vibration, and this is widely accepted as the

threshold for passive anti-icing surfaces.⁷⁴ Both thresholds have been reached by manipulating the physicochemical properties of various materials. Kreder and coworkers published an excellent review of state-of-the-art anti-icing/deicing materials in 2016.²⁶ An effort has been made to here expand upon this review by looking backward at historical accounts of anti-icing testing, as well as research done in 2016 and later, which will have an enormous impact on the field moving forward, with a focus on passive deicing. Kreder and coworkers' system of classification is useful for breaking up the breadth of work. materials may be described as smooth, textured, or lubricated. Textured surfaces are primarily comprised of dewetting/anti-icing SHS, which for the reasons outlined above will not be further discussed. These types of textured surfaces are covered in depth by Sojoudi *et al.*²⁰

Smooth icephobic materials refer to those with no intended micro-/nanostructure, relying on surface chemistry and rheology to shed ice, eliminating much of the concern of mechanical adhesion that might be observed on textured surfaces. Smooth materials are perhaps the longest studied for their potential as passive anti-icing coatings, with research having started in the early 1900s, shortly after the advent of synthetic polymers.^{1, 26} Self-assembled monolayers have been explored, but the materials here described are all polymeric coatings.^{56, 74-77} Polymer coatings were selected because of their considerably lower surface energies than metals and glass, which greatly reduces hydrogen bonding and thus ice adhesion strength. It is not unreasonable to say that scientists applying polymer

coatings have “tried everything”; virtually all industrially relevant polymer has been trialed as an icephobic coating (**Figure 1.11**).

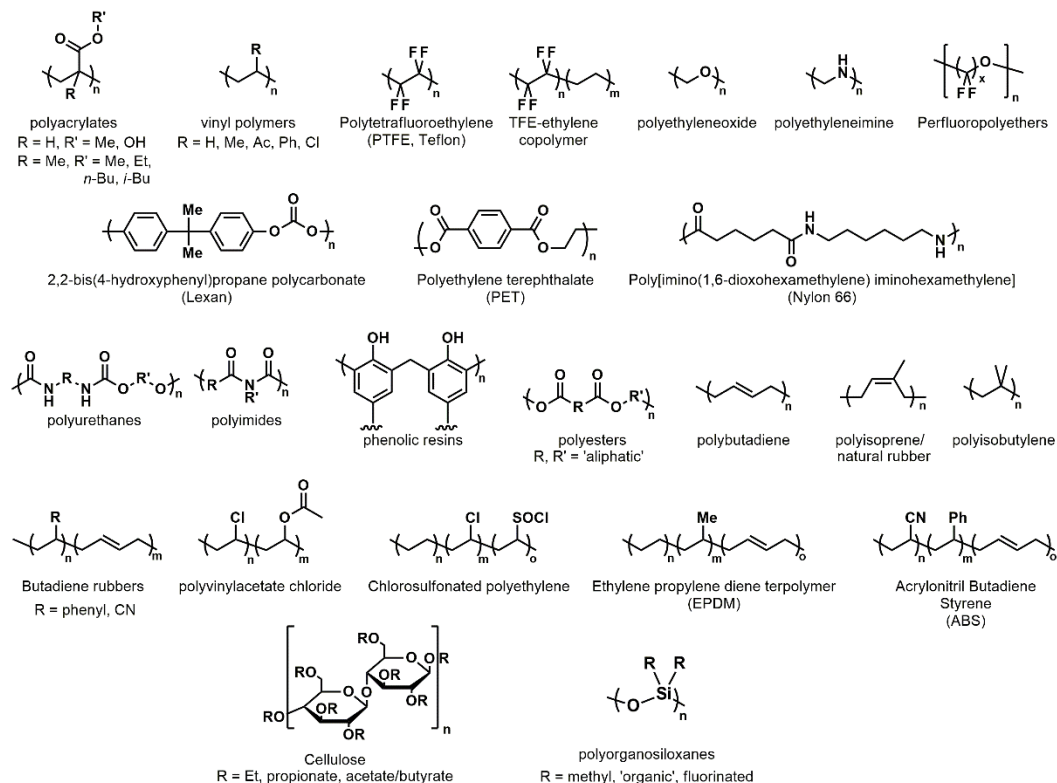


Figure 1.11: Chemical structures of polymers used in anti-icing / deicing research.

Nearly all the polymers presented in **Figure 1.11** reduce ice adhesion to a given substrate significantly. However, only a select few can be considered icephobic, and the instances in which they were observed to be icephobic required them to be modified through plasticization or lubrication. Fluorinated acrylates, polyvinyl chloride, polytetrafluoroethylene (PTFE) and copolymers, perfluoropolyethers, aliphatic polyurethane elastomers, polyisobutylene, and polyorganosiloxanes (usually polydimethylsiloxane) have shown ice adhesion ~100 kPa, but the other candidates fall in the range between of >100 kPa to 1000 kPa. These values were extracted primarily from the works of Andersson, He, and Golovin.^{16, 68, 78} Measurements of ice adhesion on polymers has shown overwhelmingly that elastomers tend to have lower ice adhesion than thermoplastics, owing to their viscoelasticity allowing for interfacial cavitation or slippage,^{16, 26} and initiation of cracks in the ice.^{12, 79-80} This ‘flexible substrate idea’ was

proposed by Sewell in the 1970s and has continued to be an important concept in icephobic materials today.⁸¹ Most of these polymers are attractive potential solutions because of their low ice adhesion and the scale on which they are produced makes them inexpensive. The two polymer types which have regularly performed better than all others (without modification) are fluorinated organic polymers, and polyorganosiloxanes. These each have drawbacks. Fluorinated organic molecules are a well-known environmental hazard and are more expensive to produce than non-fluorinated analogues.⁸² They also share a problem of low durability with polysiloxanes. Both materials perform poorly in abrasion and erosion testing, meaning that for applications where vigorous wear might occur (e.g. wind turbines, aircraft) they are not suitable.^{1, 16} Composite materials have been explored to improve the hardness and wear characteristics of these polymers.^{68, 79} Inorganic fillers like carbon black and silica have been used, and typically lead to improved abrasion resistance of the coatings.⁸³⁻⁸⁴ Unfortunately, most inorganic fillers have higher surface energy than polymers, and therefore increase the strength with which ice adheres. Copolymerization or blending of polymers may also be an interesting routes to more durable materials, as beneficial properties of multiple polymers may be combined this way. Block copolymers have been explored, with early work by Jellinek showing that copolymer coatings of polydimethylsiloxane and polycarbonate allow for ice release.¹⁷ More work has been done with copolymers, but largely the materials are fluorinated, and ice adhesion has not been directly measured.⁸⁵ Polymer coatings have been modified to improve the anti-icing characteristics through the introduction of lubricants that allow for beneficial interfacial effects to occur.

Lubricants such as greases, oils, chemicals, and paints have been tested as ‘semi-permanent’ deicing solutions for the full lifetime of ice repellency research.¹ Some have proven effective enough to stand the test of time, such as the use of glycol mixtures to deice airplanes before takeoff. This is a niche application, as the requirement of the airplane to remain ice free while in flight is mostly taken care of by the high speed of the craft, wind shear, and vibration experienced in flight. Some elements of the craft are also heated electrically or by the engine / exhaust, such as the propeller. Most other applications have sought something much more durable, and so temporary solutions like sprays and greases have largely been avoided. There are also concerns with groundwater contamination when

impermanant means of ice prevention (i.e. deicing fluids) are used. Recently lubricants were introduced into interfacial materials to mimic interesting surfaces found in nature.⁸⁶ These bio-inspired surfaces were shown to have extraordinary dewetting and self-cleaning characteristics, which can be seen as a broader extension of passive deicing. Recent materials in this vein are called slippery lubricant-infused porous surfaces (SLIPS) and consist of porous substrates ‘filled’ with a lubricating fluid (**Figure 1.12**).

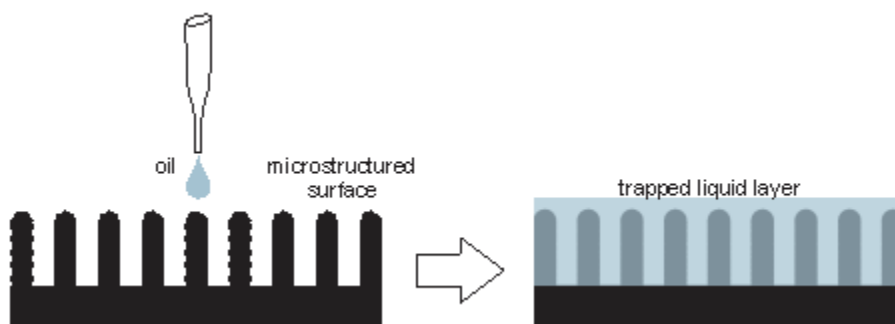


Figure 1.12: Fabrication of a generic slippery lubricant-infused porous surface, showing the formation of a trapped fluid layer deeper than the microstructure.

A variety of porous media including have been chemically modified and infused with lubricants to prepare these materials, such as nanofibres,⁸⁶ anodized aluminum,⁸⁷⁻⁸⁸ silica,⁸⁹ fabrics,⁹⁰ and patterned surfaces.⁹¹ A lubricating fluid, such as a fluorinated organic compound, organic oil or silicone oil, ‘overfills’ the pores of the substrate, creating a smooth liquid layer at the interface. This liquid layer is interesting for anti-icing applications because of its low surface energy, smoothness, and fluidity. Low surface energy decreases hydrogen bonding interactions with the surface, smoothness prevents anchoring to the surface, and fluidity allows interfacial cavitation to further decrease ice adhesion, and masking of the substructure can prevent ice anchoring seen in SHSs. Most importantly, SLIPS have demonstrated ice adhesion below 10 kPa, making them promising passive anti-icing materials.⁹² Some significant drawbacks have been observed, however. Lubricating layers in SLIPS are not mechanically stable, and can be easily removed through abrasion, or by leeching action of water on the surface.⁹³ In the case of icing, some examples of SLIPS can lose their lubricant and icephobicity properties after only one icing event. Oftentimes the lubricants used are fluorinated organic molecules, which cause harm

when they enter the environment.⁸² Scalability is also a concern with respect to some methods of creating porous substrates. Many porous coatings are not applicable on a large scale, depending on the method used to create surface architecture, so except for smaller scale applications such as in heat exchanging appliances, SLIPS are tricky to employ.⁹⁴ Lubricants and/or plasticizers incorporated into polymers might be better suited than lubricated porous materials. Different gel-type materials applied to deicing research, with varying degrees of exploration.^{86, 17, 95-97} The less explored are hydrated icephobic materials that utilize water as a lubricant. These materials are interesting because they offer low ice adhesion ~ 50 kPa, and do not have the same concerns of lubricant loss as SLIPS because there is virtually no concern with water entering the environment, and if the lubricant is depleted it may even be replaced by water from the atmosphere.⁹⁸⁻⁹⁹ From a classical standpoint it is not obvious why hydrophilic materials, or those containing water should be interesting as icephobic materials. Polyelectrolyte brushes were shown to inhibit ice attachment on the surface through an ion-exchange mechanism with the first few layers of the brush, which disrupts the formation of ice crystals.⁹⁹ A second example showed water that hydrates a gel experiences a significant depression in its freezing point to below -20 °C, remaining fluid well below temperatures where ice forms on the surfaces and preventing strong attachment of ice. More work in the field would certainly be interesting, particularly if highly durable systems could be created. Organogels are more extensively researched, and many examples of polymers lubricated with organic or silicone oils exist in the literature.

Golovin and coworkers have published exceptional works in the last few years that outline methods of utilizing lubricated and plasticized polymer coatings as icephobic materials, in cases achieving ice adhesion below 1 kPa.^{16, 100-101} Their 2016 work showcased a large library of different polymers lubricated with synthetic and natural oils, drawing connections between the cross-link density of their gels and ice adhesion. Ice adhesion strength was shown to decrease with cross-link density regardless of the polymer identity. Lubrication was shown to alter the ice delamination mechanism from ‘ordinary’ detachment to detachment involving interfacial slippage (**Figure 1.13**).

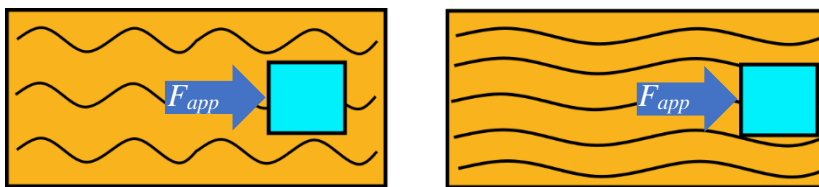


Figure 1.13: Extension and concomitant contraction of viscoelastic polymer chains in response to stress on the ice/polymer interface (F_{app}). This contraction causes cleavage where the media meet due to interfacial slippage.

The mobility of un-crosslinked polymer chains (i.e. the lubricant chains) at the surface allows for extension/contraction in response to an applied force, leading to slippage between the ice and polymer coatings, and therefore ultralow ice adhesion. However, it was shown that the surfaces were ‘dry’, and there was no lubricant at the interface. Even after several abrasion cycles, the materials exhibited ultra-low ice adhesion. The term used in the paper is “inherent icephobicity”: the ice adhesion is a property of the gels, and not of simply the lubricant, or a surface substructure. Therefore, not only do they have exceptionally low ice adhesion, but they are perhaps the most durable yet developed.

1.7 Remaining Challenges and Scope of Thesis

Despite large strides having been made in developing icephobic materials, some challenges remain in the field. This dissertation explores methods of improving the durability of a variety of icephobic materials through different means. Chapter 2 focuses on slippery lubricant-infused porous surfaces (SLIPS). Using a method of repeated ice growth and removal, we demonstrated that the incorporation of UV cross-linked materials at the interface of these materials improves their durability. Ice adhesion below 100 kPa was maintained for more than 10 deicing cycles on modified SLIPS, with minimum ice adhesion below 20 kPa.¹⁰² Chapter 3 focuses on a potential route to durable patterned icephobic surfaces, obtained by laser ablation patterning of UV-cured polymer networks. Smooth, self-supporting polymer networks were prepared and characterized at Western, and subsequently underwent laser ablation at McGill University. Analysis of the lasing parameters and fabricated surface structures gave insight into the effects of different comonomers in creating new surfaces, which may have potential as icephobic surfaces.¹⁰³

Chapter 4 focuses on the synthesis and testing icephobic PDMS-based copolymer networks. Copolymerization may be an interesting route to more durable materials, as the properties of polymers can be altered this way. Three additives, methyl methacrylate, lauryl methacrylate, and styrene were added in varying amounts to a commercially available PDMS resin in order to observe their effects on cross-link density, ice adhesion, and durability through successive deicing cycles. Interestingly, increasing additive in the networks greatly improved the durability of the materials, in some cases with little effect on the strength of ice adhesion. Some coatings showed ice adhesion ~50 kPa consistently up to 50 deicing cycles. Chapter 5 focuses on the preparation and testing of periodically-detached arrays on commercial adhesive films. In past investigations, we noted that areas of film detached from their aluminum substrate exhibited noticeably lower ice adhesion compared to fully-adhered areas of the same film. A series of significantly different commercial adhesive tapes were imparted with arrays of detachments, giving rise to extraordinarily low ice adhesion values, decreasing ice adhesion values by approximately 50%. Different methods of testing durability were attempted, highlighting the effects of detachment and detachment size on film durability. Lastly, Chapter 6 includes conclusive remarks about the presented works, and a collection of recommendations for future project directions.

1.8 References Cited

1. Sayward, J. M. *Seeking Low Ice Adhesion*; CRREL: Hanover, New Hampshire, USA, 1979; p 87.
2. Frankenstein, S.; Tuthill, A. M., Ice Adhesion to Locks and Dams: Past Work; Future Directions? *J. Cold Regions Eng.* **2002**, *16*, 83.
3. Arnhym, A. A., De-Icing and Anti-Icing Progress. *Aero Digest* 1944.
4. Constant, C. City will remove snow, ice left by last week's storm starting tonight. <https://www.cbc.ca/news/canada/montreal/montreal-snow-removal-1.4507396> (accessed August 14).
5. Mackey, M. Here's what it costs to keep Toronto safe in the winter. <https://www.theweathernetwork.com/news/articles/toronto-snow-removal-winter-safety-salt-roads-winter-driving-conditions-city-snow-removal-budget/117026> (accessed August 14).

6. Porter, K. Ottawa blows through snow budget for 7th straight year. (accessed August 14th).
7. Hopper, T., The awesome price we pay for road de-icing: Melting cars, collapsing bridges, billions in damage. *National Post* 2017.
8. Alcoba, N., Toronto ice storm cost expected to soar to \$106-million, as extreme weather costs city \$171-million in 2013. *National Post* January 8 2014, 2014.
9. Marilla Steuter-Martin, L. P., Looking back on the 1998 ice storm 20 years later. In *Photos*, CBC News: 2018.
10. Landrock, A., *Adhesives Technology Handbook*. 2nd ed.; William Andrew: Norwich, NY, USA, 2008; p 363.
11. D.D. Eley, D. T., Fundamentals of Adhesive Joints. In *Adhesion*, Eley, D. D., Ed. Oxford University Press: Oxford, 1961; pp 1.
12. Andersson, L.-O.; Golander, C.-G.; Persson, S., Ice adhesion to rubber materials. *J. Adhes. Sci. Technol.* **1994**, 8, 117.
13. Mattox, D. M., Chapter 1 - Introduction. In *Handbook of Physical Vapor Deposition (PVD) Processing (Second Edition)*, Mattox, D. M., Ed. William Andrew Publishing: Boston, 2010; pp 1.
14. German, R. M., 1 - Thermodynamics of sintering. In *Sintering of Advanced Materials*, Fang, Z. Z., Ed. Woodhead Publishing: 2010; pp 3.
15. Mattox, D. M., Chapter 2 - Substrate ("Real") Surfaces and Surface Modification. In *Handbook of Physical Vapor Deposition (PVD) Processing (Second Edition)*, Mattox, D. M., Ed. William Andrew Publishing: Boston, 2010; pp 25.
16. Golovin, K.; Kobaku, S. P. R.; Lee, D. H.; DiLoreto, E. T.; Mabry, J. M.; Tuteja, A., Designing durable icephobic surfaces. *Sci. Adv.* **2016**, 2.
17. Jellinek, H. H. G.; Kachi, H.; Kittaka, S.; Lee, M.; Yokota, R., Ice releasing block-copolymer coatings. *Colloid. Polym. Sci.* **1978**, 256, 544.
18. Makkonen, L., Ice Adhesion —Theory, Measurements and Countermeasures. *J. Adhes. Sci. Technol.* **2012**, 26, 413.
19. Sun, X.; Damle, V. G.; Liu, S.; Rykaczewski, K., Bioinspired Stimuli-Responsive and Antifreeze-Secreting Anti-Icing Coatings. *Adv. Mater. Interfaces* **2015**, 2, 1400479.
20. Sojoudi, H.; Wang, M.; Boscher, N. D.; McKinley, G. H.; Gleason, K. K., Durable and scalable icephobic surfaces: similarities and distinctions from superhydrophobic surfaces. *Soft Matter* **2016**, 12, 1938.

21. Chaudhury, M. K.; Kim, K. H., Shear-induced adhesive failure of a rigid slab in contact with a thin confined film. *Eur. Phys. J. E* **2007**, *23*, 175.
22. Kendall, K., The adhesion and surface energy of elastic solids. *J. Phys. D: Appl. Phys.* **1971**, *4*, 1186.
23. Newby, B.-m. Z.; Chaudhury, M. K.; Brown, H. R., Macroscopic Evidence of the Effect of Interfacial Slippage on Adhesion. *Science* **1995**, *269*, 1407.
24. Ghatak, A.; Vorvolakos, K.; She, H.; Malotky, D. L.; Chaudhury, M. K., Interfacial Rate Processes in Adhesion and Friction. *J. Phys. Chem. B* **2000**, *104*, 4018.
25. Migler, K. B.; Hervet, H.; Leger, L., Slip transition of a polymer melt under shear stress. *Phys. Rev. Lett.* **1993**, *70*, 287.
26. Kreder, M. J.; Alvarenga, J.; Kim, P.; Aizenberg, J., Design of anti-icing surfaces: smooth, textured or slippery? *Nat. Rev. Mater.* **2016**, *1*, 15003.
27. Laforte, J. L.; Allaire, M. A.; Laflamme, J., State-of-the-art on power line de-icing. *Atmos. Res.* **1998**, *46*, 143.
28. R. W. Gent, N. P. D., J. T. Cansdale, Aircraft Icing. *Philos. Trans. Royal Soc.* **2000**.
29. Jin, S.; Liu, J.; Lv, J.; Wu, S.; Wang, J., Interfacial Materials for Anti-Icing: Beyond Superhydrophobic Surfaces. *Chemistry – An Asian Journal* **2018**, *13*, 1406.
30. Adam, N. K., *The physics and chemistry of surfaces*. 3rd ed.; Oxford University Press: London, 1941.
31. Cassie, A. B. D.; Baxter, S., Wettability of porous surfaces. *J. Chem. Soc. FaradayTrans.* **1944**, *40*, 546.
32. Wang, G.; Shen, Y.; Tao, J.; Luo, X.; Zhang, L.; Xia, Y., Fabrication of a superhydrophobic surface with a hierarchical nanoflake–micropit structure and its anti-icing properties. *RSC Advances* **2017**, *7*, 9981.
33. Kietzig, A.-M.; Hatzikiriakos, S. G.; Englezos, P., Patterned Superhydrophobic Metallic Surfaces. *Langmuir* **2009**, *25*, 4821.
34. D'Acunzi, M.; Mammen, L.; Singh, M.; Deng, X.; Roth, M.; Auernhammer, G. K.; Butt, H.-J.; Vollmer, D., Superhydrophobic surfaces by hybrid raspberry-like particles. *Faraday Discuss.* **2010**, *146*, 35.
35. Chanda, J.; Ionov, L.; Kirillova, A.; Synytska, A., New insight into icing and de-icing properties of hydrophobic and hydrophilic structured surfaces based on core–shell particles. *Soft Matter* **2015**, *11*, 9126.

36. Wang, Y.; Li, M.; Lv, T.; Wang, Q.; Chen, Q.; Ding, J., Influence of different chemical modifications on the icephobic properties of superhydrophobic surfaces in a condensate environment. *J. Mater. Chem. A* **2015**, *3*, 4967.
37. He, M.; Zhou, X.; Zeng, X.; Cui, D.; Zhang, Q.; Chen, J.; Li, H.; Wang, J.; Cao, Z.; Song, Y.; Jiang, L., Hierarchically structured porous aluminum surfaces for high-efficient removal of condensed water. *Soft Matter* **2012**, *8*, 6680.
38. Gao, L.; McCarthy, T. J., Contact Angle Hysteresis Explained. *Langmuir* **2006**, *22*, 6234.
39. Boreyko, J. B.; Chen, C.-H., Self-Propelled Dropwise Condensate on Superhydrophobic Surfaces. *Phys. Rev. Lett.* **2009**, *103*, 184501.
40. Patil, N. D.; Bhardwaj, R.; Sharma, A., Droplet impact dynamics on micropillared hydrophobic surfaces. *Exp. Therm Fluid Sci.* **2016**, *74*, 195.
41. Khojasteh, D.; Kazerooni, M.; Salarian, S.; Kamali, R., Droplet impact on superhydrophobic surfaces: A review of recent developments. *J. Ind. Eng. Chem.* **2016**, *42*, 1.
42. Meuler, A. J.; McKinley, G. H.; Cohen, R. E., Exploiting Topographical Texture To Impart Icephobicity. *ACS Nano* **2010**, *4*, 7048.
43. Kulinich, S. A.; Farhadi, S.; Nose, K.; Du, X. W., Superhydrophobic Surfaces: Are They Really Ice-Repellent? *Langmuir* **2011**, *27*, 25.
44. Boinovich, L. B.; Emelyanenko, A. M.; Ivanov, V. K.; Pashinin, A. S., Durable Icephobic Coating for Stainless Steel. *ACS Appl. Mater. Interfaces* **2013**, *5*, 2549.
45. Foroughi Mobarakeh, L.; Jafari, R.; Farzaneh, M., The ice repellency of plasma polymerized hexamethyldisiloxane coating. *Appl. Surf. Sci.* **2013**, *284*, 459.
46. Li, W.; Zhang, X.; Yang, J.; Miao, F., In situ growth of superhydrophobic and icephobic films with micro/nanoscale hierarchical structures on the aluminum substrate. *J. Colloid Interface Sci.* **2013**, *410*, 165.
47. Alizadeh, A.; Yamada, M.; Li, R.; Shang, W.; Otta, S.; Zhong, S.; Ge, L.; Dhinojwala, A.; Conway, K. R.; Bahadur, V.; Vinciguerra, A. J.; Stephens, B.; Blohm, M. L., Dynamics of Ice Nucleation on Water Repellent Surfaces. *Langmuir* **2012**, *28*, 3180.
48. Alizadeh, A.; Bahadur, V.; Kulkarni, A.; Yamada, M.; Ruud, J. A., Hydrophobic surfaces for control and enhancement of water phase transitions. *MRS Bull.* **2013**, *38*, 407.

49. Chen, J.; Liu, J.; He, M.; Li, K.; Cui, D.; Zhang, Q.; Zeng, X.; Zhang, Y.; Wang, J.; Song, Y., Superhydrophobic surfaces cannot reduce ice adhesion. *Appl. Phys. Lett.* **2012**, *101*, 111603.
50. Jung, S.; Dorrestijn, M.; Raps, D.; Das, A.; Megaridis, C. M.; Poulikakos, D., Are Superhydrophobic Surfaces Best for Icephobicity? *Langmuir* **2011**, *27*, 3059.
51. Jung, S.; Tiwari, M. K.; Doan, N. V.; Poulikakos, D., Mechanism of supercooled droplet freezing on surfaces. *Nat. Commun.* **2012**, *3*, 615.
52. Varanasi, K. K.; Deng, T.; Smith, J. D.; Hsu, M.; Bhate, N., Frost formation and ice adhesion on superhydrophobic surfaces. *Appl. Phys. Lett.* **2010**, *97*, 234102.
53. Kulinich, S. A.; Farzaneh, M., On ice-releasing properties of rough hydrophobic coatings. *Cold Reg. Sci. Technol.* **2011**, *65*, 60.
54. Maitra, T.; Antonini, C.; Tiwari, M. K.; Mularczyk, A.; Imeri, Z.; Schoch, P.; Poulikakos, D., Supercooled Water Drops Impacting Superhydrophobic Textures. *Langmuir* **2014**, *30*, 10855.
55. Wang, Y.; Xue, J.; Wang, Q.; Chen, Q.; Ding, J., Verification of Icephobic/Anti-icing Properties of a Superhydrophobic Surface. *ACS Appl. Mater. Interfaces* **2013**, *5*, 3370.
56. Farhadi, S.; Farzaneh, M.; Kulinich, S. A., Anti-icing performance of superhydrophobic surfaces. *Appl. Surf. Sci.* **2011**, *257*, 6264.
57. Meuler, A. J.; Smith, J. D.; Varanasi, K. K.; Mabry, J. M.; McKinley, G. H.; Cohen, R. E., Relationships between Water Wettability and Ice Adhesion. *ACS Appl. Mater. Interfaces* **2010**, *2*, 3100.
58. Fitzner, M.; Soso, G. C.; Cox, S. J.; Michaelides, A., The Many Faces of Heterogeneous Ice Nucleation: Interplay Between Surface Morphology and Hydrophobicity. *J. Am. Chem. Soc.* **2015**, *137*, 13658.
59. Karthika, S.; Radhakrishnan, T. K.; Kalaichelvi, P., A Review of Classical and Nonclassical Nucleation Theories. *Cryst. Growth Des.* **2016**, *16*, 6663.
60. Turnbull, D.; Vonnegut, B., Nucleation Catalysis. *J. Ind. Eng. Chem.* **1952**, *44*, 1292.
61. Tourkine, P.; Le Merrer, M.; Quéré, D., Delayed Freezing on Water Repellent Materials. *Langmuir* **2009**, *25*, 7214.
62. Schutzius, T. M.; Jung, S.; Maitra, T.; Eberle, P.; Antonini, C.; Stamatopoulos, C.; Poulikakos, D., Physics of Icing and Rational Design of Surfaces with Extraordinary Icephobicity. *Langmuir* **2015**, *31*, 4807.

63. Boinovich, L. B.; Emelyanenko, A. M.; Emelyanenko, K. A.; Maslakov, K. I., Anti-icing properties of a superhydrophobic surface in a salt environment: an unexpected increase in freezing delay times for weak brine droplets. *PCCP* **2016**, *18*, 3131.
64. Eberle, P.; Tiwari, M. K.; Maitra, T.; Poulikakos, D., Rational nanostructuring of surfaces for extraordinary icephobicity. *Nanoscale* **2014**, *6*, 4874.
65. Jung, S.; Tiwari, M. K.; Poulikakos, D., Frost halos from supercooled water droplets. *PNAS* **2012**, *109*, 16073.
66. Jin, Y.; He, Z.; Guo, Q.; Wang, J., Control of Ice Propagation by Using Polyelectrolyte Multilayer Coatings. *Angew. Chem. Int. Ed.* **2017**, *56*, 11436.
67. Heydari, G.; Thormann, E.; Järn, M.; Tyrode, E.; Claesson, P. M., Hydrophobic Surfaces: Topography Effects on Wetting by Supercooled Water and Freezing Delay. *J. Phys. Chem. C* **2013**, *117*, 21752.
68. Andersson, L.-O. Ice Accretion and Ice Adhesion to Polymer Materials. Luleå University of Technology, Luleå, Sweden, 1993.
69. Frederking, R. K., *J. Laboratory Tests on Ice Sheet Adhesion Strength on Piles of Different Materials*; Technical Research Centre of Finland: Espoo, Finland, 1981.
70. Oksanen, P. *Adhesion strength of ice*; VTT Technical Research Centre of Finland: Espoo, Finland, 1982.
71. LANDY, M.; FREIBERGER, A., AN APPROACH TO THE SHIPBOARD ICING PROBLEM. *Nav. Eng. J.* **1968**, *80*, 63.
72. Sojoudi, H.; Arabnejad, H.; Raiyan, A.; Shirazi, S. A.; McKinley, G. H.; Gleason, K. K., Scalable and durable polymeric icephobic and hydrate-phobic coatings. *Soft Matter* **2018**, *14*, 3443.
73. Hejazi, V.; Sobolev, K.; Nosonovsky, M., From superhydrophobicity to icephobicity: forces and interaction analysis. *Sci. Rep.* **2013**, *3*, 2194.
74. Dou, R.; Chen, J.; Zhang, Y.; Wang, X.; Cui, D.; Song, Y.; Jiang, L.; Wang, J., Anti-icing Coating with an Aqueous Lubricating Layer. *ACS Appl. Mater. Interfaces* **2014**, *6*, 6998.
75. Zhang, Q.; He, M.; Zeng, X.; Li, K.; Cui, D.; Chen, J.; Wang, J.; Song, Y.; Jiang, L., Condensation mode determines the freezing of condensed water on solid surfaces. *Soft Matter* **2012**, *8*, 8285.
76. Kulinich, S. A.; Honda, M.; Zhu, A. L.; Rozhin, A. G.; Du, X. W., The icephobic performance of alkyl-grafted aluminum surfaces. *Soft Matter* **2015**, *11*, 856.

77. Kulinich, S. A.; Farzaneh, M., Alkylsilane self-assembled monolayers: modeling their wetting characteristics. *Appl. Surf. Sci.* **2004**, *230*, 232.
78. He, Z.; Vågnes, E. T.; Delabahan, C.; He, J.; Zhang, Z., Room Temperature Characteristics of Polymer-Based Low Ice Adhesion Surfaces. *Sci. Rep.* **2017**, *7*, 42181.
79. Zhang, K.; Li, X.; Zhao, Y.; Zhu, K.; Li, Y.; Tao, C.; Yuan, X., UV-curable POSS-fluorinated methacrylate diblock copolymers for icephobic coatings. *Prog. Org. Coat.* **2016**, *93*, 87.
80. Good, R. J., Theory of “Cohesive” vs “Adhesive” Separation in an Adhering System. *J. Adhesion* **1972**, *4*, 133.
81. Sewell, J. H. *The Design and Development of New Ice-Shedding Coatings*; United States Army Aviation Engineering Flight Activity: California, 1974; pp 37.
82. Key, B. D.; Howell, R. D.; Criddle, C. S., Fluorinated Organics in the Biosphere. *Environ. Sci. Technol.* **1997**, *31*, 2445.
83. Rajiv, S.; Kumaran, S.; Sathish, M., Long-term-durable anti-icing superhydrophobic composite coatings. *J. Appl. Polym. Sci.* **2019**, *136*, 47059.
84. Liu, J.; Janjua, Z. A.; Roe, M.; Xu, F.; Turnbull, B.; Choi, K.-S.; Hou, X., Super-Hydrophobic/Icephobic Coatings Based on Silica Nanoparticles Modified by Self-Assembled Monolayers. *Nanomaterials (Basel, Switzerland)* **2016**, *6*, 232.
85. Li, X.; Li, Y.; Ren, L.; Zhu, K.; Zhao, Y.; Yuan, X., Self-crosslinking coatings of fluorinated polysiloxanes with enhanced icephobicity. *Thin Solid Films* **2017**, *639*, 113.
86. Wong, T.-S.; Kang, S. H.; Tang, S. K. Y.; Smythe, E. J.; Hatton, B. D.; Grinthal, A.; Aizenberg, J., Bioinspired self-repairing slippery surfaces with pressure-stable omniphobicity. *Nature* **2011**, *477*, 443.
87. Song, T.; Liu, Q.; Liu, J.; Yang, W.; Chen, R.; Jing, X.; Takahashi, K.; Wang, J., Fabrication of super slippery sheet-layered and porous anodic aluminium oxide surfaces and its anticorrosion property. *Appl. Surf. Sci.* **2015**, *355*, 495.
88. Wang, P.; Zhang, D.; Lu, Z.; Sun, S., Fabrication of Slippery Lubricant-Infused Porous Surface for Inhibition of Microbially Influenced Corrosion. *ACS Appl. Mater. Interfaces* **2016**, *8*, 1120.
89. Huang, Y.; Hu, M.; Yi, S.; Liu, X.; Li, H.; Huang, C.; Luo, Y.; Li, Y., Preparation and characterization of silica/fluorinated acrylate copolymers hybrid films and the investigation of their icephobicity. *Thin Solid Films* **2012**, *520*, 5644.
90. Cicely, S.; Noah, M.; Tak-Sing, W.; Philseok, K.; Joanna, A., Fabrics coated with lubricated nanostructures display robust omniphobicity. *Nanotechnology* **2014**, *25*, 014019.

91. Schellenberger, F.; Xie, J.; Encinas, N.; Hardy, A.; Klapper, M.; Papadopoulos, P.; Butt, H.-J.; Vollmer, D., Direct observation of drops on slippery lubricant-infused surfaces. *Soft Matter* **2015**, *11*, 7617.
92. Zhuo, Y.; Håkonsen, V.; He, Z.; Xiao, S.; He, J.; Zhang, Z., Enhancing the Mechanical Durability of Icephobic Surfaces by Introducing Autonomous Self-Healing Function. *ACS Appl. Mater. Interfaces* **2018**, *10*, 11972.
93. Lv, J.; Song, Y.; Jiang, L.; Wang, J., Bio-Inspired Strategies for Anti-Icing. *ACS Nano* **2014**, *8*, 3152.
94. Wexler, J. S.; Jacobi, I.; Stone, H. A., Shear-Driven Failure of Liquid-Infused Surfaces. *Phys. Rev. Lett.* **2015**, *114*, 168301.
95. Zhu, L.; Xue, J.; Wang, Y.; Chen, Q.; Ding, J.; Wang, Q., Ice-phobic Coatings Based on Silicon-Oil-Infused Polydimethylsiloxane. *ACS Appl. Mater. Interfaces* **2013**, *5*, 4053.
96. Urata, C.; Dunderdale, G. J.; England, M. W.; Hozumi, A., Self-lubricating organogels (SLUGs) with exceptional syneresis-induced anti-sticking properties against viscous emulsions and ices. *J. Mater. Chem. A* **2015**, *3*, 12626.
97. Wang, Y.; Yao, X.; Chen, J.; He, Z.; Liu, J.; Li, Q.; Wang, J.; Jiang, L., Organogel as durable anti-icing coatings. *SCMs* **2015**, *58*, 559.
98. Chen, D.; Gelenter, M. D.; Hong, M.; Cohen, R. E.; McKinley, G. H., Icephobic Surfaces Induced by Interfacial Nonfrozen Water. *ACS Appl. Mater. Interfaces* **2017**, *9*, 4202.
99. Chernyy, S.; Järn, M.; Shimizu, K.; Swerin, A.; Pedersen, S. U.; Daasbjerg, K.; Makkonen, L.; Claesson, P.; Iruthayaraj, J., Superhydrophilic Polyelectrolyte Brush Layers with Imparted Anti-Icing Properties: Effect of Counter ions. *ACS Appl. Mater. Interfaces* **2014**, *6*, 6487.
100. Golovin, K.; Dhyani, A.; Thouless, M. D.; Tuteja, A., Low–interfacial toughness materials for effective large-scale deicing. *Science* **2019**, *364*, 371.
101. Golovin, K.; Tuteja, A., A predictive framework for the design and fabrication of icephobic polymers. *Sci. Adv.* **2017**, *3*.
102. Coady, M. J.; Wood, M.; Wallace, G. Q.; Nielsen, K. E.; Kietzig, A.-M.; Lagugné-Labarthet, F.; Ragogna, P. J., Icephobic Behavior of UV-Cured Polymer Networks Incorporated into Slippery Lubricant-Infused Porous Surfaces: Improving SLIPS Durability. *ACS Appl. Mater. Interfaces* **2018**, *10*, 2890.
103. Wood, M. J.; Coady, M. J.; Aristizabal, F.; Nielsen, K.; Ragogna, P. J.; Kietzig, A.-M., Femtosecond laser micromachining of co-polymeric urethane materials. *Appl. Surf. Sci.* **2019**, *483*, 633.

Chapter 2

2 Icephobic behavior of UV-cured polymer networks incorporated into slippery lubricant-infused porous surfaces: Improving SLIPS durability

2.1 Introduction

Power generation infrastructure such as wind turbines and transmission towers/lines can be damaged by ice accumulation making ice buildup a dangerous and costly problem.¹ Damage is primarily the result of the sheer weight of ice that accumulates on the surface of the installations, or of ice growth in joints and seams of the structures. The danger and economic impact of infrastructural damage caused by wide spread icing are evidenced by the impact of North American ice storms. An ice storm in Atlantic North America caused \$5 billion in damage in Canada alone in 1998, with thousands being left without heat and electricity for months, where ice must be removed from these installations before failure occurs. Contemporary methods of ice abatement are rudimentary. Processes involving the physical removal by scraping, melting, or vibration can undermine the integrity of the structure. These methods also require the input of significant energy, in the form of heat or human-power, which increases operational cost.² Surfaces that can prevent or shed accumulating ice without energy input are actively being investigated to mitigate damage and expense caused by icing. Materials with this capability are called ‘passive’ anti-icing agents (icephobic).³

Icephobic materials development is undergoing a rapid expansion.⁴ Classification of a material as icephobic requires ice adhesion forces be ≤ 20 kPa in order to effectively shed ice.⁵ Only a few materials have achieved this threshold. Lubricant-infused polymers⁶⁻⁷ and slippery lubricant-infused porous surfaces (SLIPS⁸⁻¹⁰) are the most noteworthy. These materials have demonstrated persistently low ice adhesion values that reach far below 20kPa, and are presently viewed as the state-of-the-art.⁴

Slippery lubricant-infused porous surfaces (SLIPS) have been prepared in several ways, all involving a porous substrate and a lubricating fluid.^{8-9, 11-16} SLIPS have been employed as icephobic materials, where they exhibited ice adhesion between 15 and 25 kPa.¹¹⁻¹² A lubricant layer extends beyond the depth of substrate pores, creating an extremely flat surface to which ice will not stick. This is the source of SLIPS' exceptional icephobicity. However, the trapped liquid layer is also its greatest drawback with respect to ice repellency. A deicing event can cause substantial surface damage, and as the liquid layer is leached or abraded from the surface, ice adhesion values quickly increase. Such surface damage may occur after only one icing/deicing cycle.^{4, 17} Stabilizing the surface fluid layer of SLIPS will yield icephobic surfaces with enhanced durability. The problem of durability, and another drawback of SLIPS may be solved through careful selection of materials. An additional drawback with many SLIPS is the reliance on fluorinated lubricants, which are well established as an environmental concern. The effectiveness of the nature-inspired SLIPS technology in anti-icing roles cannot be ignored, but significant headway must be made toward bolstering the durability of these materials. In this context, we have developed an approach that utilizes UV cross-linked, interpenetrated siloxane polymer networks to enhance their durability. **Figure 2.1** illustrates the method used to prepare UV-cured SLIPS.

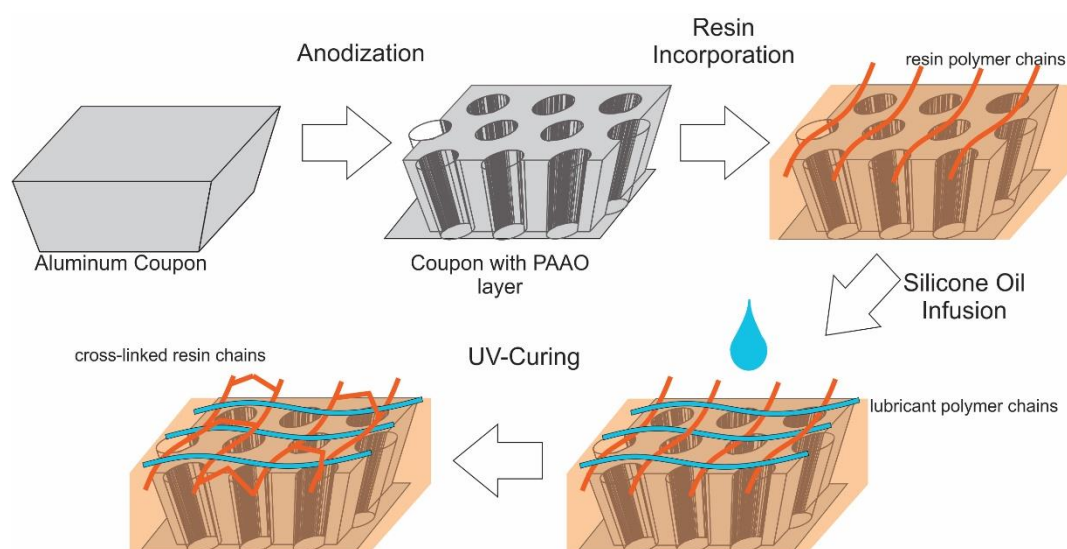


Figure 2.1: Process diagram for the fabrication of UV-cured SLIPS

These surfaces demonstrated promisingly low ice adhesion values (~50kPa) and could withstand successive deicing cycles up to 10 times. UV curable SLIPS formulations that combined cross-linked silicone resins with silicone oil were prepared in order to observe the effects of crosslinking on SLIPS icephobicity and durability. Two different acrylate-functionalized resins were used to probe the impact of degree of acrylate functionality on surface performance and durability. As a benchmark surface, “oil only” SLIPS were prepared by infusing porous anodic aluminum oxide (PAAO) with silicone oil. All SLIPS were subjected to ice adhesion testing using a custom-built centrifuge (‘The Icefuge’). This work has revealed that UV-curable resins effectively improve the durability and icephobicity of SLIPS.

2.2 Experimental

Oxalic acid dihydrate (99.5 %; Allied Chemical) was used as received and dissolved in DI water to obtain a 0.3 M solution. Ebecryl 350, Ebecryl 1360, 2-hydroxy-2-methylpropiophenone (HDMAP) were used as received (Allnex). Hexanes were dried over 4 Å molecular sieves prior to use. 6061 aluminum bar stock was purchased from McMaster Carr and cut in to 2.5 by 5.0 cm coupons. Coupons were polished using a 1000-grit (Presi P1000, silicon carbide) polishing pad on a wheel ($S_a \sim 0.2 \mu\text{m}$). S_a was measured using a KLA Tencor P-7 stylus profiler. Anodization followed a modified procedure similar to Norek *et al.*¹⁸ Anodization was performed in an open 1 L electrochemical cell, using a GW GPR-30H10D Laboratory Power Supply purchased from Test Equipment Depot, with a platinum counter electrode. 0.3 M oxalic acid in DI water was used as the electrolyte, with fresh electrolyte used for each sample. A constant voltage of 40 V was applied to the cell with rapid stirring. The temperature of the cell was raised to 40 °C for the first 20 min of anodization, after which the heating was turned off. Voltage was applied for a total of 45 min. The oxide layer on the anodized coupons was analyzed using a LEO Zeiss 154XB scanning electron microscope (SEM) equipped with a focused ion beam (FIB). Coupons were rinsed with DI water before being dried overnight at 100 °C. PAAO was functionalized using established methods.¹⁵ *n*-decyltrichlorosilane (97 %), and silicone oil (bp >140 °C) were purchased from Sigma-Aldrich and used as received. Each coupon was submerged in a flask containing 50 mL of hexanes with 100 µL of *n*-decyltrichlorosilane.

These flasks were agitated for approximately 12 hrs on a wrist-action shaker. Subsequently, the samples were rinsed with hexanes, and dried at 100 °C for 4 h. Silicone oil was pipetted onto the surface of the functionalized coupons and the assembly was allowed to rest for 12 hrs. Excess oil was drained from the surface, forming SLIPS. Excess oil remaining on SLIPS was removed using a stream of compressed air. In the case of UV-cured SLIPS, coupons were fully submerged in Ebecryl 350 or 1360, mixed with 1 wt% 2-hydroxy-2-methylpropiophenone (photoinitiator). Excess resin was then removed from the surface using compressed air. Oil infusion was carried out on the resin-infused coupons in the same way as on coupons containing no resin. The oil+resin infused coupons were cured. UV-curing was performed using a modified UV-curing system purchased from UV Process and Supply Inc. equipped with a medium pressure mercury vapor lamp ($\lambda = 200\text{-}600\text{ nm}$). The measured intensities of UVA, UVB, and UVC for this source were 165, 150, and 40 mW/cm². These intensities were measured using a Power Puck II (EIT Inc.). Excess silicone oil was removed from the SLIPS after curing. Ice adhesion tests were done at -15 °C in the Cold Weather Biome at Western's Biotron facility. A tubular metal weight with an inner diameter of 6 mm was aligned on the substrate. The weight and the substrate cooled over 10 min. Degassed DI water at 0 °C was injected into the centre cavity of the weight using a syringe. Samples were left to freeze for 25 min before testing. An image of the coupon assemblies is shown in **Appendix A**. The coupon assemblies were tested in the Icefuge, which records the highest speed reached just before deicing occurs. Ice adhesion was calculated using the following $F_c = mr\left(\frac{2\pi}{T}\right)^2$ Equation 1.4.

In cases where ice adhesion was very low, a weight was not used. Corel PHOTO-PAINT X8 (photo editing software) was used to determine the contact area of ice in these instances, by using scale photographs containing a ruler. Atomic force microscopy (AFM) experiments were conducted using a Bioscope Catalyst AFM (Bruker) equipped with $\mu\text{masch NSC15}$ tips (40 N/m, 325 kHz). $5\text{ }\mu\text{m} \times 5\text{ }\mu\text{m}$ areas were measured using silicon tips in non-contact mode. A Hitachi S-3400N SEM at the Biotron was used for SEM/EDX. SLIPS were imaged in variable pressure mode with a backscattering electron detector. An INCA EDAX system was used for EDX. The acceleration voltage was varied between 5 kV and 30 kV, using aperture 1 of the microscope. The probe current was set to 60 V. EDX spectra were collected at 2500x magnification at both acceleration voltages. Spectra for

each sample were normalized relative to each other using the INCA software. Differential scanning calorimetry used a DSC Q20 TA instrument. ~5 mg of polymer was put in an aluminum Tzero pan and cycled between 50 °C and -150 °C three times, at a rate of 5 °C/min. Data were acquired from the third heating cycle. Finally, contact angle measurements were made using a Kruss DSA100 contact angle goniometer. MilliQ water (conductivity = 18.2 megohm-cm) was used with a 0.5 mm bore stainless steel syringe. Advancing and receding contact angle (ARCA) measurements were done using a glass capillary. A 10 μ L droplet was placed on the substrate surface and increased to 30 μ L at a rate of 30 μ L/min to measure advancing contact angle. The same droplet was then removed from the surface at a rate of -30 μ L/min to attain receding contact angle. Video of both events was recorded, and contact angles were calculated using the DSA software.

2.3 Results and Discussion

UV cross-linkable siloxane polymers and silicone oil were selected as potential anti-icing materials because they posed solutions to the two major problems with SLIPS. Firstly, cross-linking of polymers is well-known to improve their resistance to abrasion. Second, siloxanes are more environmentally friendly than fluorinated materials. Siloxanes degrade back to amorphous silica and carbon dioxide in the environment and have not shown toxicity toward soil-dwelling or aquatic organisms. Silicone oil has previously been used as a lubricant in SLIPS. Ebecryl 350 and 1360 were selected as UV-curable resins because they are siloxane resins and are therefore miscible with silicone oil.

Fabrication of SLIPS: SLIPS based upon PAAO have been previously reported, but their efficacy as icephobic surfaces has not been explored.^{14, 16} PAAO surfaces are robust, and straightforward to prepare, therefore a strong candidate for withstanding ice adhesion testing. Our PAAO coupons with reproducible topography were prepared with pore sizes of approximately 60 nm (**Figure 2.2 left**). All anodized coupons were examined using SEM prior to use to ensure that a uniform surface was prepared. The thickness of the porous oxide layer was measured from representative samples and found to be 17 μ m (avg.) in thickness (**Figure 2.2 right**). The roughness of a coupon was measured after anodization using profilometry, giving an S_a value of ~ 0.1 μ m. Successfully anodized coupons were subsequently silylated and infused with silicone oil.

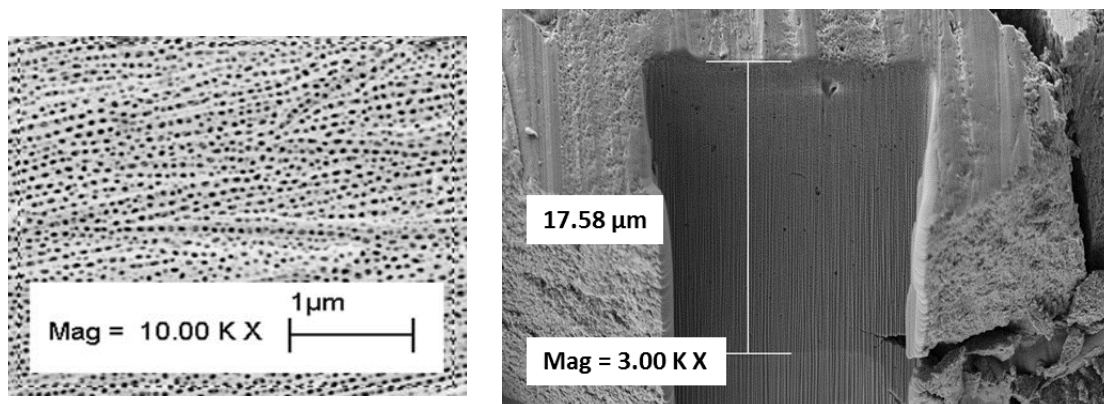


Figure 2.2: (*left*) SEM image of porous structure of anodized coupons. (*right*) FIB-etched cross-section of coupon edge used to measure approximate depth of porous oxide layer. Both images captured at 3.00 kV.

Native PAAO showed strongly hydrophilic character, such that contact angle could not be measured. Silylation increased hydrophobicity, giving contact angles up to 150°. This behaviour signified that the surface hydroxyl groups with the aliphatic silane were capped, while maintaining the porous architecture (a textured surface is required in order to support a droplet with a contact angle >120°). Following oil infusion, contact angles decreased to approximately 100°, indicative of re-establishing a smooth topography and indicative of a captive fluid layer (**Figure 2.3**).

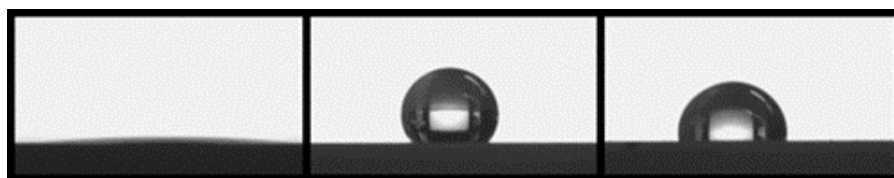


Figure 2.3: Comparison of wetting contact angle PAAO (*left*), silylated PAAO (*mid*) and oil-infused PAAO SLIPS (*right*).

SLIPS Characterization: Atomic force microscopy (AFM) was utilized to assess the presence of a trapped liquid layer in the oil-only SLIPS, and to observe whether the UV-cured SLIPS remain fluid-like after crosslinking. Golovin *et al.* demonstrated that oil-infused polymers exhibit wave-like patterns in AFM height images.⁶ Surfaces that are rigid

will not have these patterns, showing a relatively smooth height image. Oil-only, oil+350, and oil+1360 SLIPS were each tested using tapping-mode AFM, as were cured samples of both Ebecryl 350 and 1360 that contained no oil. Oil-only SLIPS showed wave-like deflections in the height image, supporting the conclusion that a trapped liquid layer was present (**Figure 2.4 left**). Ebecryl 1360 behaved as expected in this experiment showing a smooth height image (**Figure 2.4 mid**). This suggests that Ebecryl 1360 is somewhat rigid when cured. When infused with oil, Ebecryl 1360 gave a wavy image, indicating a lubricant layer was present (**Figure 2.4 right**).

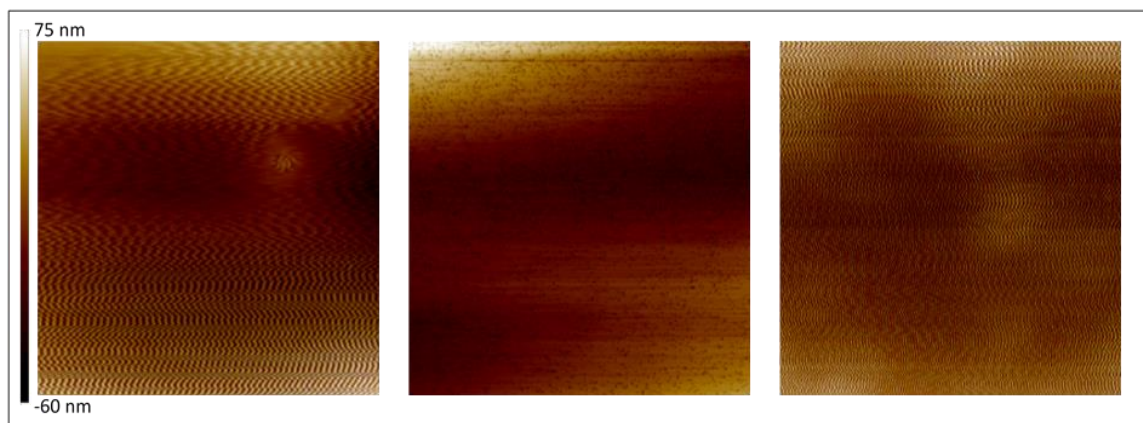


Figure 2.4: AFM height images of 5 μm by 5 μm area of a) oil-only, b) Ebecryl 1360 and c) Ebecryl 1360 plus oil

AFM results for samples that included Ebecryl 350 were not as simple. Coupons infused with Ebecryl 350 with and/or without oil, showed wave-like AFM images (see **Appendix A**). This finding prompted thermal analysis of these cured polymers.

DSC was used to probe the thermal transitions of cured Ebecryl 350 and 1360. A step transition indicating the glass transition temperature (T_g) of Ebecryl 1360 occurred at $-66\text{ }^\circ\text{C}$. A similar T_g was seen for Ebecryl 350 at $-59\text{ }^\circ\text{C}$. A transition at $-32\text{ }^\circ\text{C}$ for Ebecryl 350 was also observed. The signal was a melt transition, indicating that above $-32\text{ }^\circ\text{C}$, Ebecryl 350 is fluid-like. A fluid-like cured resin explains why even without being infused with oil, Ebecryl 350 appeared wavelike using AFM.

Ice adhesion and wettability of UV-cured SLIPS: Silylated PAAO, oil-only SLIPS, cured Ebecryl 350 and 1360, and UV-cured SLIPS made using one of the Ebecryl resins

(oil+350 and oil+1360 SLIPS) were tested repeatedly for ice adhesion strength (**Table 2.1**).

Table 2.1: Ice adhesion and wetting data for SLIPS and selected surfaces

Sample Type	Advancing Contact Angle (°)	Receding Contact Angle (°)	Icing Replicates	Initial Adhesion (kPa)	After Testing (kPa)
Silylated PAAO			4	22 ± 13	359 ± 13
Oil-only SLIPS	100 ± 2	81 ± 5	10	36 ± 5	115 ± 80
Ebecryl 350			3	12 ± 3	96 ± 17
Ebecryl 1360			3	23 ± 1	255 ± 26
Oil+350 SLIPS	77 ± 1	29 ± 3	5	8 ± 0.8	17 ± 3
Oil+1360 SLIPS	84 ± 0.9	50 ± 2	5	7 ± 0.6	22 ± 2

This table also gives values of the advancing and receding contacts angles for the SLIPS surfaces. No trend was observed relating dynamic contact angle to ice adhesion on SLIPS. Silylated aluminum, oil-only SLIPS, and crosslinked resins containing no added oil all showed dramatic increases in ice adhesion strength after only four deicing tests. UV cured SLIPS showed more resilience towards icing/deicing cycles, up to fourteen repeats (**Figure 2.5**).

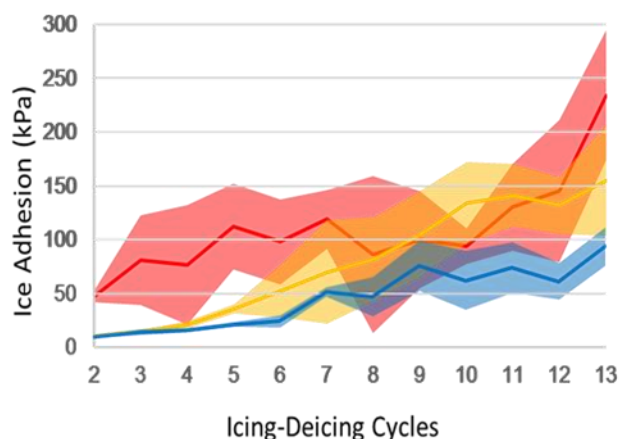


Figure 2.5: Deicing results for oil-only (red), oil+1360 (yellow) and oil+350 (blue) SLIPS samples. Solid lines indicate the mean values measured after n deicing cycles, while the shaded areas correspond to the standard error associated with those measurements.

SLIPS UV-cured resins showed lower initial ice adhesion than the oil-only SLIPS. The reason for lowered adhesion to the cured SLIPS is not obvious. Most likely, removal of

lubricant from the un-cured SLIPS happens upon the introduction of water at the interface, decreasing the efficacy of the lubricating layer during the first round of adhesion tests. UV-cured SLIPS do not lose lubricant, as interpenetration of the polymer networks retains the silicone oil. This causes the initial ice adhesion of the UV-cured SLIPS to be lower than the oil-only counterparts. SLIPS prepared using Ebecryl 350 performed best out of the three types prepared. Ice adhesion values for these types of SLIPS are among the lowest of those tested (min. 10 kPa) and maintained ice adhesion below 50 kPa for 8 deicing cycles. The high-level performance of the oil+350 SLIPS stems from the crosslinked structure of the diacrylated resin. Crosslinking makes these SLIPS more resistant to lubricant loss compared the oil-only SLIPS. Enhanced durability compared to the oil+1360 is also explained as the higher proportion of crosslinking in the hexacrylated resin (Ebecryl 1360) causes the films to become brittle, and easily damaged by ice removal. AFM and DSC support this notion, as from these tests it was concluded that the oil+350 SLIPS are softer than the oil+1360 SLIPS. Similar results were observed by Golovin *et al.*, who found that lightly cross-linked polymer coatings tended toward lower ice adhesion than more highly crosslinked polymers.⁶ Visible damage occurred to oil+1360 coated coupons during testing (**Appendix A**). Results from ice adhesion testing support the hypothesis that SLIPS durability can be improved using UV-crosslinkable resins. The cause of increasing ice adhesion with successive measurements was therefore investigated in further surface characterization experiments using SEM/EDX.

SEM/EDX experiments were conducted to better understand why ice adhesion on the SLIPS surfaces increased with subsequent deicing cycles. Lubricant depletion is accepted as the primary mechanism for decreasing performance in SLIPS, yet we hypothesize that interpenetration of silicone oil within a UV-cured resin prevented oil from being removed. EDX was used to determine the relative amounts of silicon and aluminum in the samples, which indicated how much oil was removed from the surfaces over the course of ice adhesion testing. Spectra obtained using oil-only SLIPS were straightforward in that depletion of oil from the surfaces was evident (**Figure 2.6**).

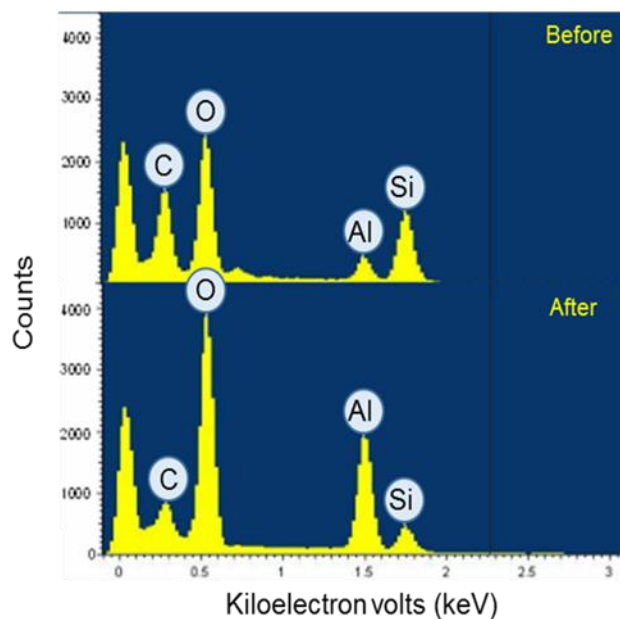


Figure 2.6: EDX spectra of oil-only SLIPS. Top image taken of area where ice was not grown. Bottom image taken in a deiced area.

An appreciable decrease in the intensity of the silicon signal relative to aluminum was apparent. This is interpreted as the removal of silicone oil from the porous surface of the PAAO coupons, which led to increased ice adhesion. EDX results from the resin-containing SLIPS were more complicated, as SEM images of the deiced areas on these samples showed two distinctly different areas: one bright and one dark. The bright area was identified as exposed aluminum, where both the oil and UV-curable resin were completely removed from the surface. Darker areas are those where the coating persists (**Figure 2.7**).

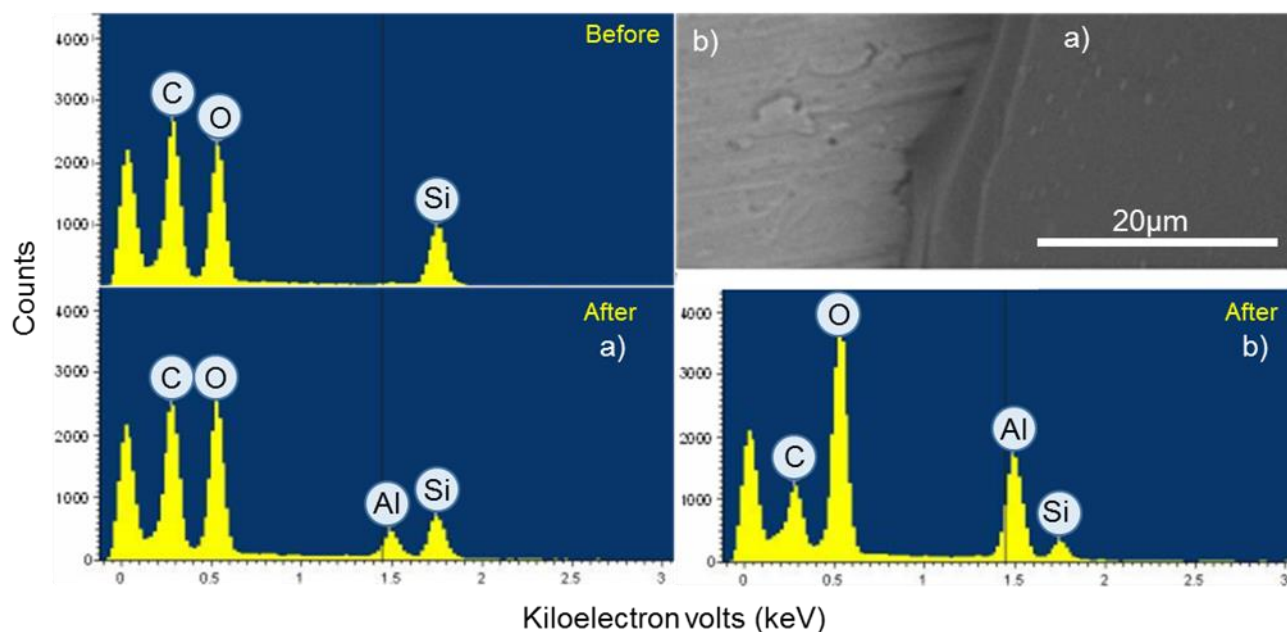


Figure 2.7: Oil+350 resin EDX and SEM results. (*Top left*) Spectrum before icing, with no aluminum seen at the surface. (*Bottom*) Spectra representing different areas observed by SEM after deicing, correlated to the SEM image (*top right*): a) where much of the silicon still resides in the surface, and b) where the coating has been completely removed.

From the SEM images and the EDX spectra, the primary mechanism of increasing ice adhesion in UV-cured SLIPS is because of complete removal of the coating and not simply lubricant depletion. Exposed aluminum indicated the coating was stripped away, which exposed the textured PAAO surface, allowing ice to nucleate and strongly bind to the surface. The darker areas where the coating persisted showed evidence for depleted silicone oil. However, because of variance in the thickness of the crosslinked siloxane resin, EDX results are not always consistent because of the different distance the beam needed to traverse to conduct the analysis. This in turn caused a change in the relative intensity of the Al and Si peaks despite all the spectra being obtained from the same samples.

2.4 Conclusions

UV-cured SLIPS based upon PAAO displayed excellent potential for icephobic surfaces. Silylated PAAO was infused with silicone oil and characterized with contact angle and AFM measurements to confirm the presence of a trapped liquid layer. Incorporating UV-cured resins Ebecryl 350 and 1360 to the SLIPS formulations weakened ice adhesion and improved surface longevity. SLIPS that included the diacrylated silicone resin Ebecryl 350 exhibited ice adhesion below 10kPa. Adhesive forces below 50kPa for up to seven deicing cycles were seen for these materials. Investigations of the SLIPS using SEM/EDX showed that the primary cause for increasing ice adhesion in the UV-cured samples was removal of the resin/oil layer, and not simply lubricant depletion. Future work will be aimed at using resins that are more resistant to abrasion, so that ice adhesion below 10kPa can be maintained.

2.5 References Cited

1. Lv, J.; Song, Y.; Jiang, L.; Wang, J., Bio-Inspired Strategies for Anti-Icing. *ACS Nano* **2014**, *8*, 3152.
2. Laforge, J. L.; Allaire, M. A.; Laflamme, J., State-of-the-art on power line de-icing. *Atmos. Res.* **1998**, *46*, 143.
3. Kulinich, S. A.; Farzaneh, M., Alkylsilane self-assembled monolayers: modeling their wetting characteristics. *Appl. Surf. Sci.* **2004**, *230*, 232.
4. Kreder, M. J.; Alvarenga, J.; Kim, P.; Aizenberg, J., Design of anti-icing surfaces: smooth, textured or slippery? *Nat. Rev. Mater.* **2016**, *1*, 15003.
5. Wang, Y.; Li, M.; Lv, T.; Wang, Q.; Chen, Q.; Ding, J., Influence of different chemical modifications on the icephobic properties of superhydrophobic surfaces in a condensate environment. *J. Mater. Chem. A* **2015**, *3*, 4967.
6. Golovin, K.; Kobaku, S. P. R.; Lee, D. H.; DiLoreto, E. T.; Mabry, J. M.; Tuteja, A., Designing durable icephobic surfaces. *Sci. Adv.* **2016**, *2*.
7. Zhu, L.; Xue, J.; Wang, Y.; Chen, Q.; Ding, J.; Wang, Q., Ice-phobic Coatings Based on Silicon-Oil-Infused Polydimethylsiloxane. *ACS Appl. Mater. Interfaces* **2013**, *5*, 4053.
8. Wong, T.-S.; Kang, S. H.; Tang, S. K. Y.; Smythe, E. J.; Hatton, B. D.; Grinthal, A.; Aizenberg, J., Bioinspired self-repairing slippery surfaces with pressure-stable omniphobicity. *Nature* **2011**, *477*, 443.

9. Cicely, S.; Noah, M.; Tak-Sing, W.; Philseok, K.; Joanna, A., Fabrics coated with lubricated nanostructures display robust omniphobicity. *Nanotechnology* **2014**, *25*, 014019.
10. Wilson, P. W.; Lu, W.; Xu, H.; Kim, P.; Kreder, M. J.; Alvarenga, J.; Aizenberg, J., Inhibition of ice nucleation by slippery liquid-infused porous surfaces (SLIPS). *PCCP* **2013**, *15*, 581.
11. Yin, X.; Zhang, Y.; Wang, D.; Liu, Z.; Liu, Y.; Pei, X.; Yu, B.; Zhou, F., Integration of Self-Lubrication and Near-Infrared Photothermogenesis for Excellent Anti-Icing/Deicing Performance. *Adv. Funct. Mater.* **2015**, *25*, 4237.
12. Kim, P.; Wong, T.-S.; Alvarenga, J.; Kreder, M. J.; Adorno-Martinez, W. E.; Aizenberg, J., Liquid-Infused Nanostructured Surfaces with Extreme Anti-Ice and Anti-Frost Performance. *ACS Nano* **2012**, *6*, 6569.
13. Huang, X.; Chrisman, J. D.; Zacharia, N. S., Omniphobic Slippery Coatings Based on Lubricant-Infused Porous Polyelectrolyte Multilayers. *ACS Macro Lett.* **2013**, *2*, 826.
14. Song, T.; Liu, Q.; Liu, J.; Yang, W.; Chen, R.; Jing, X.; Takahashi, K.; Wang, J., Fabrication of super slippery sheet-layered and porous anodic aluminium oxide surfaces and its anticorrosion property. *Appl. Surf. Sci.* **2015**, *355*, 495.
15. Wang, P.; Zhang, D.; Lu, Z.; Sun, S., Fabrication of Slippery Lubricant-Infused Porous Surface for Inhibition of Microbially Influenced Corrosion. *ACS Appl. Mater. Interfaces* **2016**, *8*, 1120.
16. Wang, Y.; Zhang, H.; Liu, X.; Zhou, Z., Slippery liquid-infused substrates: a versatile preparation, unique anti-wetting and drag-reduction effect on water. *J. Mater. Chem. A* **2016**, *4*, 2524.
17. Chen, J.; Liu, J.; He, M.; Li, K.; Cui, D.; Zhang, Q.; Zeng, X.; Zhang, Y.; Wang, J.; Song, Y., Superhydrophobic surfaces cannot reduce ice adhesion. *Appl. Phys. Lett.* **2012**, *101*, 111603.
18. Norek, M.; Krasinski, A., Controlling of water wettability by structural and chemical modification of porous anodic alumina (PAA): Towards super-hydrophobic surfaces. *Surf. Coat. Technol.* **2015**, *276*, 464.

Chapter 3

3 Fundamentals of Lasing Elastomeric Urethane Coatings to Prepare Icephobic Microstructures

Chapter 3 has been adapted for this dissertation from the original work ‘Femtosecond laser micromachining of co-polymeric urethane materials’ by Michael J. Wood, Matthew J. Coady, Felipe Aristizabal, Kent Nielsen, Paul J. Ragona, and Anne-Marie Kietzig.¹

3.1 Introduction

A variety of anti-icing materials have been explored in recent years in order to combat concerns with ice growing on structural surfaces, particularly in areas like infrastructure and aerospace.² Textured superhydrophobic surfaces (SHS) have been the subject of many studies aimed at promoting water/droplet removal under icing conditions, prior to freezing.³ Some of these trials have shown reasonable success, with the ability to repel water under atmospheric icing conditions.⁴⁻⁵ However, the use of SHS as ice repellent surface remains controversial in the field of anti-icing materials.⁶⁻⁹ The greatest point of contention comes from the observed ‘interlocking’ or ‘anchoring’ of ice to SHS, occurring when water infiltrates surfaces texture and subsequently freezes (**Figure 3.1**)

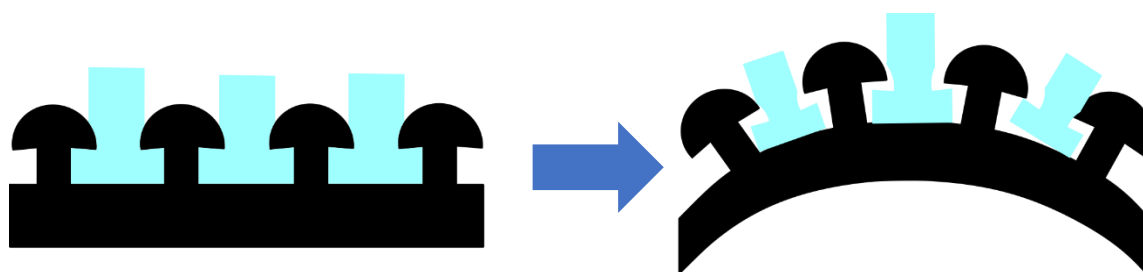


Figure 3.1: (left) Ice interlocking with structure surface. (right) Release of ice occurring when a pillared surface is flexible.

Interlocking causes increased ice adhesion strength and is also likely to damage the brittle surface architecture that imparts water/ice repellency characteristics. Water may infiltrate surface texture through condensation or through high-velocity impact, both of which will be encountered outdoors. Concerns of anchoring may be circumvented through the

inclusion of lubricants in the materials,¹⁰ or through the selection of tough, flexible materials that can release anchored ice due to flexion, ideally to resist structural damage. Lei Wang and coworkers demonstrated this idea by creating a flexible SHS based upon ZnO nanohairs and PDMS, but ice adhesion strength was not measured.¹¹ Liu *et al.* recently used similar materials to create flexible microneedles which repelled condensed droplets.¹²

A relatively unexplored approach to weakening adhesion of interlocked ice is to utilize tough and flexible, patterned polymer coatings. These materials could allow for greater durability when encased with ice, given the passive deicing characteristics observed for un-patterned elastomeric materials.¹³ There are a variety of methods which might be used to generate textured surfaces, and a recently developed example is femtosecond laser (fs-laser) micromachining.¹⁴ Femtosecond-laser micromachining uses a rastered laser beam to directly impart patterns on a surface, which vary depending on the path of the laser, and the intensity and number of pulses of light supplied. Studies using this technique principally involve micromachining conductive substrates, such as stainless steel,¹⁵⁻¹⁷ titanium,^{15, 18-20} copper,²¹⁻²⁴ and aluminum.^{15, 25-27} Some works have explored fs-laser patterning of polymeric materials, but these studies are confined to homopolymeric, semicrystalline polymers, such as polyethylene,²⁸⁻²⁹ polyimide,³⁰⁻³³ poly(methyl methacrylate),³⁴⁻³⁷ polycarbonates,^{30, 38-40} and polytetrafluoroethylene.⁴¹⁻⁴⁴ The present work seeks to expand our understanding of femtosecond laser ablation of polymeric materials beyond semicrystalline homopolymers by utilizing cross-linked, amorphous network copolymers as lasing substrates. The types of microstructures created are of particular interest. Copolymer networks are interesting materials because of the tunability of their properties; the flexibility, durability, hardness, etc. may all be influence by changing the proportion of the comonomeric units within the network. This tunability could broaden the scope for which lased polymeric surface are applicable, allowing access to a variety of new applications, such as icephobic surfaces.

3.2 Experimental

The following work was performed at Western University:

Preparation of Polymeric Materials

UCECOAT 6569 (urethane) acrylate urethane resin from Solvay, Inc. was used as the base polymer. The co-monomers: ethyl acrylate (EA, 99%), ethyl methacrylate (EMA, 98%), methacrylic acid (MAA, 99%), and 2-hydroxy-2-methylpropiophenone (photoinitiator, 97%) were purchased from Sigma Aldrich Co. and used as received. The co-monomers: benzyl methacrylate (BzMA, 98%) and styrene (Sty, 99.5%) were purchased from Alfa Aesar, Inc. Inhibitor was removed from styrene by washing with 5% aqueous NaOH prior to use. The comonomer triethyl(4-vinylbenzyl)phosphonium chloride (P⁺) was prepared using the methods of Cuthbert *et al.*⁴⁵ Urethane was dissolved in the co-monomers above to make solutions with weight ratios of 25:75, or 50:50 co-monomer to urethane. Five weight percent of 2-hydroxy-2-methylpropiophenone relative to the total mass of the urethane/co-monomer mixture was added with stirring. Mixtures were injected into a polytetrafluoroethylene (PTFE) mould with a glass cover to create smooth surfaces for fs-laser micromachining. Mixtures then underwent UV-curing, using LZC-4V photochemical cell (Luzchem Research, Inc.) equipped with 360 nm lamps. Curing took place over 1 h, with an illuminance of 150 ± 5 lx. The polymer samples, as prepared, were 10 mm \times 40 mm \times 2 mm thick and possessed a smooth face that was in contact with the PTFE mould and an opposing rough face. To make these surfaces suitable for femtosecond laser micromachining, they were mounted parallel to metal back plates. The smooth faces were mounted outwards to be incident to the laser beam using a two-part marine epoxy (Henkel Canada, Corp.) which also served to level the rough faces with respect to the metal plates. After a curing period, the mounted samples were sonicated in reverse-osmosis water for 15 min to remove any loose particles. Polymeric materials were swelled to measure gel content and investigate their cross-link density. Three 250 mg samples of each polymer were swollen in 25 mL of acetone. The solvent was replaced several times to ensure all leachable materials were removed from the networks. Subsequently, the remaining cross-linked materials were dried in a vacuum oven over a few days until the masses stopped decreasing. Gel content was calculated as the percent of mass remaining. Swelling experiments were later repeated using toluene as a solvent.

The following work was performed at McGill University. For the complete lasing setup, parameters, and theory, refer to Wood *et al.*¹

A Coherent Libra Ti: sapphire femtosecond laser system (Coherent, Inc.) was used to perform all laser micromachining experiments. This system has an inherent wavelength of 800 nm, pulse duration $\tau_p < 100$ fs, repetition rate $f_p = 1$ kHz, and a maximal output power $P = 4$ W. The beam passed through an OPerA Solo optical parametric amplifier (Coherent, Inc.) in order to isolate 275 nm and 550 nm UV light. The beam diameters at these wavelengths were 1.275 mm and 5.500 mm. The beam was attenuated with a continuously variable reflective neutral density filter and focused onto a linear x-z T-LSM050A translation stage (Zaber Technologies, Inc.) translational stage using a SPX028AR.16 200 mm plano-convex lens (Newport Corp). The polymer materials were mounted within the focal plane of the beam. Lines were ablated into the coatings translating the stage only in the x direction, moving with a velocity to provide a predetermined number of pulses per spot (PPS). The machined samples were sonicated to remove loose particles. UV-vis absorbance was measured using an Evolution 300 PC UV-Vis spectrophotometer (ThermoFischer Scientific, Inc.) and a wavelength range of 200 to 1100 nm. A FEI Inspect F50 scanning electron microscope (SEM) was used to capture images of the ablated surfaces. Images were taken using a spot size of 2.0 nm and a voltage of 10 nm. The materials were sputter coated with gold prior to observation. Line width measurements were made using ImageJ software. Surface chemistry was analyzed using an Axis Ultra DLD X-ray photoelectron spectrometer (XPS) (Kratos Analytical, Ltd.).

3.3 Results and Discussion

Copolymer networks were created by mixing commercial UCECOAT 6569 urethane resin with one of six different comonomers (**Figure 3.2**):

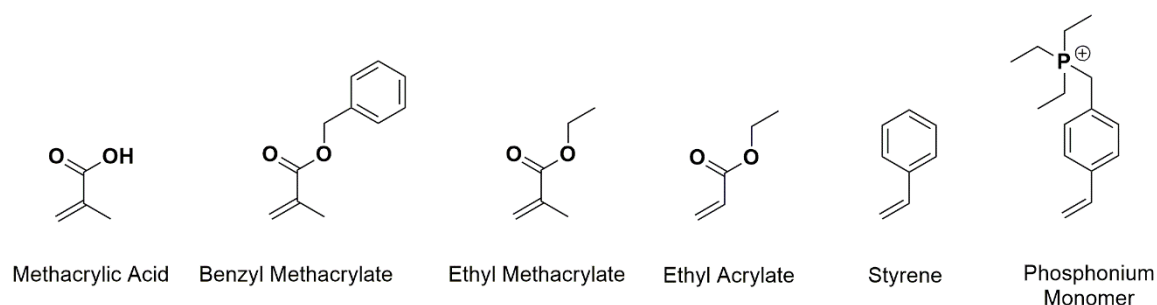


Figure 3.2: Chemical structures of comonomers for lasing study

Ethyl acrylate (EA) was selected based upon prior work done in the Ragogna group, and it was known that it could form copolymer networks with UCECOAT 6569. The other comonomers were selected as variations of EA which should have an effect on the networks' properties. Ethyl methacrylate (EMA) introduced a methyl group into the polymer backbone, which is also present in methacrylic acid (MAA). MAA does not contain an ethyl group, though. Benzyl methacrylate (BzMA) contains the same methyl group, and introduces a phenyl ring, which could have interesting absorption in the UV region. Styrene (Sty) retains this phenyl group but does not contain any acrylate functionality. Triethyl(4-vinylbenzyl) phosphonium chloride (P⁺) is essentially a decorated styrene group, which was expected to have similar properties. UV-curing of the mixtures yielded self-supporting films. Samples of each film were subsequently lased with 275 and 550 nm wavelength laser beams to inscribe new surface morphologies. SEM investigation of the lased surfaces showed the formation of surface morphologies that varied with the wavelength of laser used (**Figures 3.3** and **3.4**).

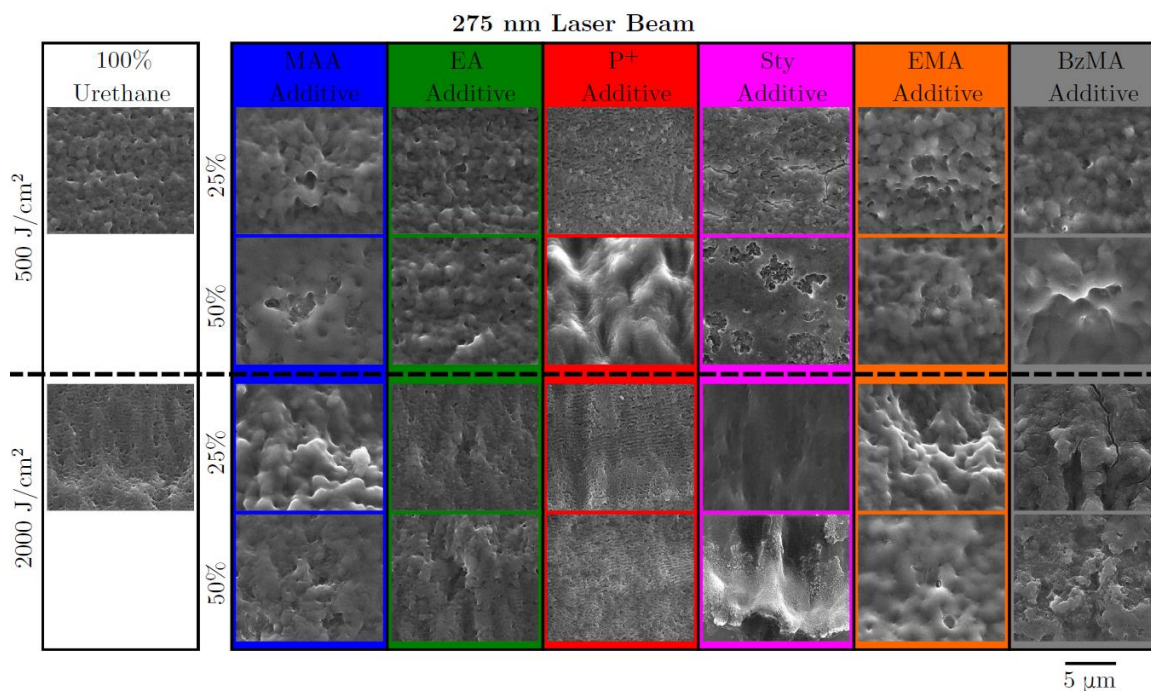


Figure 3.3: Scanning electron micrographs of the microstructures induced on the surface of the studied co-polymer materials irradiated with a 275 nm laser beam. Taken from Wood *et al* with permission.

Irradiation at 275 nm resulted in various morphologies that appeared to be the result of a re-solidified melt phase. In contrast, 550 nm irradiation presented more consistent morphologies between materials. These morphologies were similar in appearance to those reported by Assaf *et al.*, who showed that a porous morphology is the result of explosive boiling in the material as the localized heating causes the surface to melt.²⁸ Increasing total fluence to 2000 J/cm² from 500 J/cm² had differing effects on the materials and depended upon the irradiation wavelength: at 275 nm, topography became smoother suggesting increased melting of the substrate, and at 550 nm the visibility of the pores was enhanced, likely the result of further boiling. In all cases, results align with those gathered through the lasing of homopolymers in the literature, and the topographies suggest following the mechanisms proposed by Assaf.²⁹

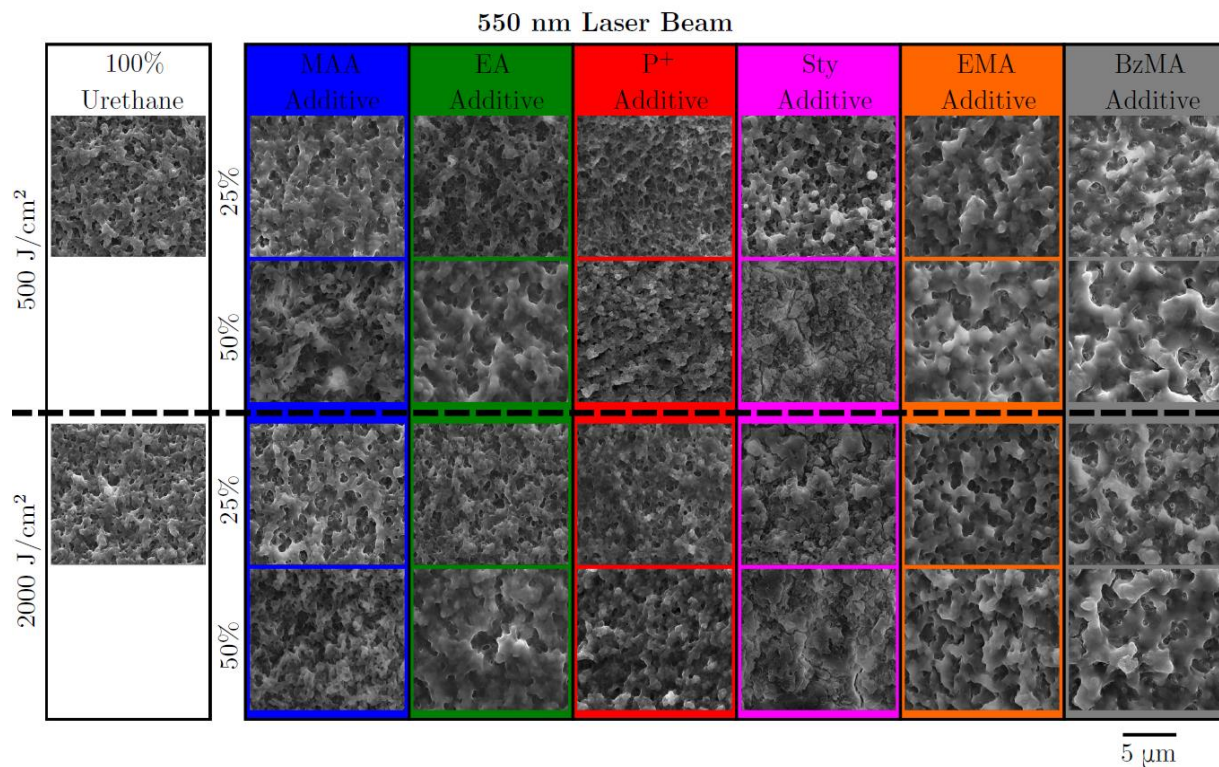


Figure 3.4: Scanning electron micrographs of the microstructures induced on the surface of the studied co-polymer materials irradiated with a 550 nm laser beam. Taken from Wood et al with permission.

The effects of comonomer identity and proportion on threshold fluence were next explored. Threshold fluence describes the amount of energy per unit area, expressed as J cm⁻², required for ionization / ablation of material from a surface. A higher threshold fluence means more energy must be supplied to a surface before ablation occurs and is associated with boiling and porous structure formation in polymer surfaces. A lower threshold fluence means a material is easier to ablate at a particular wavelength and tends to form smoother looking surfaces. Threshold fluences for the prepared materials were measured at both 275 and 550 nm to discern the effects of comonomer identity and concentration. It was observed that all networks have higher threshold fluence at 550 nm than at 275 nm, which agrees with the observed microstructures (**Figure 3.5**).

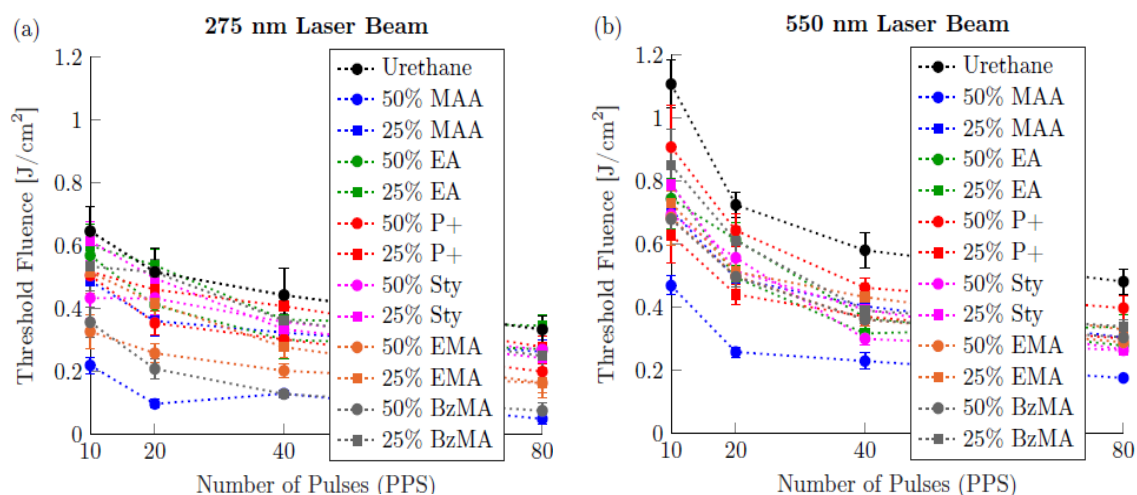


Figure 3.5: Experimentally determined ionization threshold fluences of UV-cured polymer materials, irradiated with (a) 275 nm, and (b) 550 nm fs-laser beam, presented as a function of the number of laser pulses. Error bars represent the 95% confidence interval. Note that in many cases the error bar is smaller than the data marker. Adapted from Wood *et al* with permission.

The addition of any comonomer resulted in a lowering of the threshold fluence of the copolymer networks relative to neatly cured UCECOAT 6569, regardless of the chemical structure. Furthermore, increasing comonomer content to 50 wt% from 25 wt% served to decrease threshold fluence to a greater extent. This effect was first hypothesized to be a result of increased laser absorption at the materials surface, since increased absorption of a wavelength decreases the threshold fluence of a material. This reasoning was disproved by performing UV-vis measurements. These experiments showed that at 275 nm there was virtually no difference between the absorption of any copolymer network and UCECOAT 6569 (**Figure 3.6**).

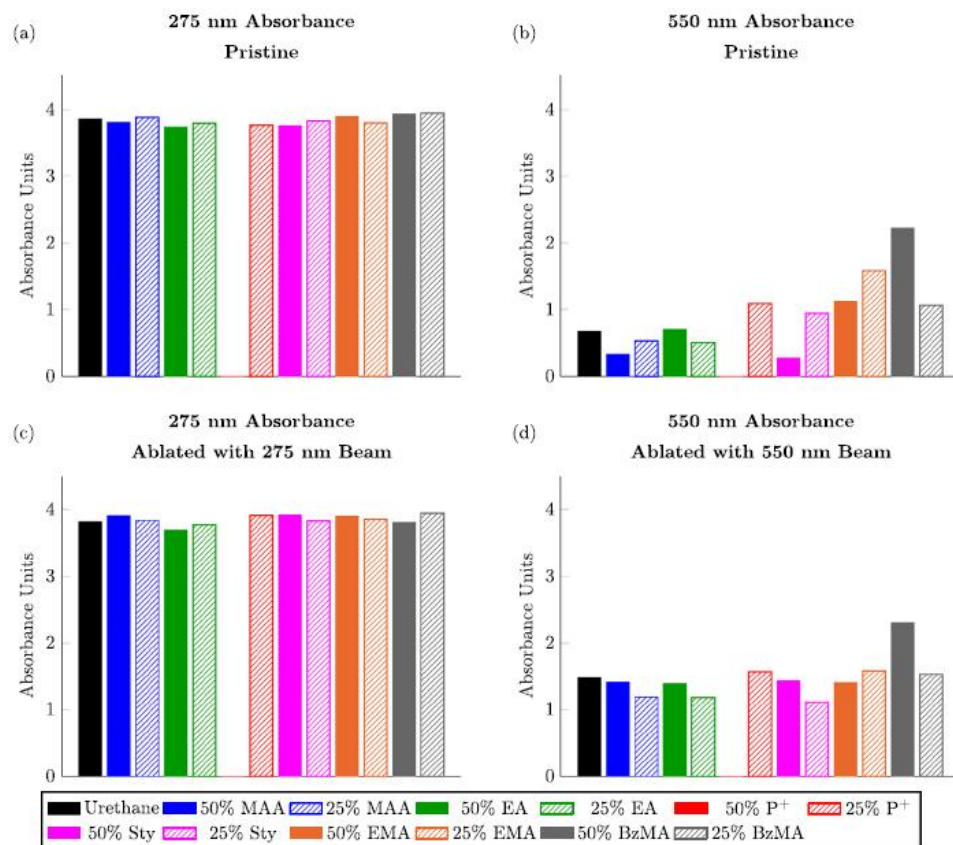


Figure 3.6: Absorbance of (a) 275 nm wavelength light by the pristine polymer substrates, (b) 550 nm wavelength light by the pristine polymer substrates, (c) 275 nm wavelength light by the polymer substrates after ablation, and (d) 550 nm wavelength light after ablation. Used with permission.

The threshold fluence and UV-vis absorption measurements revealed no discernable relationship between the chemistry of the comonomers and the lasing parameters. Studies of other material properties were performed, since absorption measurement results could not adequately explain changes in the observed threshold fluence. Swelling experiments were done to determine the gel content of the copolymer networks. It was found that regardless of comonomer content, gel content remained consistent at both 25 and 50 wt% (Table 3.1).

Table 3.1: Gel content and swelling of polymer networks. Adapted with permission.

		Gel Content	Swelling	
Material		% Cross-linked Material	% change in acetone	% change in toluene
100 %	UCECOAT 6569	84.8 ± 1.0	43.6 ± 1.1	26.6 ± 0.4
25 %	EA	76.5 ± 1.2	74.1 ± 2.2	49.9 ± 1.0
50 %	EA	77.9 ± 0.4	111.1 ± 1.7	94.0 ± 2.2
25 %	EMA	85.0 ± 0.6	56.7 ± 0.3	42.0 ± 0.1
50 %	EMA	84.0 ± 0.1	86.5 ± 0.3	81.7 ± 0.4
25 %	BzMA	83.5 ± 0.2	50.9 ± 0.2	35.9 ± 0.1
50 %	BzMA	84.3 ± 0.2	65.5 ± 0.1	63.7 ± 0.6
25 %	Sty	84.9 ± 0.2	54.2 ± 0.4	40.6 ± 0.5
50 %	Sty	85.2 ± 0.2	65.9 ± 0.7	86.1 ± 0.6

This consistency in gel content allowed us to qualitatively compare the relative cross-link densities of the materials by observing the percent change in mass of the materials when swollen in acetone and toluene. A higher degree of swelling indicates lower cross-link density, as more lightly cross-linked polymers allow for more solvent to infiltrate the network. It was found that for all materials that increasing comonomer proportion to 50 wt% from 25 wt% led to more swelling, and thus lower cross-link density. We concluded that this lower cross-link density decreased the required energy for ablation to occur.

Incubation effects and changes in surface chemistry were next studied. Incubation describes a process through which a material becomes easier to ablate with successive laser pulses. The incubation coefficient ξ therefore describes the magnitude of this change, with

$\xi = 1$ indicating no incubation effects. All the materials prepared showed some incubation effects (**Figure 3.7**).

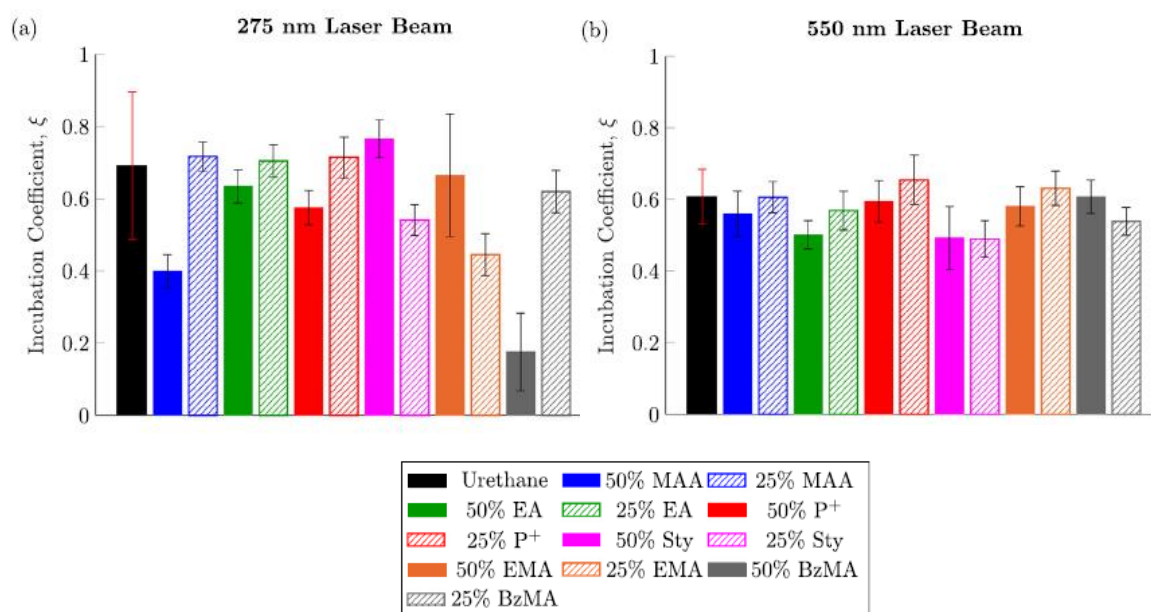


Figure 3.7: Experimentally determined incubation coefficients ξ of UV-cured polymer materials irradiated with (a) 275 nm, and (b) 550 nm fs-laser beam. Error bars represent the 95% confidence interval. Adapted with permission.

No trends relating incubation effects and comonomer chemistry, wt%, or crosslink density of the material were identified. Surface chemistry was examined using X-ray photoelectron spectroscopy (XPS) to observe any changes in relative O, N, or C content in the materials. Very little change in the materials' surface chemistry was observed after ablation: there was no significant change in relative O, N, or C content, and no change in hybridization that would indicate preferential ablation of the comonomer over the urethane resin.

3.4 Conclusions

Our work is the first to explore femtosecond laser micromachining of crosslinked amorphous copolymer networks and has uncovered that their response to laser irradiation is similar to that of homopolymers previously reported. Surface morphologies observed were strongly dependent upon the threshold fluence of the materials, and the wavelength of illumination: melt-like topography resulted on materials with low ablation thresholds, and rougher, porous morphologies were observed at higher threshold fluence. It was found that threshold fluence decreased for materials with lower cross-link density, independent of the identity of the added comonomer. Surfaces were stable to ablation under atmospheric conditions, showing little to no change in surface chemistry after ablation. Other trends in the data were difficult to assess. No correlations between IR cure and incubation coefficient were observed with comonomer identity, threshold fluence, or cross-link density. Future explorations will be aimed at applying these materials to anti-icing applications and studying the wetting and icing characteristics of different surface morphologies.

3.5 References Cited

1. Wood, M. J.; Coady, M. J.; Aristizabal, F.; Nielsen, K.; Ragogna, P. J.; Kietzig, A.-M., Femtosecond laser micromachining of co-polymeric urethane materials. *Appl. Surf. Sci.* **2019**, *483*, 633.
2. Kreder, M. J.; Alvarenga, J.; Kim, P.; Aizenberg, J., Design of anti-icing surfaces: smooth, textured or slippery? *Nat. Rev. Mater.* **2016**, *1*, 15003.
3. Jin, S.; Liu, J.; Lv, J.; Wu, S.; Wang, J., Interfacial Materials for Anti-Icing: Beyond Superhydrophobic Surfaces. *Chemistry – An Asian Journal* **2018**, *13*, 1406.
4. Wang, Y.; Li, M.; Lv, T.; Wang, Q.; Chen, Q.; Ding, J., Influence of different chemical modifications on the icephobic properties of superhydrophobic surfaces in a condensate environment. *J. Mater. Chem. A* **2015**, *3*, 4967.
5. Yeong, Y. H.; Milionis, A.; Loth, E.; Sokhey, J.; Lambourne, A., Atmospheric Ice Adhesion on Water-Repellent Coatings: Wetting and Surface Topology Effects. *Langmuir* **2015**, *31*, 13107.
6. Nosonovsky, M.; Hejazi, V., Why Superhydrophobic Surfaces Are Not Always Icephobic. *ACS Nano* **2012**, *6*, 8488.

7. Kulinich, S. A.; Farhadi, S.; Nose, K.; Du, X. W., Superhydrophobic Surfaces: Are They Really Ice-Repellent? *Langmuir* **2011**, *27*, 25.
8. Chen, J.; Liu, J.; He, M.; Li, K.; Cui, D.; Zhang, Q.; Zeng, X.; Zhang, Y.; Wang, J.; Song, Y., Superhydrophobic surfaces cannot reduce ice adhesion. *Appl. Phys. Lett.* **2012**, *101*, 111603.
9. Jung, S.; Dorrestijn, M.; Raps, D.; Das, A.; Megaridis, C. M.; Poulikakos, D., Are Superhydrophobic Surfaces Best for Icephobicity? *Langmuir* **2011**, *27*, 3059.
10. Wong, T.-S.; Kang, S. H.; Tang, S. K. Y.; Smythe, E. J.; Hatton, B. D.; Grinthal, A.; Aizenberg, J., Bioinspired self-repairing slippery surfaces with pressure-stable omniphobicity. *Nature* **2011**, *477*, 443.
11. Wang, L.; Gong, Q.; Zhan, S.; Jiang, L.; Zheng, Y., Robust Anti-Icing Performance of a Flexible Superhydrophobic Surface. *Adv. Mater.* **2016**, *28*, 7729.
12. Liu, X.; Zhao, H.; Li, P.; Pang, Y.; Fan, Y.; Zhang, B.; Wang, L.; Zheng, Y.; Wang, Z., Robust Icephobic Performance of Flexible Needles. *ChemNanoMat* **2019**, *5*, 175.
13. Andersson, L.-O.; Golander, C.-G.; Persson, S., Ice adhesion to rubber materials. *J. Adhes. Sci. Technol.* **1994**, *8*, 117.
14. Sugioka, K.; Xu, J.; Wu, D.; Hanada, Y.; Wang, Z.; Cheng, Y.; Midorikawa, K., Femtosecond laser 3D micromachining: a powerful tool for the fabrication of microfluidic, optofluidic, and electrofluidic devices based on glass. *Lab on a Chip* **2014**, *14*, 3447.
15. Ahmmed, K. M. T.; Ling, E. J. Y.; Servio, P.; Kietzig, A.-M., Introducing a new optimization tool for femtosecond laser-induced surface texturing on titanium, stainless steel, aluminum and copper. *Opt. Laser Eng.* **2015**, *66*, 258.
16. Yahng, J. S.; Nam, J. R.; Jeoung, S. C., The influence of substrate temperature on femtosecond laser micro-processing of silicon, stainless steel and glass. *Opt. Laser Eng.* **2009**, *47*, 815.
17. Wu, B.; Zhou, M.; Li, J.; Ye, X.; Li, G.; Cai, L., Superhydrophobic surfaces fabricated by microstructuring of stainless steel using a femtosecond laser. *Appl. Surf. Sci.* **2009**, *256*, 61.
18. Tsukamoto, M.; Asuka, K.; Nakano, H.; Hashida, M.; Katto, M.; Abe, N.; Fujita, M., Periodic microstructures produced by femtosecond laser irradiation on titanium plate. *Vacuum* **2006**, *80*, 1346.
19. Vorobyev, A. Y.; Guo, C., Femtosecond laser structuring of titanium implants. *Appl. Surf. Sci.* **2007**, *253*, 7272.

20. Lehr, J.; Kietzig, A.-M., Production of homogenous micro-structures by femtosecond laser micro-machining. *Opt. Laser Eng.* **2014**, *57*, 121.
21. Biswas, S.; Karthikeyan, A.; Kietzig, A.-M., Effect of Repetition Rate on Femtosecond Laser-Induced Homogenous Microstructures. *Materials (Basel, Switzerland)* **2016**, *9*, 1023.
22. Preuss, S.; Demchuk, A.; Stuke, M., Sub-picosecond UV laser ablation of metals. *Appl. Phys. A* **1995**, *61*, 33.
23. Chichkov, B. N.; Momma, C.; Nolte, S.; von Alvensleben, F.; Tünnermann, A., Femtosecond, picosecond and nanosecond laser ablation of solids. *Appl. Phys. A* **1996**, *63*, 109.
24. Vorobyev, A. Y.; Guo, C., Femtosecond laser nanostructuring of metals. *Opt. Express* **2006**, *14*, 2164.
25. Valette, S.; Audouard, E.; Le Harzic, R.; Huot, N.; Laporte, P.; Fortunier, R., Heat affected zone in aluminum single crystals submitted to femtosecond laser irradiations. *Appl. Surf. Sci.* **2005**, *239*, 381.
26. Robinson, G. M.; Jackson, M. J., Femtosecond laser micromachining of aluminum surfaces under controlled gas atmospheres. *J. Mater. Eng. Perform.* **2006**, *15*, 155.
27. Mahmood, A. S.; Venkatakrishnan, K.; Tan, B., 3-D aluminum nanostructure with microhole array synthesized by femtosecond laser radiation for enhanced light extinction. *Nanoscale Res. Lett.* **2013**, *8*, 477.
28. Assaf, Y.; Zhao, M.; Kietzig, A.-M., Femtosecond laser-induced porosity on poly(ethylene) surfaces—A crystallographic and rheological study. *J. Appl. Phys.* **2018**, *124*, 023103.
29. Assaf, Y.; Kietzig, A.-M., Optical and chemical effects governing femtosecond laser-induced structure formation on polymer surfaces. *Mater. Today Commun.* **2018**, *14*, 169.
30. J. Krüger, W. K., Ultrashort pulse laser interaction with dielectrics and polymers. *Adv. Polym. Sci.* **2004**, *168*, 247.
31. Baudach, S.; Bonse, J.; Kautek, W., Ablation experiments on polyimide with femtosecond laser pulses. *Appl. Phys. A* **1999**, *69*, S395.
32. Baudach, S.; Kr; Uuml; Ger, J.; ouml; rg; Kautek, W., Femtosecond Laser Processing of Soft Materials. *Rev. Laser Eng.* **2001**, *29*, 705.

33. Forster, M.; Kautek, W.; Faure, N.; Audouard, E.; Stoian, R., Periodic nanoscale structures on polyimide surfaces generated by temporally tailored femtosecond laser pulses. *PCCP* **2011**, *13*, 4155.
34. Srinivasan, R.; Sutcliffe, E.; Braren, B., Ablation and etching of polymethylmethacrylate by very short (160 fs) ultraviolet (308 nm) laser pulses. *Appl. Phys. Lett.* **1987**, *51*, 1285.
35. De Marco, C.; Eaton, S. M.; Suriano, R.; Turri, S.; Levi, M.; Ramponi, R.; Cerullo, G.; Osellame, R., Surface Properties of Femtosecond Laser Ablated PMMA. *ACS Appl. Mater. Interfaces* **2010**, *2*, 2377.
36. Klinger, D.; Sobierajski, R.; Nietubyc, R.; Krzywiński, J.; Pelka, J.; Juha, L.; Jurek, M.; Żymierska, D.; Guizard, S.; Merdji, H., Surface modification of polymethylmethacrylate irradiated with 60fs single laser pulses. *Radiat. Phys. Chem.* **2009**, *78*, S71.
37. Watanabe, W.; Sowa, S.; Tamaki, T.; Itoh, K.; Nishii, J., Three-Dimensional Waveguides Fabricated in Poly(methyl methacrylate) by a Femtosecond Laser. *JJAP* **2006**, *45*, L765.
38. Baudach, S.; Bonse, J.; Krüger, J.; Kautek, W., Ultrashort pulse laser ablation of polycarbonate and polymethylmethacrylate. *Appl. Surf. Sci.* **2000**, *154-155*, 555.
39. Tao Qi, L.; Ping Hu, J., *Experimental Investigation on Femtosecond Laser Ablation of Polycarbonate*. 2013; Vol. 652-654, p 2359.
40. Klein-Wiele, J.-H.; Simon, P., Fabrication of periodic nanostructures by phase-controlled multiple-beam interference. *Appl. Phys. Lett.* **2003**, *83*, 4707.
41. Liang, F.; Lehr, J.; Danielczak, L.; Leask, R.; Kietzig, A.-M., Robust Non-Wetting PTFE Surfaces by Femtosecond Laser Machining. *Int. J. Mol.* **2014**, *15*, 13681.
42. Küper, S.; Stuke, M., Ablation of polytetrafluoroethylene (Teflon) with femtosecond UV excimer laser pulses. *Appl. Phys. Lett.* **1989**, *54*, 4.
43. Hashida, M.; Mishima, H.; Tokita, S.; Sakabe, S., Non-thermal ablation of expanded polytetrafluoroethylene with an intense femtosecond-pulse laser. *Opt. Express* **2009**, *17*, 13116.
44. Yong, J.; Fang, Y.; Chen, F.; Huo, J.; Yang, Q.; Bian, H.; Du, G.; Hou, X., Femtosecond laser ablated durable superhydrophobic PTFE films with micro-through-holes for oil/water separation: Separating oil from water and corrosive solutions. *Appl. Surf. Sci.* **2016**, *389*, 1148.
45. Cuthbert, T. J.; Guterman, R.; Ragogna, P. J.; Gillies, E. R., Contact active antibacterial phosphonium coatings cured with UV light. *J. Mater. Chem. B* **2015**, *3*, 1474.

Chapter 4

4 Highly cross-linked UV-cured siloxane copolymer networks as icephobic coatings

4.1 Introduction

Preventing ice growth on surfaces is a significant engineering challenge particularly relevant to large infrastructure installations and aerospace, as their operational efficiency is reduced and they are often damaged by the accumulation of ice.¹ Repairing or replacing infrastructure, such as power generators or downed transmission lines can cost billions of dollars.² Materials that repel ice are of great interest, as they can prevent damage, reduce repair costs and limit infrastructure down time.³ Several technologies have been developed that follow three primary approaches to ice abatement:⁴ ice repellence through (i) the rapid dewetting of surfaces before freezing occurs; (ii) controlling ice growth through freezing delay or nucleation control, and (iii) decreasing the force of ice adhesion to ease removal. Reducing ice adhesion strength is the most practical of these approaches, as measuring ice adhesion allows a direct rating for the performance of a given material.⁵ Two benchmarks have been identified for classifying low ice adhesion surfaces, where icephobic materials exhibit ice adhesion ≤ 100 kPa. Passive anti-icing materials require considerably lower adhesion, on the order of 20 kPa,⁶ as below this threshold, ice can reasonably be removed by environmental means, such as wind, gravity, or vibration.⁷ For passive anti-icing materials, ice delamination occurs without extraneous energy input (e.g. scraping, heating, smashing), making them key targets of interest, especially when an installation susceptible to icing is located in a remote area or dangerous to access such as off shore wind turbines.⁸ There have been significant advances in anti-icing materials, which vary drastically in their composition and properties. Over all they can be divided into two broad categories: textured and smooth.³ Texture imposes lower ice adhesion when water freezes in a Cassie-Baxter-type wetting state, and contact area between ice and surface is minimized by the formation of an air pocket beneath water at the interface.⁹⁻¹¹ While some effective rough surfaces have been reported, the use of surface texture as a means toward reducing the force of ice adhesion is controversial.¹²⁻¹⁵ Ice adhesion strength increases when water

freezes in a Wentzel-type wetting state as it leads to the interlocking of ice with the surface texture. These observations, coupled with durability and scalability concerns for mass producing micro-/nanostructured surfaces make textured materials less than promising candidates for anti-icing.¹⁶ In contrast, smooth materials utilize low surface energy and interfacial effects to minimize ice adhesion, and are more easily scaled.^{6, 17}

Smooth materials can be further divided into wet- and dry-type icephobic surfaces. This distinction has become important owing to the success of wet (i.e. lubricated) materials in reducing ice adhesion to well below 20 kPa.¹⁸⁻¹⁹ Such wet materials contain lubricating fluids that impart icephobicity through interfacial effects. Two prominent examples of these materials are slippery lubricant-infused porous surfaces (SLIPS),¹⁹⁻²⁰ consisting of a porous substrate filled with a lubricant, lubricated polymer networks (gels) and self-lubricating coatings,^{6, 21-23} such as those containing micellar structures. Despite observed ultra-low ice adhesion, few of these materials are durable enough to show consistently low ice adhesion over repeated deicing cycles. Lubricants are readily removed from the surface by the action of water or ice, ultimately yielding increased ice adhesion to the surfaces.³ An elegant study by Golovin *et al.* exhibited a library of cross-linked polymers with incorporated non-cross-linking polymer chains, giving soft, lightly cross-linked icephobic coatings.⁶ They showed that their coatings were durable up to 100 deicing cycles, with a key finding that regardless of polymer identity, lowering the cross-link density of the coatings yielded lower ice adhesion. The decreased in cross-link density was achieved by (i) incorporating a non-cross-linking polymer chains or oils; and (ii) changing the number of cross-linkable moieties with respect to un-crosslinked chains. This work inspired our interest in expanding on the idea of reducing crosslink density to achieve icephobic coatings. To this end, we looked to the incorporation of a comonomer with a telechelic, UV-curable polydimethylsiloxane (PDMS) resin, to create copolymer network coatings (**Figure 4.1**).

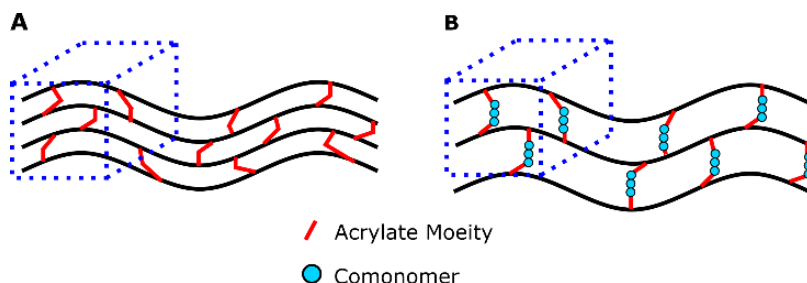


Figure 4.1: Illustration of the differing cross-link densities in cured polymer networks with no comonomer (A) and with comonomer included (B).

Copolymers as icephobic coatings have been employed,²⁴⁻²⁵ but usually incorporate fluorinated materials, which is a waning approach given the environmental persistence of organofluorine fragments.²⁶ Many studies also do not include tests of material durability to successive deicing tests. Using light curing approaches is attractive because of their short cure times, and scalability.²⁷ Our approach uses PDMS because of its low surface energy, together with methyl methacrylate (MMA), lauryl methacrylate (LMA), or styrene (Sty) as the comonomers. These monofunctional groups were chosen based on their differing hydrophobicity. We hypothesized that incorporating varying amounts of comonomer into the polymer networks would decrease cross-link density, and a reduction in ice adhesion force may be observed. Effects of comonomer proportion on hardness, surface topography, and durability to successive deicing tests were also measured, to better understand how these characteristics are affected by comonomer content. In this context, the prepared coatings showed very promising icephobicity, with initial ice adhesion values close to 20 kPa, maintained for up to 50 deicing cycles. This work has revealed interesting trends in the behavior of cross-linked copolymer networks as icephobic coatings.

4.2 Experimental

Ebecryl 1360 PDMS resin was received from Allnex. Lauryl methacrylate (monomer, 96%), phenylbis(2,4,6-trimethylbenzoyl)phosphine oxide (BAPO, photoinitiator, 97%), and 2-hydroxy-2-methylpropiophenone (photoinitiator, 97%) were purchased from Sigma-Aldrich. Methylmethacrylate (monomer, 99%) and Styrene (monomer, 99%) were purchased from Alfa Aesar. All chemicals were used as received,

except styrene, which was washed with 5% NaOH prior to use, to remove the inhibitor (4-*tert*-butylcatechol). Aluminum 6061 bar stock was purchased from McMaster Carr and cut into 2.5 by 5.0 cm coupons. The coupons were polished with an 80-grit polishing pad and rinsed with ethanol prior to coating. Coating formulations were prepared by mixing Ebecryl 1360 with 5, 10, or 25 wt% of a comonomer. To these mixtures were added compatible photoinitiators: 2-hydro-2-methylpropiophenone for the methacrylates, and phenylbis(2,4,6-trimethylbenzoyl)phosphine oxide for styrene. 1 wt% photoinitiator was used for 5-10% monomer formulations, and 2 wt% photoinitiator was used for 25% comonomer formulations. Formulations were applied to aluminum substrates using a #90 Mayer rod without dilution. The coupons were placed in a partially sealed bag, that was purged 10 times with N₂. The bag was sealed, and UV-curing performed. UV-curing was done using a modified system purchased from UV Process and Supply Inc., equipped with a medium pressure mercury vapor lamp ($\lambda = 200\text{-}600\text{ nm}$). The maximum measured intensities of UVA, UVB, and UVC for this source were 890, 820, and 200 mW cm⁻². These intensities were measured with a Power Puck II from EIT Inc. Self-supporting films for swelling experiments were prepared using the same equipment but were cured in a poly(tetrafluoroethylene) mould, yielding ingots approximately 10 by 30 by 2 mm in size. Ice adhesion measurements were carried out in the Cold Weather Biome at Western's Biotron Facility, using our previously described centrifuge method.²⁸ Material hardness was measured with a Micro Materials Nano Test Machine equipped with a Berkovich Indenter. Nine indents were made on each sample, at depths from 1 to 5 μm . The load/unload rates were 0.0013 mN sec⁻¹, and the dwell time was 5 seconds. Differential scanning calorimetry was done using a DSC Q20 from TA Instruments. Approximately 6 mg of sample was loaded into an aluminum T-zero pans. All samples underwent a heat/cool/heat profile at 40 °C min⁻¹ under a nitrogen atmosphere. Data were acquired from the final cooling cycle of this profile. Swelling experiments were carried out in triplicate, in sealed jars using toluene as the. Self-supporting films were cut into 3 approximately equal pieces, totaling 0.5 g. These pieces were put into jars and allowed to swell in toluene for 10 days; Fresh solvent was exchanged semi-daily. Cross-link density (v_e) was calculated according to ASTM D618.²⁹ Material density was measured via water displacement in a 5 mL volumetric flask. The displaced mass of water was measured using

a Mettler-Toledo AB304-S balance. Contact angle measurements were conducted using a Kruss DSA100 drop shape analyzer and Milli-Q water ($18.2 \text{ M}\Omega \text{ cm}$) was dispensed using a glass capillary. Initial droplets were $10 \text{ }\mu\text{L}$, placed on the surface, and increased to $30 \text{ }\mu\text{L}$ at a rate of $30 \text{ }\mu\text{L min}^{-1}$ (advancing contact angle). The same droplet was then removed from the surface at a rate of $-30 \text{ }\mu\text{L/min}$ (receding contact angle). Video of both events were recorded, and contact angles were determined using the DSA software. Scanning electron microscopy (SEM) was performed at Western's Nanofabrication facility using a Zeiss LEO 1530 field-emission SEM for all measurements with a $30 \text{ }\mu\text{m}$ aperture, 2.00 kV accelerating voltage, and 10k times magnification. Surface topography of the samples was measured using a Multimode AFM with NanoScope V controller and a Bruker AS-130VLR-2 scanner covering a maximum horizontal range of about $12 \text{ }\mu\text{m}$. The ScanAsyst mode was used with silicon nitride cantilevers of spring constant 0.4 N m^{-1} and resonant frequency 70 KHz . The scanning rate was 1 Hz and all measurements were taken at room temperature. Images were analyzed using Bruker NanoScope Analysis software to calculate properties of the samples such as ripple width and roughness. Notes on data treatment can be found in **Appendix C**.

4.3 Results and Discussion

Three series of coating formulations were prepared by mixing containing Ebecryl 1360 (EB1360), and 5, 10, and 25% of methyl methacrylate (MMA), lauryl methacrylate (LMA), or styrene (Sty) comonomers. The mixtures formed homogeneous mixtures and when cured yielded visually smooth films upon which shear ice adhesion (τ_{ice}) was tested to gauge their suitability as anti-icing materials (**Figure 4.2**).

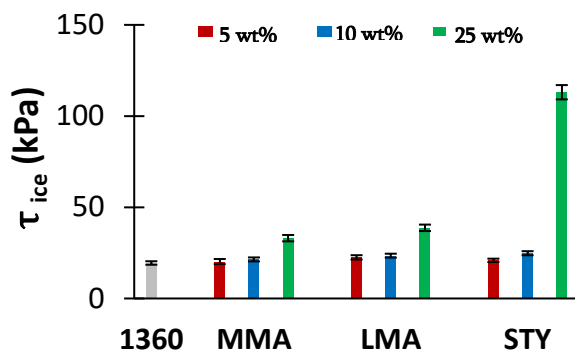


Figure 4.2: Initial ice adhesion data of the three series of prepared coatings compared to EB1360. Red, blue, and green columns denote 5, 10 and 25 wt% comonomer. Error bars are the standard error of the measurements ($n = 5$).

Overall, little change in τ_{ice} was observed upon the addition of up to 10 wt% of MMA, LMA, or STY. These coatings showed ice adhesion near 20 kPa, the threshold needed for passive deicing. τ_{ice} increased modestly as the proportion of MMA (33 kPa) or LMA (39 kPa) was increased to 25 wt% from 10%, maintaining their classification as icephobic. The 25% styrene formulation showed an increase in τ_{ice} to 113 kPa and was the only coating to exceed the icephobic range. Notably, τ_{ice} did not decrease with the addition of MMA, LMA or Sty comonomers as expected. Cross-link density, hardness, and surface roughness were measured to shed light on the measured values.

Swelling experiments were conducted to determine the cross-link density of the materials. Cross-link density, v_e , decreased as additional MMA, LMA, or styrene was added to the networks. For example, v_e decreases from 14.5 to 5.7×10^3 chains m^{-3} as LMA content is increased from 5% to 25%, showing a decrease in cross-link density of approximately 60%. v_e for 5% MMA and LMA decreased relative to EB1360, but 5% Sty coatings showed an increase, which was attributed to the use of BAPO photoinitiator in place of 2-hydroxy-2-methylpropiophenone as photoinitiator: necessary because of the UV absorption of styrene overlapping with 2-hydroxy-2-methylpropiophenone. Despite this observation, the trend of v_e decreasing with increased Sty content held true. Decreased cross-link density for all coating series was expected to give a parallel decrease in τ_{ice} , as observed by Golovin *et al.*,⁶ however this was not the

Table 4.1: Table of physical data measured for the prepared icephobic coatings.

Formulation	τ_{ice} (kPa)	ν_e (10^3 chains m^{-3})	Hardness (10^{-5} GPa)
EB1360	19 ± 1	19.6 ± 0.8	539 ± 9
5% MMA	20 ± 1	16.9 ± 0.1	524 ± 5
10% MMA	21 ± 1	14.8 ± 1.2	508 ± 8
25% MMA	33 ± 2	9.4 ± 0.7	415 ± 3
5% LMA	23 ± 1	14.5 ± 1.0	537 ± 9
10% LMA	23 ± 1	12.0 ± 0.2	586 ± 20
25% LMA	39 ± 2	5.7 ± 0.4	481 ± 8
5% Sty	21 ± 1	30.9 ± 0.6	491 ± 5
10% Sty	25 ± 1	16.1 ± 0.3	365 ± 8
25% Sty	113 ± 4	5.3 ± 0.2	194 ± 5

case. It was reasoned that τ_{ice} was being influenced by the physical properties of the coatings other than ν_e . Hardness measurements resulting from nanoindentation experiments showed that in general, hardness decreased in parallel with cross-link density, for example from 520 to 415 $\times 10^{-5}$ GPa between 5 and 25% MMA, and from 419 to 194 $\times 10^{-5}$ GPa from between 5 and 25% Sty. The hardness and cross-link density results are coherent, as decreasing cross-link density typically decreases hardness in polymers. It was concluded that increased hardness of the coatings was not the cause of rising τ_{ice} , which agreed with the findings of He *et al.*, who reported no correlation between the room temperature hardness of a material and ice adhesion.³⁰ Surface topography was then examined using scanning electron (SEM) and atomic force microscopy (AFM) to search for changes which may have led to increased τ_{ice} .

Imaging copolymer network surfaces by SEM revealed that the materials did indeed have a wrinkled surfaces, a well-known artifact from UV-curing.³¹⁻³² Qualitatively, it appeared that the surfaces of coatings which contained LMA, MMA, and styrene (**Figure 4.3**) were considerably more wrinkled than neat EB1360, with the apparent wrinkle width increasing with higher proportions of Sty.

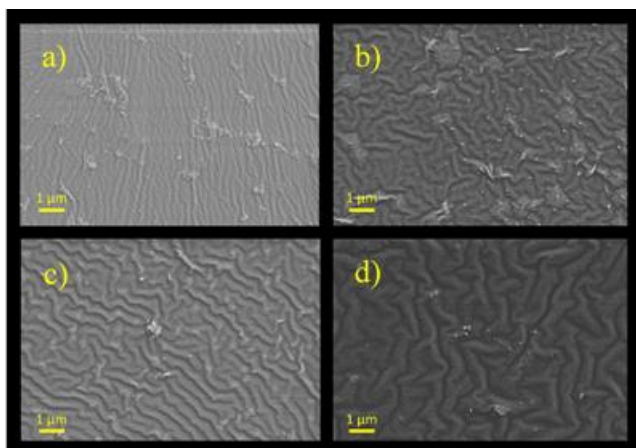


Figure 4.3: SEM images showing wrinkling on surfaces of EB1360:Styrene coatings: a) EB1360, b) 5 wt% Sty, c) 10% Sty, d) 25 wt% Sty.

The widths of wrinkles were measured by AFM, and showed that for any given comonomer, wrinkle width increased as comonomer was increased to 25 wt% from 5 wt % (**Figure 4.4**).

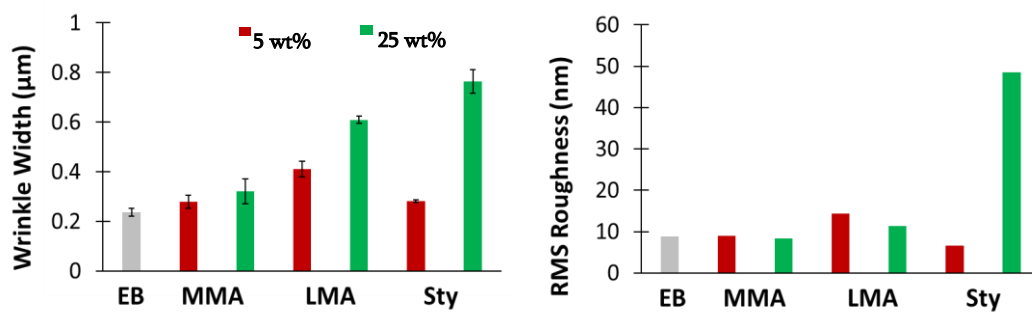


Figure 4.4: a) average wrinkle width and b) root-mean square roughness of copolymer network coatings measured by AFM.

Changes in width as comonomer content increased from 5 wt% to 25 wt% coincides well with the τ_{ice} data: width increases of 0.28 to 0.32, 0.41 to 0.61, and 0.28 to 0.76 μm for MMA, LMA, and Sty align with τ_{ice} increases from 20 to 33, 23 to 39, and 21 kPa to 113 kPa. Styrene-containing coatings show the largest increase in wrinkle width, and therefore the largest increase in τ_{ice} . Root mean square (RMS) roughness on the coatings was measured, as well (**Figure 4.4**). These results show that the RMS roughness of 25 % styrene coatings was at least three-times that of any of the other coatings, further illustrating the

cause for drastically increased ice adhesion. Lastly, the range of height measured in the AFM height images in 25% Sty coatings was considerably greater than the other coatings (**Figure 4.5**).

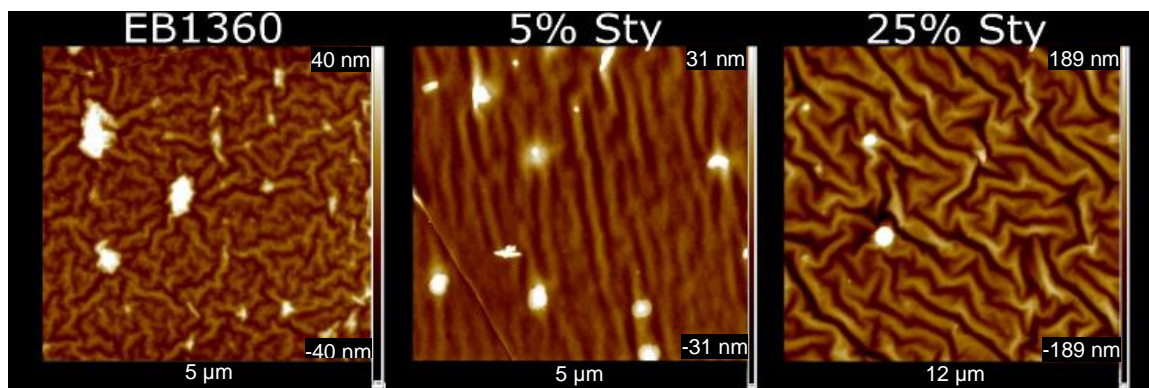


Figure 4.5: AFM height images showing wrinkles present in EB1360:Sty copolymer films.

The height ranges measured by AFM for EB1360, compared to 5 and 25 wt% Sty coatings. The range measured on 25% styrene coatings was ~ 400 nm, which is nearly five-times greater than the range measured on EB1360 and on 5% Sty. Therefore, it was concluded that surface wrinkling had a comparatively greater effect on raising τ_{ice} than v_e did on lowering it. It is important to note that Golovin *et al.* explored cross-link density on the order of 10 to 1000 mol·m⁻³ in the work where they observed significant decreases in ice adhesion. Since the observed cross-link densities in the present work are much higher and cover a narrower range, we do not observe the same decreases in ice adhesion.

A major goal of this work was to measure changes in durability of the UV-cured coatings with the inclusion of comonomer into the polymer networks. Three series of coatings were subjected to successive deicing experiments to examine how ice adhesion changed over time (**Figure 4.6**).

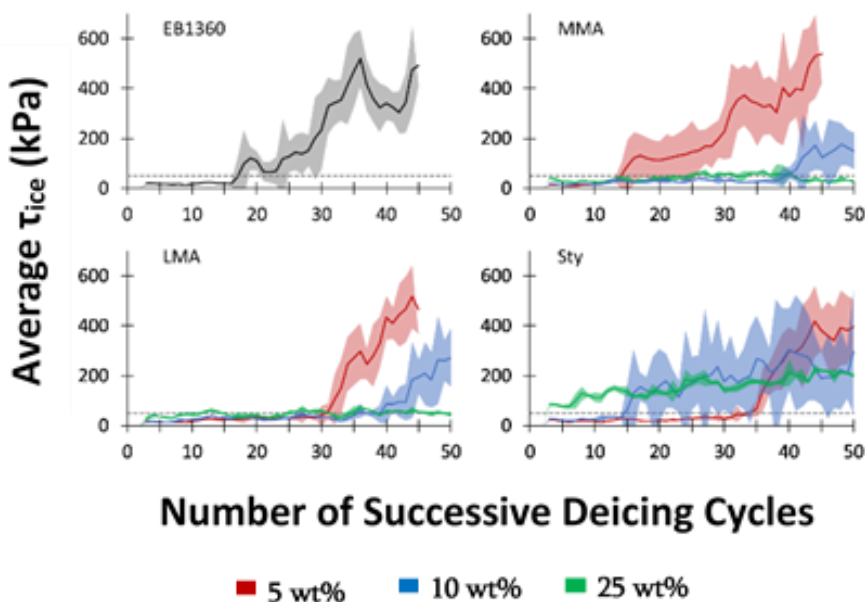


Figure 4.6: Plots showing ice adhesion over time measure on prepared copolymer networks. Red, blue, and green data series represent 5, 10 and 25 wt% comonomer.

Plots of τ_{ice} against the number of deicing cycles imposed on samples of the three series, and on neat EB1360 show a drastic increase in τ_{ice} after ~15 deicing cycles on EB1360 containing no additives, with similar changes seen for the 5 wt% MMA. 5 wt% Sty and LMA coatings showed improved durability, with no significant increase in τ_{ice} . Increasing MMA and LMA proportions to 10 from 5 wt%, yielded a later onset of increased τ_{ice} , ~40 deicing cycles. When MMA or LMA content was further elevated, virtually no increase in ice adhesion was observed throughout testing, indicating icephobicity to at least 50 deicing cycles. The Sty-containing coatings showed different behavior than the others. 10 wt% styrene had a relatively early onset of high ice adhesion, around 15 cycles, and 25 wt% Sty coatings showed a gradual increase in ice adhesion over the course of testing from 113 to ~200 kPa. The hardness of these coatings was notably lower than for all the other coatings, which may have contributed to earlier onset of surface damage, yielding these findings.

During the deicing experiments, it was observed that an increase in ice adhesion was typically noted when visible damage on a coating had occurred, such as delamination

of the coating. Damage was tracked and plotted against ice adhesion and the number of deicing cycles to create durability plots (**Figure 4.7**).

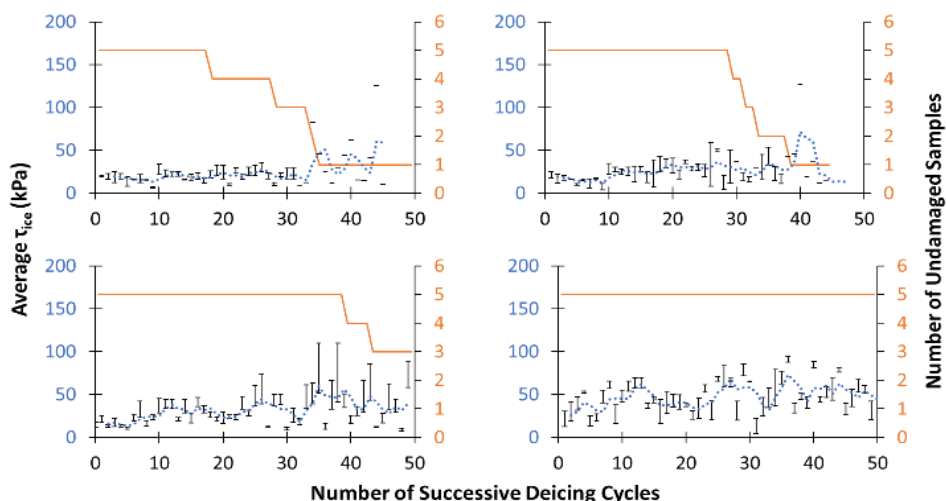


Figure 4.7: Plots showing durability of coatings to successive deicing tests. Samples visibly damaged from testing were removed from the complement as damage occurred. The average τ_{ice} values in blue were calculated from intact samples only, and the orange plot shows the number of samples with no visible damage.

Average ice adhesion on undamaged coatings is plotted along the left vertical axis, and the right vertical axis notes the number of samples remaining undamaged during testing. Taken together these data show that increased comonomer content in the networks decreased the extent to which the coatings were damaged. Coatings containing 5 wt% comonomer are damaged like of 100% EB1360, whereas no visible damage was observed on the 25 wt% MMA or LMA coatings. Fluctuations in ice adhesion on the coatings were attributed to microscale damage on the surfaces, but no obvious damage could be found when imaging the repeatedly iced/deiced surfaces using SEM. Observing enhanced durability of the coatings with the inclusion of additional comonomer presents an interesting trade-off: increased comonomer content increased the strength of ice adhesion on these materials, but also improved their durability. Therefore, preparing these types of coatings should be viewed as system-specific. If a case like the MMA-containing copolymer networks is observed, where increased comonomer content gave a modest increase in ice adhesion, but showed a comparatively large improvement in durability, a coating with maximum

comonomer content may be desired. Conversely, if a substantial increase in ice adhesion is paired with only a middling improvement in durability, such formulations would likely be ignored. The role of the wrinkles forming on the coatings should be considered, as well. Increasing comonomer content increased the durability, ice adhesion, and wrinkling of the prepared coatings. Surface wrinkling clearly increases ice adhesion, and likely also influence durability.

4.4 Conclusions

Ice accumulation on infrastructure, machinery, and appliances remains a significant engineering challenge. Icephobic coatings were successfully created, based upon a UV-curable siloxane resin with different comonomers, methyl and lauryl methacrylate, and styrene. Increasing comonomer content decreased cross-link density while also causing an increase in ice adhesion. Nevertheless, the materials proved to have promising durability, with coatings withstanding 50 deicing cycles with no visible damage occurring and while maintaining ice adhesion ~ 50 kPa. In future work, we aim to explore a broader range of curing conditions, with a wider range of cross-link densities to determine if trends reported here extend to more lightly cross-linked materials.

4.5 References Cited

1. Laforte, J. L.; Allaire, M. A.; Laflamme, J., State-of-the-art on power line de-icing. *Atmos. Res.* **1998**, *46*, 143.
2. Marilla Steuter-Martin, L. P., Looking back on the 1998 ice storm 20 years later. In *Photos*, CBC News: 2018.
3. Kreder, M. J.; Alvarenga, J.; Kim, P.; Aizenberg, J., Design of anti-icing surfaces: smooth, textured or slippery? *Nat. Rev. Mater.* **2016**, *1*, 15003.
4. Jin, S.; Liu, J.; Lv, J.; Wu, S.; Wang, J., Interfacial Materials for Anti-Icing: Beyond Superhydrophobic Surfaces. *Chemistry – An Asian Journal* **2018**, *13*, 1406.
5. Ramachandran, R.; Nosonovsky, M., Surface micro/nanotopography, wetting properties and the potential for biomimetic icephobicity of skunk cabbage *Symplocarpus foetidus*. *Soft Matter* **2014**, *10*, 7797.
6. Golovin, K.; Kobaku, S. P. R.; Lee, D. H.; DiLoreto, E. T.; Mabry, J. M.; Tuteja, A., Designing durable icephobic surfaces. *Sci. Adv.* **2016**, *2*.

7. Dou, R.; Chen, J.; Zhang, Y.; Wang, X.; Cui, D.; Song, Y.; Jiang, L.; Wang, J., Anti-icing Coating with an Aqueous Lubricating Layer. *ACS Appl. Mater. Interfaces* **2014**, *6*, 6998.
8. Frankenstein, S.; Tuthill, A. M., Ice Adhesion to Locks and Dams: Past Work; Future Directions? *J. Cold Regions Eng.* **2002**, *16*, 83.
9. Cassie, A. B. D.; Baxter, S., Wettability of porous surfaces. *J. Chem. Soc. FaradayTrans.* **1944**, *40*, 546.
10. Srinivas Begaluru Subramanyam, V. K., Jurgen Ruhe, Kripa K. Varanasi, Low Ice Adhesion on Nano-Textured Superhydrophobic Surfaces under Supersaturated Conditions. *ACS Appl. Mater. Interfaces* **2016**, *8*, 12583.
11. Quéré, D., Wetting and Roughness. *Annu. Rev. Mater. Res.* **2008**, *38*, 71.
12. Chen, J.; Liu, J.; He, M.; Li, K.; Cui, D.; Zhang, Q.; Zeng, X.; Zhang, Y.; Wang, J.; Song, Y., Superhydrophobic surfaces cannot reduce ice adhesion. *Appl. Phys. Lett.* **2012**, *101*, 111603.
13. Wang, Y.; Li, M.; Lv, T.; Wang, Q.; Chen, Q.; Ding, J., Influence of different chemical modifications on the icephobic properties of superhydrophobic surfaces in a condensate environment. *J. Mater. Chem. A* **2015**, *3*, 4967.
14. Jung, S.; Dorrestijn, M.; Raps, D.; Das, A.; Megaridis, C. M.; Poulikakos, D., Are Superhydrophobic Surfaces Best for Icephobicity? *Langmuir* **2011**, *27*, 3059.
15. Yeong, Y. H.; Milionis, A.; Loth, E.; Sokhey, J.; Lambourne, A., Atmospheric Ice Adhesion on Water-Repellent Coatings: Wetting and Surface Topology Effects. *Langmuir* **2015**, *31*, 13107.
16. Wang, N.; Xiong, D.; Pan, S.; Wang, K.; Shi, Y.; Deng, Y., Robust superhydrophobic coating and the anti-icing properties of its lubricants-infused-composite surface under condensing condition. *New J. Chem.* **2017**, *41*, 1846.
17. Golovin, K.; Dhyani, A.; Thouless, M. D.; Tuteja, A., Low-interfacial toughness materials for effective large-scale deicing. *Science* **2019**, *364*, 371.
18. Niemelä-Anttonen, H.; Koivuluoto, H.; Tuominen, M.; Teisala, H.; Juuti, P.; Haapanen, J.; Harra, J.; Stenroos, C.; Lahti, J.; Kuusipalo, J.; Mäkelä, J. M.; Vuoristo, P., Icephobicity of Slippery Liquid Infused Porous Surfaces under Multiple Freeze–Thaw and Ice Accretion–Detachment Cycles. *Adv. Mater. Interfaces* **2018**, *5*, 1800828.
19. Kim, P.; Wong, T.-S.; Alvarenga, J.; Kreder, M. J.; Adorno-Martinez, W. E.; Aizenberg, J., Liquid-Infused Nanostructured Surfaces with Extreme Anti-Ice and Anti-Frost Performance. *ACS Nano* **2012**, *6*, 6569.

20. Wang, T.; Zheng, Y.; Raji, A.-R. O.; Li, Y.; Sikkema, W. K. A.; Tour, J. M., Passive Anti-Icing and Active Deicing Films. *ACS Appl. Mater. Interfaces* **2016**, *8*, 14169.
21. Zhu, L.; Xue, J.; Wang, Y.; Chen, Q.; Ding, J.; Wang, Q., Ice-phobic Coatings Based on Silicon-Oil-Infused Polydimethylsiloxane. *ACS Appl. Mater. Interfaces* **2013**, *5*, 4053.
22. Urata, C.; Dunderdale, G. J.; England, M. W.; Hozumi, A., Self-lubricating organogels (SLUGs) with exceptional syneresis-induced anti-sticking properties against viscous emulsions and ices. *J. Mater. Chem. A* **2015**, *3*, 12626.
23. Wang, Y.; Yao, X.; Chen, J.; He, Z.; Liu, J.; Li, Q.; Wang, J.; Jiang, L., Organogel as durable anti-icing coatings. *SCMs* **2015**, *58*, 559.
24. Jellinek, H. H. G.; Kachi, H.; Kittaka, S.; Lee, M.; Yokota, R., Ice releasing block-copolymer coatings. *Colloid. Polym. Sci.* **1978**, *256*, 544.
25. Li, X.; Li, Y.; Ren, L.; Zhu, K.; Zhao, Y.; Yuan, X., Self-crosslinking coatings of fluorinated polysiloxanes with enhanced icephobicity. *Thin Solid Films* **2017**, *639*, 113.
26. Key, B. D.; Howell, R. D.; Criddle, C. S., Fluorinated Organics in the Biosphere. *Environ. Sci. Technol.* **1997**, *31*, 2445.
27. Gao, J.; Martin, A.; Yatvin, J.; White, E.; Locklin, J., Permanently grafted icephobic nanocomposites with high abrasion resistance. *J. Mater. Chem. A* **2016**, *4*, 11719.
28. Coady, M. J.; Wood, M.; Wallace, G. Q.; Nielsen, K. E.; Kietzig, A.-M.; Lagugné-Labarthe, F.; Ragogna, P. J., Icephobic Behavior of UV-Cured Polymer Networks Incorporated into Slippery Lubricant-Infused Porous Surfaces: Improving SLIPS Durability. *ACS Appl. Mater. Interfaces* **2018**, *10*, 2890.
29. Standard Test Method for Determination of Percent Devulcanization of Crumb Rubber Based on Crosslink Density. 2018.
30. He, Z.; Vågenes, E. T.; Delabahan, C.; He, J.; Zhang, Z., Room Temperature Characteristics of Polymer-Based Low Ice Adhesion Surfaces. *Sci. Rep.* **2017**, *7*, 42181.
31. Chandra, D.; Crosby, A. J., Self-Wrinkling of UV-Cured Polymer Films. *Adv. Mater.* **2011**, *23*, 3441.
32. Schubert, R.; Scherzer, T.; Hinkefuss, M.; Marquardt, B.; Vogel, J.; Buchmeiser, M. R., VUV-induced micro-folding of acrylate-based coatings: 1. Real-time methods for the determination of the micro-folding kinetics. *Surf. Coat. Technol.* **2009**, *203*, 1844.

Chapter 5

5 Creating Arrays of film/substrate detachments as a means of lowering ice adhesion strength

5.1 Introduction

Combating ice accumulation is a challenge in a number of areas, ranging from personal and industrial appliances, marine and aerospace vehicles, to public infrastructure. In order to relieve the annoyance, cost, and danger of ice in these areas, a growing number of researchers are conducting studies in fundamental and applied aspects of the icing problem.¹ Three principle design strategies of interfacial materials for anti-icing have been outlined:² (i) Water may be rapidly removed from a surface by using low surface energy or textured materials like superhydrophobic surfaces; (ii) ice nucleation or propagation may be discouraged by controlling surface chemistry and architecture; and (iii) ice adhesion strength may be greatly reduced by careful selection of coating materials based upon their physicochemical properties. ‘Icephobic’ materials utilize this third methodology, reducing the adhesion strength of surfaces to below 100 kPa, with passive delamination occurring ~20 kPa.^{1, 3-4} Recent discussion surrounding icephobic materials has stressed the importance of durability, owing both to the vigorous nature applications like on airplanes and wind turbines, and the long-term basis desired for coating use.^{3, 5-7} Regardless of which design philosophy they follow, many materials do not possess the high durability required for reliable icephobicity. It is important that new, more durable materials be actively pursued, or that methods of decreasing ice adhesion to already durable materials be found.

Golovin and coworkers have recently published groundbreaking work demonstrating ways to decrease ice adhesion strength (τ_{ice})³ and interfacial toughness (Γ)⁸ on a variety of commercially-relevant polymers by changing the cross-link density of the materials, altering the thickness of the coatings, and by incorporating lubricants / plasticizers. Their most recent publication presents coatings which shed ice under low flexion, owing to fracture resulting from limited interfacial toughness. Flexibility has long been accepted as an important material characteristic for ice repellency,⁹⁻¹⁰ in part leading to the widespread use of polysiloxanes and other elastomers as icephobic coatings,^{3, 7}

inspiring research involving lubricated materials,¹¹⁻¹² and the recent use of flexible surface structures by Liu *et al.*¹³ The use of widely available materials is beneficial because of the huge scale on which anti-icing is of interest, such as on power transmission lines¹⁴ and nascent wind turbines with blades over 100 m long.¹⁵ However, many flexible materials are not durable. Polysiloxanes are a good example because although they exhibit low ice adhesion characteristics, they also possess poor abrasion / erosion characteristics and so are unsuitable for applications where they encounter particulates at high velocity (e.g. sand or precipitation at high velocity).¹⁶ It is therefore of interest to find methods of either (a) making icephobic materials more durable, or (b) increasing the flexibility / icephobicity of already durable materials. While performing experiments toward the former, we came across an interesting example highlighting the latter.

This chapter describes the serendipitous discovery and experimentation of a method to reduce ice adhesion to commercial adhesive films (i.e. tape). During previous explorations of icephobic polymer films, we found that ice adhesion on a film greatly decreased when ice growth occurred on top of an area where a detachment between the film and substrate existed (**Figure 5.1**).

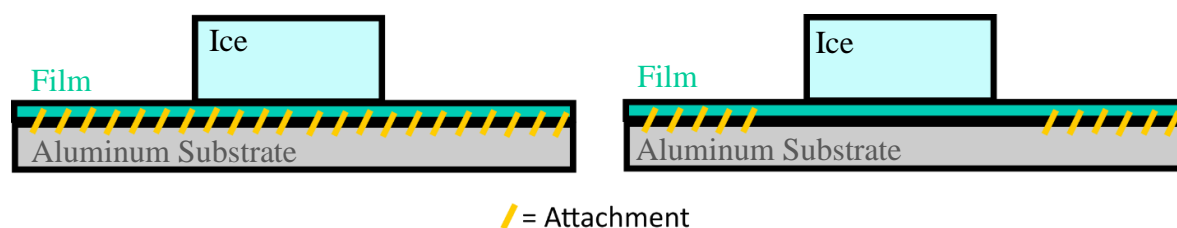


Figure 5.1: Ice grown on a film (*left*) completely (normally) attached to the substrate, or (*right*) partially detached from the substrate.

This finding was tested through a cursory experiment, which showed that ice adhesion strength (τ_{ice}) was reduced in this situation on any film tested (**Figure 5.2**).

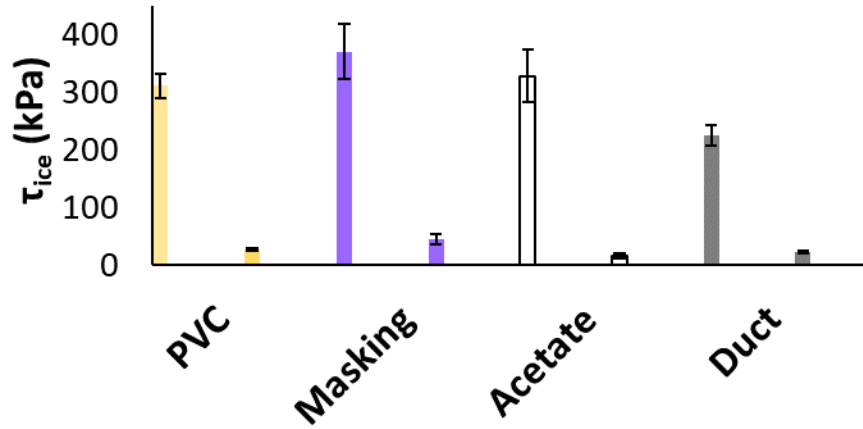


Figure 5.2: Ice adhesion τ_{ice} measured on commercial adhesive films. The right column of each series denotes films detached from the substrate under the iced area. ($A_{ice} = 0.28 \text{ cm}^2$, $A_{det} = 1 \text{ cm}^2$).

The effects of 1 cm^2 detachments on ice adhesion to four different commercial tapes: electrical, masking, Scotch (acetate), and duct tape were pronounced: adhesion on all four of the tested films was reduced by approximately one order of magnitude. This is caused by increased flexibility of the material when it is free from the surface. We were unaware of any discussion surrounding this type of methodology for reducing ice adhesion. It is hypothesized that by creating an array of smaller detachments, a decrease in τ_{ice} may be observed over areas of multiple centimeters. In this context we embarked on an exploration of ice adhesion on detached films using a simple screen-printing method, followed by durability testing through abrasion and sand-erosion. Our results display a novel approach for decreasing ice adhesion on commercially available films, using materials which do not seem immediately interesting as icephobic surfaces. This work will expand the existing library of icephobic materials to those with considerably higher durability. Some expected challenges in developing these type of materials are addressed.

5.2 Experimental

Scotch® Magic Tape, Super 33+™ electrical tape, VentureClad™ 1577-CW insulation jacketing tape, 501+ purple masking tape, 2929 general use duct tape, and 9576 double coated tape were received from 3M Canada. Where removal of adhesive was

required, toluene (99.9 %) purchased from Fisher Chemical was used. Chromatech PL Emulsion and screen-printing mesh were purchased from thescreenprintstore.ca. MAPEI Ultrabond ECO 360 was donated by Deacon Flooring Inc. in London, Ontario. Aluminum 6061 coupons were cut of stock purchased from McMaster Carr. All coupons were degreased with isopropanol prior to use. Detached films for ice adhesion on singular detachments, abrasion, and sand erosion tests were prepared by cutting out millimeter-scale squares from 9567 double-sided tape that had been attached to aluminum coupons. The backing was peeled from the tape, and the sample was pressed to the under-side of the commercial films, from which adhesive had been removed. The surfaces were subsequently cleaned with isopropanol. For screen printing, 125-mesh screens were used. CHROMA/TECH® PL Emulsion was built up on the screens into five layers using the method outlined in the data sheet. Stencils were created on transparencies using Inkscape. Screens were exposed in a UV photochemical cabinet for 1 min, and subsequently developed in a wash-out sink. MAPEI Ultrabond ECO 360 was screened onto the commercial films from which the original adhesive had been removed. ECO 360 was left to set for ~15 min before the films were attached to the 15 x 5 cm aluminum coupons. Ice adhesion measurements of singular detachments were done in the Cold Weather Biome at Western's Biotron Facility, using our previously described centrifuge method.¹⁷ Statistical ice adhesion measurements of large-scale patterns were performed using a Slip-Peel tester donated by 3M Canada. 1 cm² sections of cuvettes were placed on the substrate in random positions, generated using Inkscape's "randomize centres" function. "Unclump" was used to prevent overlap of the structures. Abrasion testing was done using a Taber ® Model 503 Standard Abrasion Tester (Teledyne Taber), generally following the procedure outlined in ASTM D4060-14 'Standard Method for Abrasion Resistance of Organic Coatings by the Taber Abraser'.¹⁸ A load of 1000 g per wheel and Calibrase ® CS-17 wheels were used to perform the tests and S-11 abrasive disks were used for resurfacing the wheels every 500 cycles / when beginning a new sample. Changes in mass were measured using a four-point balance. Sand erosion testing was done at 3M Center in Maplewood, Minnesota. 46 grit Al₂O₃ was used as the erosive medium and was blasted onto the film surfaces from ~ 8cm, at a pressure of 70 psi. This method is based upon an ASTM erosion test method.¹⁹ The mass of sand required to break through the films was recorded as the change in mass of

total sand. Any notes on data treatment and additional images of eroded / abraded surfaces can be found in **Appendix D**.

5.3 Results and Discussion

Following the first set of experiments where the reproducibility of τ_{ice} reduction on detached areas was confirmed, further probing of this phenomenon was done by varying the size of the detachment relative to the iced area (**Figure 5.3**).

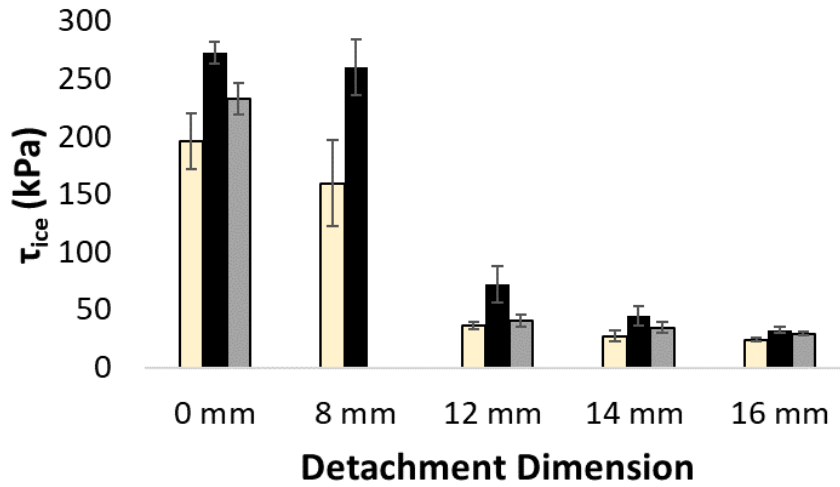


Figure 5.3: Ice adhesion (τ_{ice}) on commercial films with varied area of detachment between the film and substrate ($A_{ice} = 1 \text{ cm}^2$).

Changes in τ_{ice} occurred when the dimensions of a square detachment area were changed relative to the iced area. It was observed that larger relative detachments had greatly reduced ice adhesion in comparison with smaller detachments, but that there was little variation in τ_{ice} once the size of the detachment was greater than the iced area (in this case, greater than 1 cm^2). This agrees with the hypothesis that lower ice adhesion is promoted by flexibility of the film. If the detached area is smaller than the iced area, flexion of the film away from the substrate is significant. However, when the iced area is greater than the detached area, ice imposes rigidity on the surface, reducing the effect of a more flexible film. Film/substrate detachments therefore favor ice delamination when they are incompletely covered in ice. From a practical standpoint, singular film detachments are not interesting for reducing ice adhesion over large areas; creating very large detachments

effectively would lead to separation. Arrays of detachments were created to gauge their effect on ice adhesion on various commercial films.

Adhesive was removed from the films of interest, followed by screen printing of Ultrabond ECO 360 onto the back side of the films, yielding grid patterns of pressure sensitive adhesive (**Figure 5.4a**).

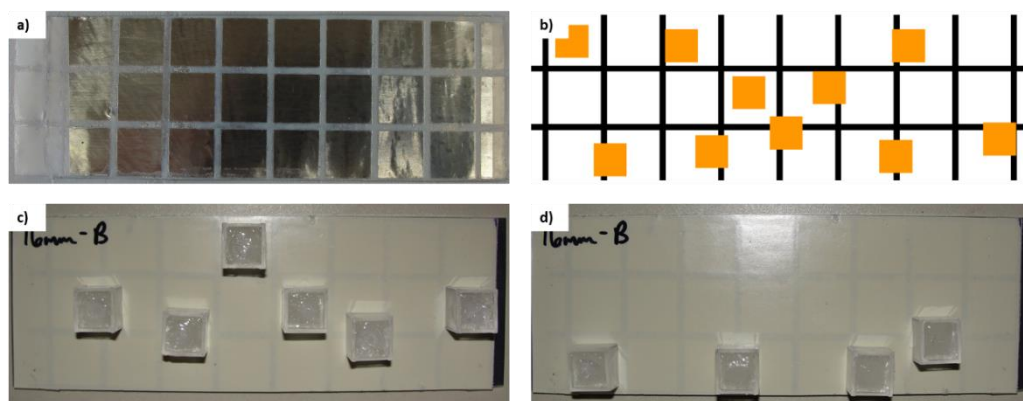


Figure 5.4: a) Image of ECO 360 applied to underside of 1577CW film, b) Pattern of ice column positions generated by Inkscape, c) and d) Ice columns corresponding to the first six and four remaining positions on the generated pattern.

This adhesive was left to set, and then pressed on to aluminum substrates, yielding periodically detached arrays over a 5 cm by 15 cm area. Next, ice adhesion on the materials was measured by creating randomized arrays of 1 cm² areas on top of the corresponding grids (**Figure 5.4b**). Sections were cut from cuvettes to serve as molds for the ice, and to give a defined area of attachment. These cuvettes were aligned on the surfaces to resemble the patterns generated by Inkscape (**Figure 5.4 c/d**). Some adjustments had to be made with the cuvette positions, but care was taken to ensure that overlap with gridlines occurred where appropriate. The τ_{ice} value measured for a given column was related to its position relative to the underlying adhesive grid. Columns overlapping with the intersection of gridlines had ice adhesion approximately the same as measurements made on normally attached films, while ice columns with no gridline overlap showed very low τ_{ice} values, similar to those measured in the initial singular detachment experiments. By examining the

average τ_{ice} values on the detached arrays, it is seen that larger detachments still yield lower ice adhesion (**Figure 5.5**)

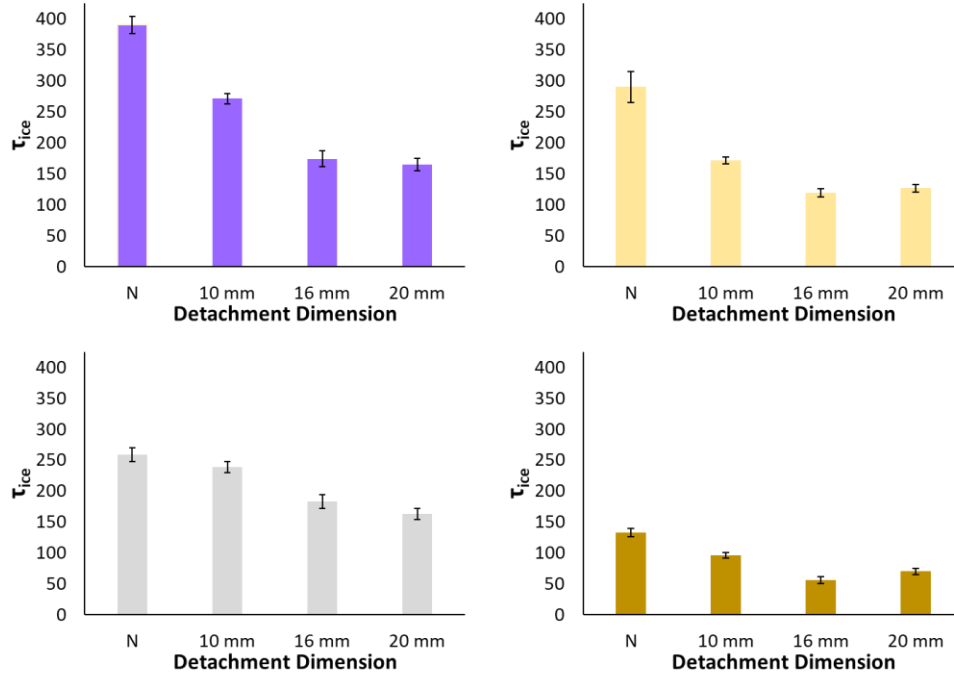


Figure 5.5: Plots of ice adhesion measured on arrays of varying detachment size for: a) Masking tape, b) PVC tape, c) Aluminum shielding tape, and d) Skived PTFE film.

Masking, PVC, insulation jacketing tape, and PTFE skived film were selected because of their varying surface chemistries, and not necessarily and all showed decreased τ_{ice} as detachment sizes increased. Little difference in τ_{ice} was observed between the 16- and 20-mm detached arrays, although the τ_{ice} values on these arrays were less than 50 % of the values measured on normally attached films: τ_{ice} decreased to 165 ± 10 kPa from 390 ± 14 kPa on masking tape, 120 ± 7 from 290 ± 25 on PVC tape, and 55 ± 6 from 133 ± 7 kPa on PTFE film. Aluminum insulating jacket tape showed the smallest reduction in τ_{ice} to 163 ± 9 kPa from 259 ± 11 kPa, which is due to it being the stiffest of the films measured. It is the only film that maintains its shape when bent, as would be expected of a thick aluminum foil. The effect of larger detachment areas on lower τ_{ice} is two-fold: i) Larger areas mean that a given film can flex a greater distance away from the substrate, which should allow for ice release;⁸ ii) They decrease the probability of ice columns overlapping with the adhesive gridlines, which were observed to give nominal τ_{ice} values. A reducing

in τ_{ice} on films varying significantly in their surface chemistry can therefore be achieved with the only modification being selective application of pressure sensitive adhesive. The question remained that if larger detachment size gives greater reduction in τ_{ice} , is there a reason not to maximize detachments in order to reduce ice adhesion? Focus was thus turned to durability which is a critically important parameter in the development of icephobic materials.

Abrasion testing was conducted using the same materials previously outlined with detachments arranged in the path of the abrasive wheels (see **Appendix D**). It was hypothesized that wear would be focused near the center of the detachments, leading to tearing of the film or increased mass loss. The mass-loss of films throughout the course of abrasion was measured, showing no significant effect of detachment size on this aspect of durability (**Figure 5.6**).

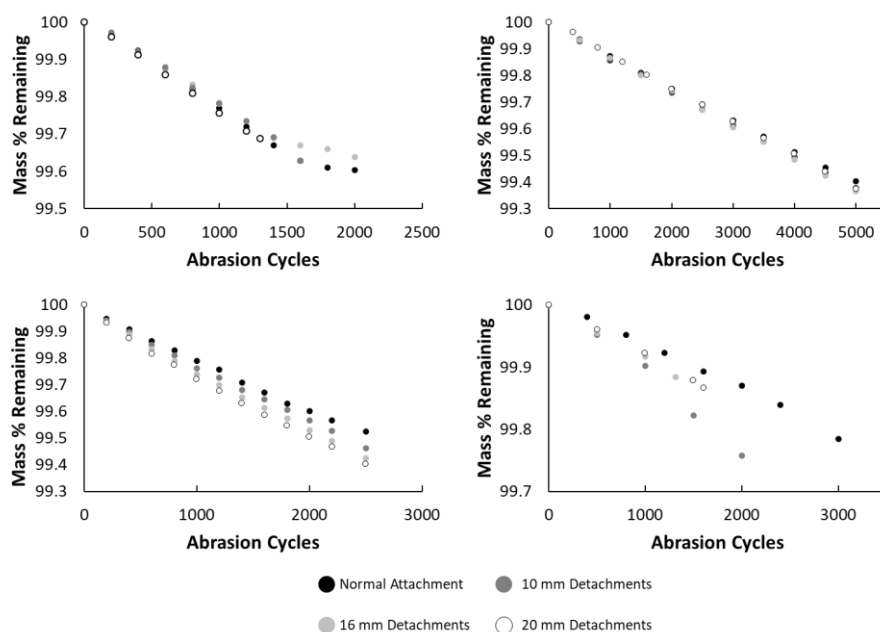


Figure 5.6: Plots showing the change in relative sample masses for films with varying detachment size: a) masking tape, b) PVC tape, c) jacketing tape, and d) PTFE skived film.

The masking and PVC tapes showed close agreement in mass loss between the normally attached films, and those with detachments of any size. Aluminum jacketing tape showed

a trend of mildly increasing rates of mass-loss as detachment size increased. This is likely a characteristic of the aluminum coating. Similar observations were made on PTFE skived film in that detached films showed greater mass loss than normally attached films, although a tidy trend was not observed. This lack of trend is the result of surface wrinkles resulting from the adhesive removal process that led to less predictable material removal. Photos of the PVC films taken during testing are shown in **Figure 5.7**, showing that abrasive damage tends to prevail around the edges of the detachments, contrary to the hypothesis of damage occurring on the area of the detachments themselves.

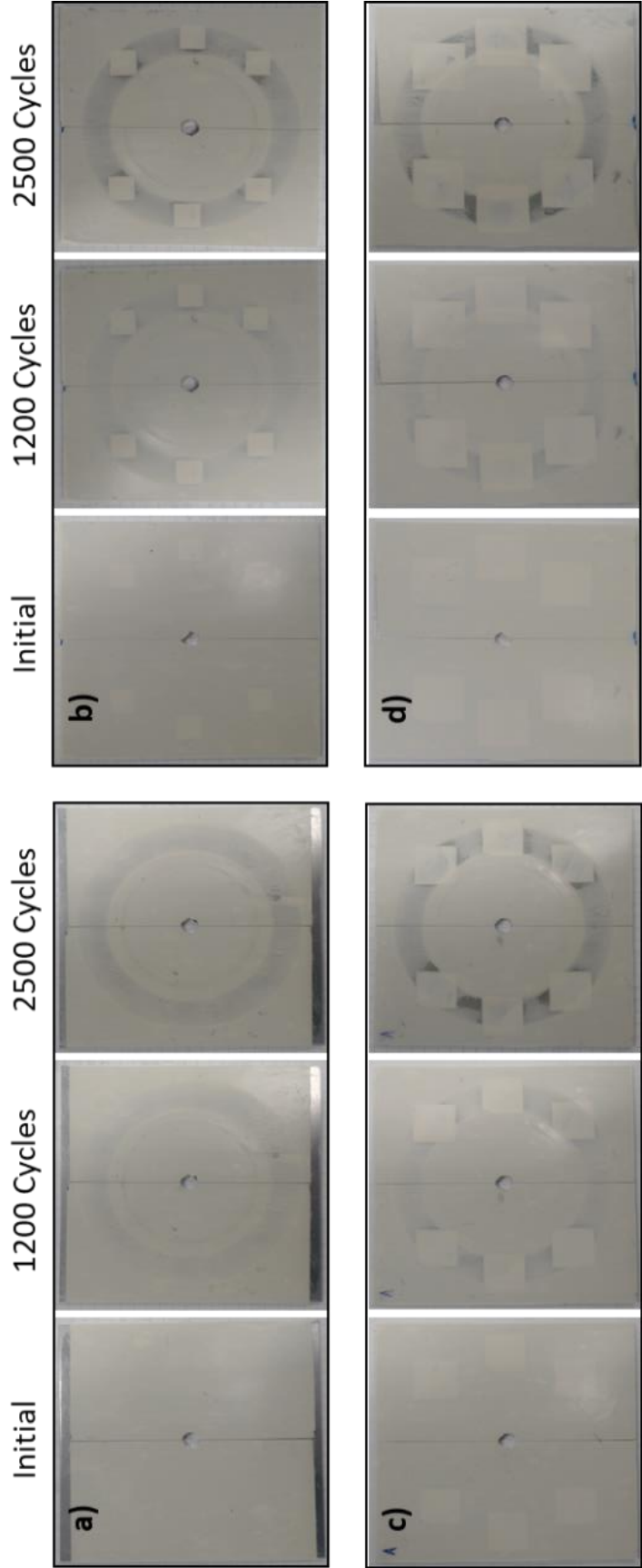


Figure 5.7: Photos showing surface damage to a) normally attached PVC film, and films with b) 10 mm, c) 16 mm, and d) 20 mm detachments in the path of the abrasive wheels.

Little damage was observed on the detached areas, and significant tearing of the films did not occur except in the case of masking tape. Tearing of the tape was not observed until most of the tape backing had worn down to the underlying adhesive (**Appendix D**). These durability results were surprising, as there appeared not to be a significant change in durability resulting from film detachment. Particle erosion was selected as a second method of durability testing to further probe changes in durability that might be caused by film detachments. Particle erosion is an important test for icephobic materials, as sand and ice particles will be encountered in the atmosphere.¹⁶ (Note: the jacketing tape was not used due to thin backing layer being eroded rapidly by the extreme conditions).

The mass of alumina required to break through the films was measured to gauge the effects of detachment size on durability (**Figure 5.8 a/b**).

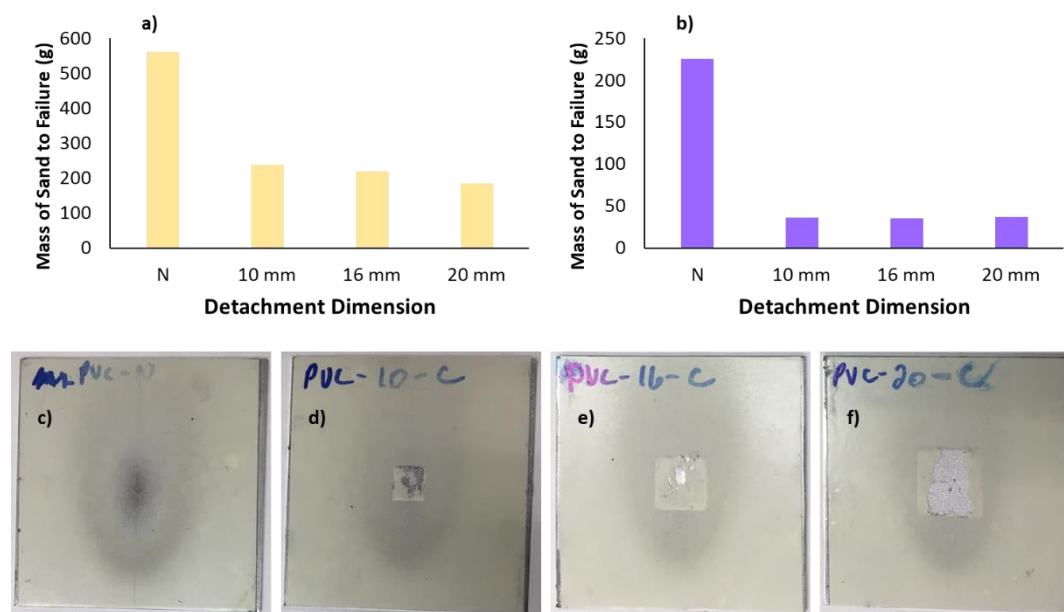


Figure 5.8: Plots showing Al_2O_3 required to break through a) PVC film and b) masking tape with different detachment sizes. Photos showing surface damage to a) normally attached PVC film, and films with b) 10 mm, c) 16 mm, and d) 20 mm detachments in the path of the Al_2O_3 particles.

It was observed that a detachment of any size on any film led to an immediate and significant decrease in the amount of alumina required to break through both films. The mass of alumina required to break through the film decreased to ~ 200 g from > 500 g for the PVC film, and to < 50 g from ~ 200 g for the masking tape. This indicates that particulates can easily puncture films when unattached to their substrate, leading to early failure. It is worth noting that this test is very intense, and beyond the designed range for both materials. When a film is securely adhered to a substrate, energy from particle impact is partially absorbed by the substrate, helping to keep the surface intact. When the coating is detached, this energy is likely dispersed in the film as deformation / tearing, which was observed. Therefore, without further modification films applied to surfaces in the manner described here likely do not exhibit the durability necessary for extreme applications such as airfoil or wind turbines. Further modification of the films / architecture may yield improved durability.

5.4 Conclusions

Developing more durable icephobic materials is a critical goal of anti-icing research. On the other hand, finding methods of making well-established, durable materials more icephobic might be an interesting route to reaching this goal. In this work an example of the latter is outlined, whereby creating arrays of detachments between the substrate and the film leads to lower ice adhesion. Singular detachments showed the promise of this method, lowering τ_{ice} on various films by one order of magnitude. Creating arrays of detachments lowered the average τ_{ice} to half that measured on normally attached films. Two tests of durability were used to probe the films. While no major change in mass-loss was observed from abrasion, increased wear was observed around the edges of the detachments, leading to eventual tearing once the backing had worn down to the adhesive layer. A significant decrease in durability was observed during particle erosion. The presence of any detachment between the film and substrate led to puncturing of the film. This work presents a new method of lowering ice adhesion, and clearly outlines the expectant challenges of further development.

5.5 References Cited

1. Kreder, M. J.; Alvarenga, J.; Kim, P.; Aizenberg, J., Design of anti-icing surfaces: smooth, textured or slippery? *Nat. Rev. Mater.* **2016**, *1*, 15003.
2. Jin, S.; Liu, J.; Lv, J.; Wu, S.; Wang, J., Interfacial Materials for Anti-Icing: Beyond Superhydrophobic Surfaces. *Chemistry – An Asian Journal* **2018**, *13*, 1406.
3. Golovin, K.; Kobaku, S. P. R.; Lee, D. H.; DiLoreto, E. T.; Mabry, J. M.; Tuteja, A., Designing durable icephobic surfaces. *Sci. Adv.* **2016**, *2*.
4. Dou, R.; Chen, J.; Zhang, Y.; Wang, X.; Cui, D.; Song, Y.; Jiang, L.; Wang, J., Anti-icing Coating with an Aqueous Lubricating Layer. *ACS Appl. Mater. Interfaces* **2014**, *6*, 6998.
5. Irajizad, P.; Al-Bayati, A.; Eslami, B.; Shafquat, T.; Nazari, M.; Jafari, P.; Kashyap, V.; Masoudi, A.; Araya, D.; Ghasemi, H., Stress-localized durable icephobic surfaces. *Mater. Horiz.* **2019**, *6*, 758.
6. Zhuo, Y.; Håkonsen, V.; He, Z.; Xiao, S.; He, J.; Zhang, Z., Enhancing the Mechanical Durability of Icephobic Surfaces by Introducing Autonomous Self-Healing Function. *ACS Appl. Mater. Interfaces* **2018**, *10*, 11972.
7. Sojoudi, H.; Wang, M.; Boscher, N. D.; McKinley, G. H.; Gleason, K. K., Durable and scalable icephobic surfaces: similarities and distinctions from superhydrophobic surfaces. *Soft Matter* **2016**, *12*, 1938.
8. Golovin, K.; Dhyani, A.; Thouless, M. D.; Tuteja, A., Low–interfacial toughness materials for effective large-scale deicing. *Science* **2019**, *364*, 371.
9. Sewell, J. H. *The Design and Development of New Ice-Shedding Coatings*; United States Army Aviation Engineering Flight Activity: California, 1974; pp 37.
10. Vasileiou, T.; Schutzius, T. M.; Poulikakos, D., Imparting Icephobicity with Substrate Flexibility. *Langmuir* **2017**, *33*, 6708.
11. Kim, P.; Wong, T.-S.; Alvarenga, J.; Kreder, M. J.; Adorno-Martinez, W. E.; Aizenberg, J., Liquid-Infused Nanostructured Surfaces with Extreme Anti-Ice and Anti-Frost Performance. *ACS Nano* **2012**, *6*, 6569.
12. Zhu, L.; Xue, J.; Wang, Y.; Chen, Q.; Ding, J.; Wang, Q., Ice-phobic Coatings Based on Silicon-Oil-Infused Polydimethylsiloxane. *ACS Appl. Mater. Interfaces* **2013**, *5*, 4053.
13. Liu, X.; Zhao, H.; Li, P.; Pang, Y.; Fan, Y.; Zhang, B.; Wang, L.; Zheng, Y.; Wang, Z., Robust Icephobic Performance of Flexible Needles. *ChemNanoMat* **2019**, *5*, 175.

14. Volat, C.; Farzaneh, M.; Leblond, A., *De-icing/Anti-icing Techniques for Power Lines: Current Methods and Future Direction*. 2005.
15. Kellner, T. A Towering Achievement: This Summer In Holland, GE Will Build The World's Largest Wind Turbine. <https://www.ge.com/reports/about/> (accessed July 24).
16. Sojoudi, H.; Arabnejad, H.; Raiyan, A.; Shirazi, S. A.; McKinley, G. H.; Gleason, K. K., Scalable and durable polymeric icephobic and hydrate-phobic coatings. *Soft Matter* **2018**, *14*, 3443.
17. Coady, M. J.; Wood, M.; Wallace, G. Q.; Nielsen, K. E.; Kietzig, A.-M.; Lagugné-Labarhet, F.; Ragogna, P. J., Icephobic Behavior of UV-Cured Polymer Networks Incorporated into Slippery Lubricant-Infused Porous Surfaces: Improving SLIPS Durability. *ACS Appl. Mater. Interfaces* **2018**, *10*, 2890.
18. Standard Test Method for Abrasion Resistance of Organic Coatings by the Taber Abraser.
19. Standard Test Method for Conducting Erosion Tests by Solid Particle Impingement Using Gas Jets.

Chapter 6

6 Summary, Conclusions and Future Work

6.1 Summary and Conclusions

This dissertation discusses the unique nature of ice adhesion to structural surfaces and highlights the material properties that can be exploited to decrease the strength with which ice adheres to these surfaces through the use of coatings. Chapters two through five demonstrate effective methods of modifying materials towards this end, with a focus on improving their durability.

Chapter Two details our effort at making state-of-the art icephobic materials more durable. Slippery lubricant-infused porous surfaces (SLIPS) have been used by others as effective anti-icing and anti-frosting surfaces but had notably poor durability. The loss of interfacial oil was observed after mild abrasion, or after one deicing event. By incorporating a UV-curable resin, lubricant retention and icephobic character ($\tau_{ice} < 50$ kPa) was stabilized for more than 10 deicing cycles. Results obtained during this first exploration were exciting and of interest to the community, though ultimately the degree of durability was still too low for vigorous applications such as on aircraft or wind turbines. Nonetheless, cross-linked SLIPS promising for applications as discussed by Kim *et al.* on heat exchangers.¹

Golovin *et al.* published work detailing highly durable icephobic materials based upon cured polymer networks with and without interfacial slippage.² Their observation of the relationship between τ_{ice} and cross-link density was intriguing, and so this avenue was pursued to develop more durable icephobic materials. The first of these approaches was done through collaborative work with the Kietzig group at McGill University and presented in Chapter Three.³ Drawbacks of superhydrophobic and patterned surfaces as a solution to ice accumulation have been discussed at length. Brittleness of micro-/nanostructures is a significant problem, as at small length scales metals, glasses, and ceramics can be easily damaged, removing any beneficial dewetting / deicing characteristics. The laser micromachining of polymeric materials presented an interesting opportunity to avoid this

concern by micromachining tough, flexible, cross-linked materials that were hypothesized to be less damage prone than more brittle materials. A fundamental study of the effects of material properties on experimental lasing parameters provided important insights, chiefly that material chemistry has little effect on material ablation threshold. This threshold was found to be related to the cross-link density of the material, with lower cross-link density leading to material removal with lower energy input. Unfortunately, the created materials did not have improved dewetting characteristics, and prohibitively long times were required to prepare areas large enough for ice adhesion testing. Reliable control over material cross-link density was achievable which in parallel with Golovin's work inspired the work presented in Chapter Four.

Ice adhesion was shown by Golovin and co-workers to decrease as cross-link density was lowered in a variety of polymers. While synthesizing and characterizing different urethane-based substrates used for lasing experiments in Chapter Three, we found that increasing proportions of comonomer with respect to a multifunctional polymer resin led to lower cross-link density. In Chapter Four we describe the use of this methodology to prepare copolymer networks of PDMS with methyl methacrylate, lauryl methacrylate, or styrene. Lower cross-link densities were attained through our method, but a decrease in τ_{ice} was not observed. Nevertheless, ice adhesion values near the 20 kPa threshold for passive deicing were measured, and improved material durability to repeated deicing tests was seen; the best-performing copolymer coatings maintained τ_{ice} values below 50 kPa for up to 50 deicing cycles. Our exploration points to surface wrinkling phenomena as a major source of increased ice adhesion in UV-cured materials, which is of great import to researchers interested in improving upon our results. The low τ_{ice} values also demonstrate that dry coatings remain promising despite the popularity of lubricated materials. Compared with materials presented in Chapter Two, those in this chapter have much higher durability. The durability of our materials improved from withstanding ~ 10 deicing cycles, to withstanding 50 deicing cycles, but even with a five-fold improvement these materials are not durable enough for commercial use. While performing successive deicing tests present in Chapter 4, we noted decreases in ice adhesion on different materials when partial delamination of the films occurred under the iced area. We performed experiments on

commercially available films designed to mimic this observation, which is described in Chapter 5.

High durability is a key characteristic in icephobic materials research. Many of the materials in recent discussion, such as those involving lubrication or delicate surface structure are not durable enough to be applied in such demanding applications as on wind turbines and aircraft. Polymer coatings are promising, due to the wide array of durable polymers already produced commercially. Chapter 5 outlines work done to decrease ice adhesion on these materials by creating arrays of detachments between films and the substrates. We observed that singular detachments between the substrate and a variety of commercial adhesive tapes could decrease τ_{ice} by approximately an order of magnitude, yielding ice adhesion around 20 kPa. Grids of detachments were subsequently created, which decreased the average ice adhesion on various materials by ~50%. It was found that ice growing over the adhered gridlines adhered with strength similar to when grown on uniformly attached films, and iced areas with little overlap of the gridlines showed much lower adhesion. This method showed promise for reducing ice adhesion on multiple centimeter areas. We tested the effects of detachment on durability by Taber abrasion, and by sand particle erosion. Although little change was seen in the abrasion testing, particle erosion showed that the presence of detachments between the film and substrate led to damage to the films. Our observations show that further development of this methodology is required, but it is promising for reducing ice adhesion on a variety of materials.

6.2 Future Work

6.2.1 Method Development

Western's capabilities for anti-icing experiments/measurements have not yet been fully detailed, except for the methods by which we conduct ice adhesion measurements.⁴ What sets Western apart from other institutions is that the instruments are fully housed in a temperature-controlled room, the Cold Weather Biome (CWB) at the Biotron. The CWB can be set to temperatures as low as $-40\text{ }^{\circ}\text{C}$.⁵ Methods involving Peltier stages and otherwise atmospheric conditions create concerns with the reproducibility of data, and how well it captures ice adhesion phenomena.⁶⁻¹⁰ Other methods require materials be exposed to outdoor weather conditions. This methodology does not guarantee consistency in results and is only viable four to five months of the year in the extreme case. The built-in water spraying apparatus in the CWB may be used to simulate winter weather conditions year-round.

6.2.1.1 Simulating Winter Weather in the Cold Weather Biome

Simulating wintry conditions in the CWB is interesting for measuring the accumulated mass of ice and snow on a variety of prepared surfaces to gauge their suitability as ice repellent surfaces. Equipment in the CWB includes (1) A network of misting heads to create mist / freezing rain; (2) A custom-made 'snow-gun';¹¹ (3) High-precision platform scales, which could be used with the end goal of measuring the mass accumulated ice over time. A new apparatus would be required to measure ice accretion, such as the one shown in **Figure 6.1**.

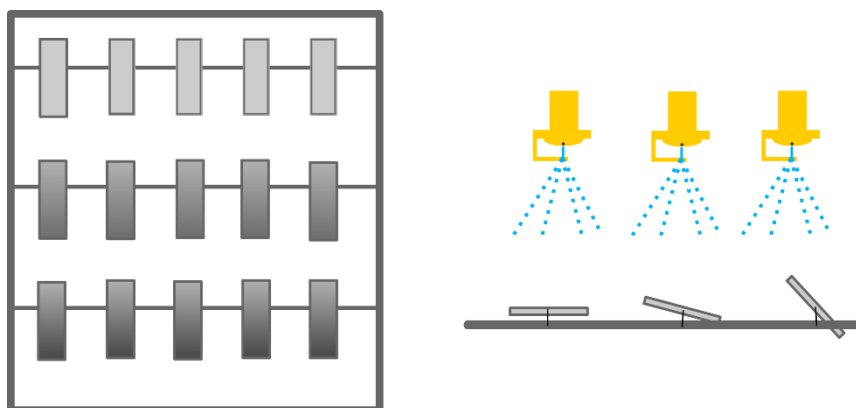


Figure 6.1: Proposed construction of a rack containing an array of coated aluminum coupons at different angles relative to spraying apparatus (left, top view; right, side view).

Arrangement of sample coupons at varying angles with respect to the spraying apparatus would allow insight into how much ice will accumulate over a given time on the selected materials. The real-life performance of the materials could thus be compared if the proper weather parameters were targeted. These parameters could be compiled from publicly available climate data, such as the historical data, and climate weather normals available from the Government of Canada.¹²

An extension of the emulation / ice accumulation work would be performing droplet impact experiments using the droplet impact apparatus (DIA) to translate droplet splashing/spreading characteristics of materials to their ice accumulation performance under emulated weather conditions. Aboud and Kietzig reported a variety of different droplet impact characteristics in their 2015 work.¹³ They showed that varying the angle and velocity of impact on different surfaces influences how droplets spread on the surface. We are unaware of any work that ties single droplet impact to ‘bulk’ surface wetting and ice accumulation, and so the results from these experiments would be of great interest. Measuring the average impact speed of water droplets from the sprayers, we can model these impacts using the DIA, and correlate different droplet spreading characteristics with the onset of surface icing. A determination of the type of surface wetting on preventing ice accretion could then be made. The droplet impact apparatus (DIA) can be housed within

the CWB, giving us access to icing temperatures for observation and comparison, which has not been completed.

The CWB at Western has not yet been used to its full capabilities but is well-equipped for modelling winter weather conditions year-round. Collaboration between researchers and technicians at Western can allow for careful study of ice accumulation on virtually any surface that is prepared. Further collaboration with McGill University would allow for modelling single-droplet impact at temperatures and velocities not yet observed by other researchers but are well within our capabilities, which could allow correlation experiments between single droplet spreading and ice accumulation would be the first of their kind.

6.2.1.2 Ice Adhesion and Interfacial Toughness

Typically, ice adhesion is expressed in terms of its strength, τ_{ice} , the maximum force value measured before detachment.⁷ However, Golovin *et al* discuss in their 2019 work that adhesion at an interface may be described by two distinct physical properties, as described by a cohesive zone model.⁶ The first zone is interfacial adhesion strength (τ_{ice}), and the second is interfacial toughness (Γ). Both parameters should be considered for a complete view of the adhesion characteristics of ice to a material. The authors discuss the two different regimes that control fracture (i.e. separation) between two interfaces, in this case ice and a variety of polymers. Beyond a critical length of interfacial contact, L_c , Γ is the prevailing property keeping the two materials together (**Figure 6.2**).

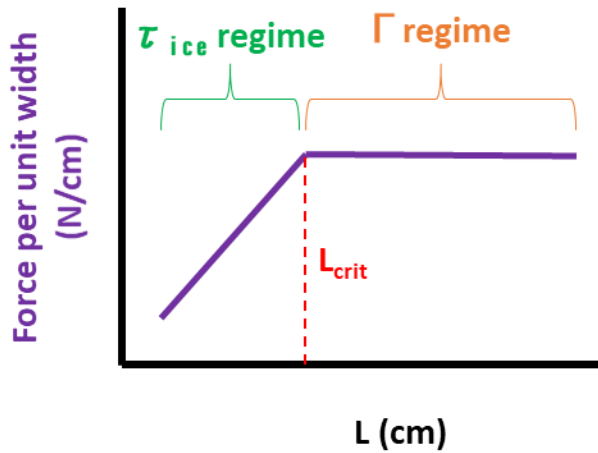


Figure 6.2: Plot of force per unit width ($x = 1\text{cm}$) versus length (L) of iced areas. Force per unit width is constant after a critical length, L_{crit} .

The existence of the Γ regime means that in applications involving meter-scale surface areas, minimizing interfacial toughness is much more important than lowering τ_{ice} . Since the applications commonly cited such as wind turbines, marine locks, aircraft, etc. all involve these length scales, we must expand our methods of measurement to include those for Γ and for L_c . The method used to determine Γ is to measure the force required to separate ice columns of varying length, L , from a given material are done (**Figure 6.3**).

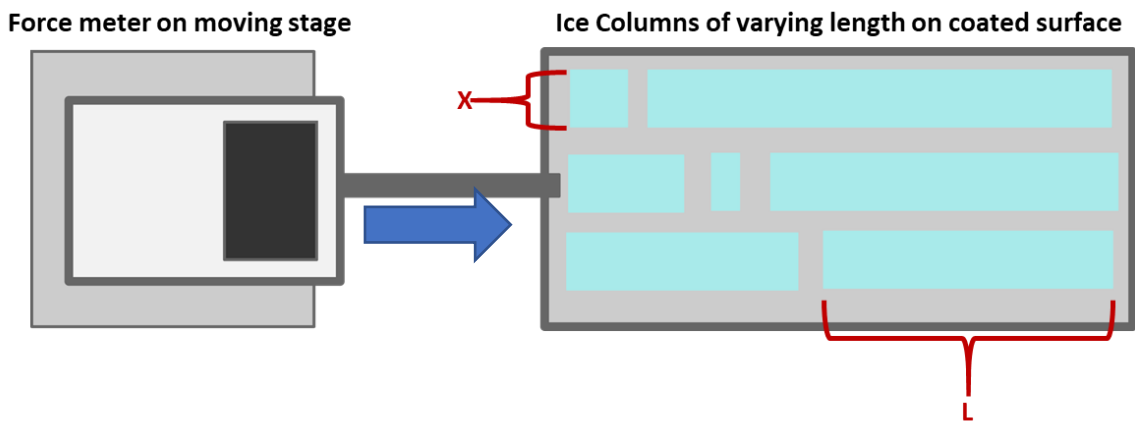


Figure 6.3: Experimental setup for measuring interfacial toughness using ice columns with a fixed width (x) and variable length (L).

By plotting force per unit width (width is constant) versus the length of the columns of ice, L_c can be observed as the transition between linearly increasing force of the interfacial adhesion strength regime, and the asymptotic value of force per unit width in the interfacial toughness regime. This methodology is well-described in the supporting information provided by Golovin.⁶ It is important to expand our methodologies to include measuring interfacial toughness, Γ , because it is the parameter of greatest importance to passive deicing on large length scales. Optimization of these tests at Western would allow for cutting-edge work to be performed in the development of passive deicing materials.

6.2.2 Material Development

Chapters Two and Four outline work done to improve the durability of materials with respect to successive deicing cycles. These materials were comprised of PDMS cross-linked polymer networks. Despite being studied extensively in the field of icephobic materials,¹⁴ PDMS is not an effective solution to ice accumulation. PDMS is not durable to abrasion or erosion, adheres weakly to many substrates, and collects dust. Given that a primary goal of developing passive deicing materials has become to develop more durable ones, we need to consider what might be the best way to achieve this. Perhaps the most effective way is by utilizing 1) polymer blends or 2) inorganic fillers.

6.2.2.1 Thermoplastic Elastomers / Vulcanizates

Thermoplastic elastomers (TPEs) are polymeric materials that combine the properties of hard thermoplastic polymers with the properties of flexible elastomers. Most often they are block or graft copolymers, containing a ‘hard block’ like polystyrene or polypropylene, and a ‘soft block’ like butadiene or isoprene rubber.¹⁵ Many of these materials are processable using the same methods as thermoplastics but can yield solid materials with properties ranging from hard plastics to soft rubbers. For example, they can be injection molded to different shapes, or extruded into films. An amazing characteristic of TPEs is their tunability. Their properties may be changed prior to polymerization by altering the relative sizes of the hard and soft phases. After polymerization, the properties may be influenced by the addition of additive such as oils and plasticizers. The effect of the additive depends upon which phase of the polymer is compatible with the additive. If the hard block is compatible with the additive, its relative volume increases, and the

material becomes harder. If the additive is soft-block compatible, the relative volume of this block increases, making the material softer. This tunability is very interesting for applying these materials as icephobic coatings, because of the ability to maintain the flexibility of an elastomer, while imparting the hardness of thermoplastic polymers. We are not aware of any works exploring the relationship of ice adhesion strength (τ_{ice}) and interfacial toughness (Γ) to parameters of TPE systems.

A broad class of TPEs are polystyrene-elastomer block copolymers. Linear members of this class have the general block structure S-E-S, where S represents a polystyrene block, and E represents an elastomeric block. There are several commercially available examples listed by Holden: Quintac® (Zeon Chemical), Finaprene® (Ato Fina), Coperflex® (Petroflex), Tufprene® and Asaprene® (Asahi), and Stereon® (Firestone).¹⁶ Styrene-block compatible additives are often ‘aromatic resins’; elastomer-block compatible additives are varied and include many types of organic oils and resins. Extrusion into films would allow observation of changes in the material properties, and the resulting changes in ice adhesion characteristics. These experiments should shed light on what concentrations of additive yield changes in polymer properties, and which may result in an inability to form a film. Once a small library of films is built the films physical properties can be measured. Determining τ_{ice} and Γ for the TPE films would be very interesting and should be accompanied by selected tests of the materials durability. In extension, a ‘wet-chemistry’ approach can be taken to this project, focusing on lab-scale polymerization techniques used to vary the hard/soft block lengths of the TPEs.

6.2.2.2 Graphene/Polymer Nanocomposites

Graphene has been called a miracle material because of its extreme physical properties. Graphene is one of the hardest measured materials (graphene = 1 TPa, diamond ~ 70-150 GPa), is electrically conductive/semi-conductive, and is flexible. These properties have made it attractive for applications like fuel cells and electronics. Graphene has even seen inclusion into polymer composites.¹⁷ An important aspect of graphene in polymers composites is the small size of loading required to greatly improve the physical properties of a polymer, such as the 128% increase in modulus observed by Wu and coworkers at 2.5 vol %.¹⁸ A challenge in using graphene as an additive is that it is difficult to prepare in

large quantities. Achieving uniform dispersion in the polymer matrix can also be difficult, since graphene can reaggregate into graphite upon compounding.

One way of generating a reasonably large amount of graphene is through graphite exfoliation using superacids.¹⁹ Chlorosulfonic acid can be used to separate sheets of graphite into graphene through protonation, generating equilibrium suspensions $\sim 2 \text{ mg mL}^{-1}$. Graphene films can be cast from these solutions, or the suspensions can be subsequently quenched followed by compounding. However, in the time between quenching and use, graphite nanoparticles might re-aggregate when deprotonated, making it difficult to capture graphene in a polymer composite. Conducting studies where the exfoliated suspensions are simultaneously quenched and incorporated into polymer matrices could be of great interest. This could be accomplished by two means (**Figure 6.4** and **Figure 6.5**):

Microcrystalline graphite can be exfoliated in chlorosulfonic acid, separating the sheets by protonation into a stable suspension. This suspension could be added to a pre-blended mixture of sodium bicarbonate and an elastomer of interest. PDMS in this case could be interesting, since it has a low Young's modulus, and its hardness might experience a drastic increase from graphene incorporation. Under a high-shear environment, sodium bicarbonate could quench any remaining acid while graphene is incorporated into the polymer matrix. This tandem quenching compounding step could prevent reaggregation of the graphene sheets, yielding to good dispersion in the elastomer.

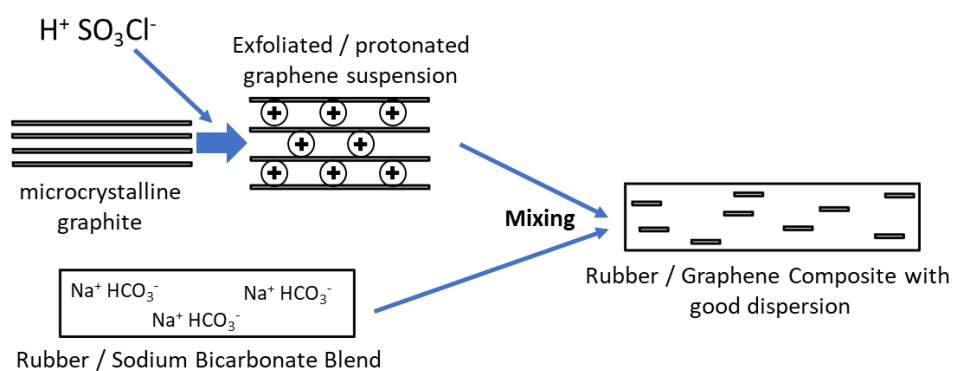


Figure 6.4: Blending of acidic graphene suspension with polymers containing sodium bicarbonate for concurrent dispersion and quenching.

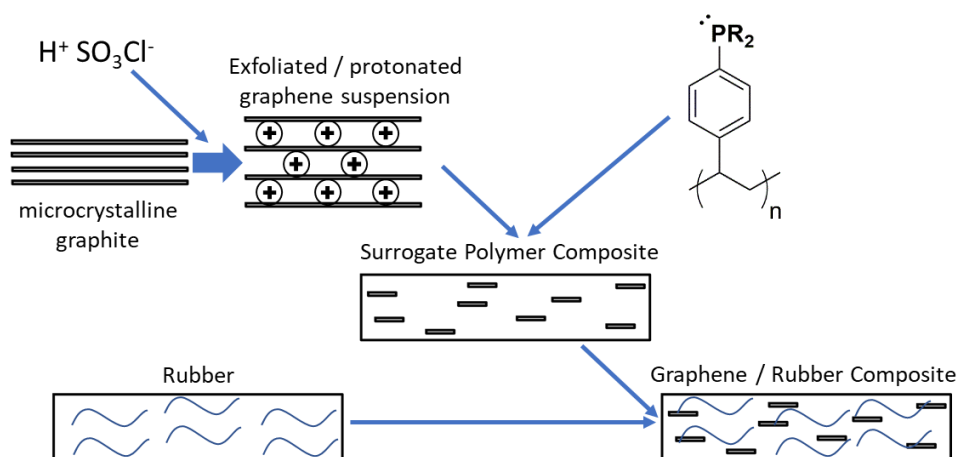


Figure 6.5: Blending of graphene suspension with ‘surrogate’ polymer containing basic phosphine functionalities, followed by blending with elastomer of interest.

Exfoliation of graphene by chlorosulfonic acid is performed as in the previous example. This suspension is subsequently blended with a polymer containing phosphine functionalities to form a surrogate polymer composite. The role of the phosphine groups is to deprotonate the exfoliated graphene during blending, yielding a neutral graphene with good dispersion. This surrogate can subsequently be blended with an elastomer to give a well-dispersed nanocomposite in the desired elastomer. This methodology avoids the generation of biproducts from the acid-base reaction from **Figure 6.4**. Composites created using both methods should be compared to a composite made through successive quenching and blending steps, utilizing Raman and x-ray photon spectroscopy to characterize the materials. Behabtu *et al* used high-resolution TEM to characterize the dispersion of graphene in the polymer matrix.¹⁹ Anti-icing and durability properties of the prepared materials could next be studied, uncovering the suitability of these new nanocomposites as passive deicing coatings.

Graphene is an exceptionally interesting material for creating new polymer composites because of its hardness, flexibility, and conductivity. Graphene has shown beneficial effects on materials abrasion and elongation characteristics in low loadings, which could feasibly translate to more durable polymer composites. A fair body of work exists on incorporating graphene into polymer matrices, but little to no work has used

graphene/polymer composites as anti-icing materials. Obtaining good incorporation of graphene into polymer composites by the outlined methodologies could yield durable anti-icing materials and would be of great interest to other researchers working with graphene nanocomposites.

6.3 References Cited

1. Kim, P.; Wong, T.-S.; Alvarenga, J.; Kreder, M. J.; Adorno-Martinez, W. E.; Aizenberg, J., Liquid-Infused Nanostructured Surfaces with Extreme Anti-Ice and Anti-Frost Performance. *ACS Nano* **2012**, *6*, 6569.
2. Golovin, K.; Kobaku, S. P. R.; Lee, D. H.; DiLoreto, E. T.; Mabry, J. M.; Tuteja, A., Designing durable icephobic surfaces. *Sci. Adv.* **2016**, *2*.
3. Wood, M. J.; Coady, M. J.; Aristizabal, F.; Nielsen, K.; Ragogna, P. J.; Kietzig, A.-M., Femtosecond laser micromachining of co-polymeric urethane materials. *Appl. Surf. Sci.* **2019**, *483*, 633.
4. Coady, M. J.; Wood, M.; Wallace, G. Q.; Nielsen, K. E.; Kietzig, A.-M.; Lagugné-Labarhet, F.; Ragogna, P. J., Icephobic Behavior of UV-Cured Polymer Networks Incorporated into Slippery Lubricant-Infused Porous Surfaces: Improving SLIPS Durability. *ACS Appl. Mater. Interfaces* **2018**, *10*, 2890.
5. Nagare, R. M.; Schincariol, R. A.; Quinton, W. L.; Hayashi, M., Moving the Field into the Lab: Simulation of Water and Heat Transport in Subarctic Peat. *Permafrost Periglac.* **2012**, *23*, 237.
6. Golovin, K.; Dhyani, A.; Thouless, M. D.; Tuteja, A., Low-interfacial toughness materials for effective large-scale deicing. *Science* **2019**, *364*, 371.
7. Makkonen, L., Ice Adhesion —Theory, Measurements and Countermeasures. *J. Adhes. Sci. Technol.* **2012**, *26*, 413.
8. Gonzalo, J.; López, D.; Domínguez, D.; García, A.; Escapa, A., On the capabilities and limitations of high altitude pseudo-satellites. *Prog. Aerosp. Sci.* **2018**, *98*, 37.
9. Guo, P.; Zheng, Y.; Wen, M.; Song, C.; Lin, Y.; Jiang, L., Icephobic/anti-icing properties of micro/nanostructured surfaces. *Advanced materials (Deerfield Beach, Fla.)* **2012**, *24*, 2642.
10. Lv, J.; Song, Y.; Jiang, L.; Wang, J., Bio-Inspired Strategies for Anti-Icing. *ACS Nano* **2014**, *8*, 3152.
11. Meyer, T.; Lei, Y. D.; Wania, F., Measuring the Release of Organic Contaminants from Melting Snow under Controlled Conditions. *Environ. Sci. Technol.* **2006**, *40*, 3320.

12. Historical Climate Data. <http://climate.weather.gc.ca/> (accessed 22 August 2019).
13. Aboud, D. G. K.; Kietzig, A.-M., Splashing Threshold of Oblique Droplet Impacts on Surfaces of Various Wettability. *Langmuir* **2015**, *31*, 10100.
14. Sojoudi, H.; Wang, M.; Boscher, N. D.; McKinley, G. H.; Gleason, K. K., Durable and scalable icephobic surfaces: similarities and distinctions from superhydrophobic surfaces. *Soft Matter* **2016**, *12*, 1938.
15. Holden, G.; Kricheldorf, H. R.; Quirk, R. P., *Thermoplastic Elastomers*. Hanser: 2004.
16. Holden, G. H., D.R., Applications of Thermoplastic Elastomers. In *Thermoplastic Elastomers*, 3rd ed.; Holden, G. K., H.R.; Quirk, R.P., Ed. Hanser Publishers: Munich, 2004; pp 493.
17. Kim, H.; Abdala, A. A.; Macosko, C. W., Graphene/Polymer Nanocomposites. *Macromolecules* **2010**, *43*, 6515.
18. Xu, Y.; Hong, W.; Bai, H.; Li, C.; Shi, G., Strong and ductile poly(vinyl alcohol)/graphene oxide composite films with a layered structure. *Carbon* **2009**, *47*, 3538.
19. Behabtu, N.; Lomeda, J. R.; Green, M. J.; Higginbotham, A. L.; Sinitskii, A.; Kosynkin, D. V.; Tsentalovich, D.; Parra-Vasquez, A. N. G.; Schmidt, J.; Kesselman, E.; Cohen, Y.; Talmon, Y.; Tour, J. M.; Pasquali, M., Spontaneous high-concentration dispersions and liquid crystals of graphene. *Nat. Nanotechnol.* **2010**, *5*, 406.

Appendices

Appendix A: Supporting Information for Chapter 2

This appendix contains notes on ice growth and ice adhesion measurements performed in Chapter 2. Additional EDX spectra can be found in the Supporting Information, available at DOI: [10.1021/acsami.7b14433](https://doi.org/10.1021/acsami.7b14433)

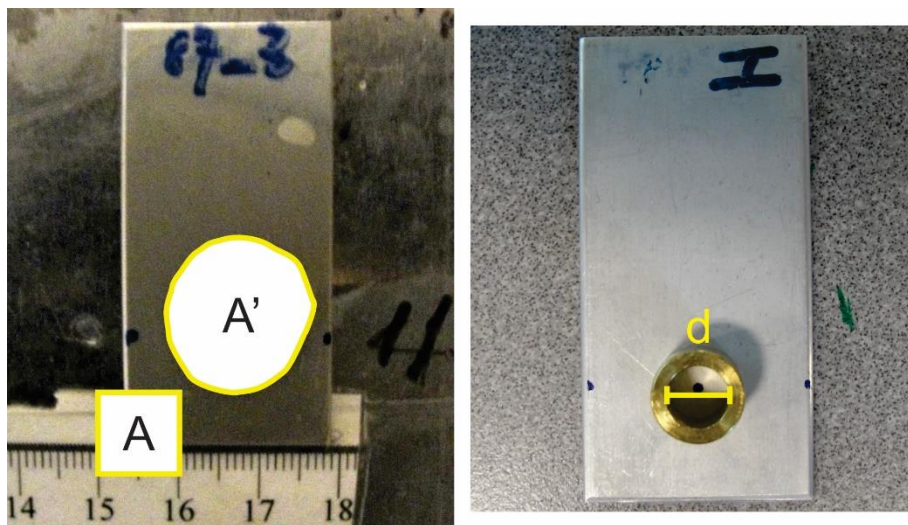


Figure A 1: (*left*) illustration of ice growth on coupon when a weight is not used. The footprint of the ice is compared to a 1 cm^2 area in the same photograph. The ratio of the number of pixels in area A' to the number of pixels in area A gives the area of the ice footprint in cm^2 . This is converted to m^2 to calculate kPa. (*right*) photograph of tubular metal weight on coupon surface. The weight is aligned with its centre approximately at the position of a mark made on the coupon. The diameter d is used to calculate the area of the ice footprint in this case, by calculating the area of a circle.



Figure A 2: (*left*) bucket of the centrifuge used to measure ice adhesion. The radius r of the arm is that used with Equation 1 from the main text to calculate adhesion. r is measured from the centre of the centrifuge arm to the position of the ice on the coupon. (*right*) digital display on the icefuge that gives the maximum speed of rotation reached before detachment. The limit RPM dial and Ramp time dial are used to adjust the speed the centrifuge will reach. The same limit and ramp time were used for all samples: 4900 RPM, and 60 sec.

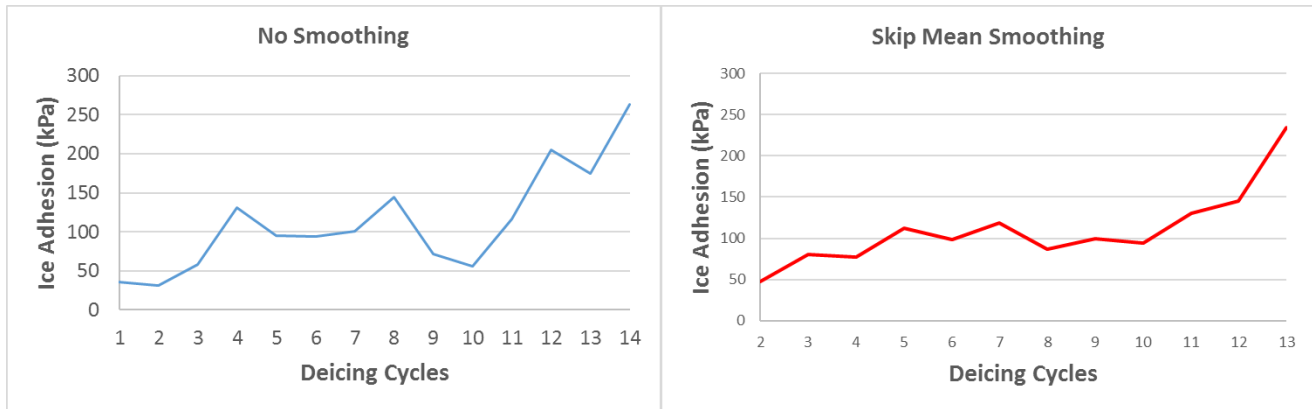


Figure A 3: (*left*) average ice adhesion measured on oil-only SLIPS over the course of testing, without any applied data processing. (*right*) the same data set after having applied skip mean smoothing, where each point becomes the average between the point preceding and the point following it. For example, point ‘2’ in the right-hand plot is the average of points ‘1’ and ‘3’ on the left. An outcome of this processing is that points 1 and 14 are missing from the final plot. This type of smoothing was chosen because it improved the appearance of our plot, but did not require the removal of any data points. All measured values of ice adhesion for every sample were used in calculating averages and standard error. We feel this is important when measuring ice adhesion, as the sample replicates may all be damaged differently, and at different stages of the testing.

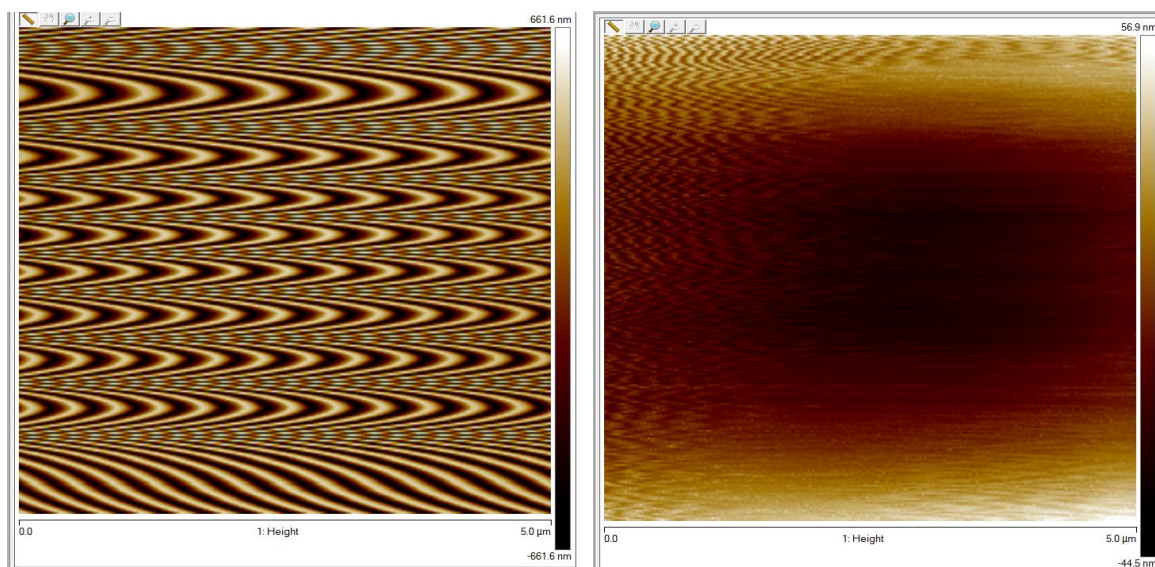


Figure A 4: AFM height images collected for (*left*) cured Ebecryl 350, and (*right*) 350+oil SLIPS. Both images showed wave-like deflections in the height images.

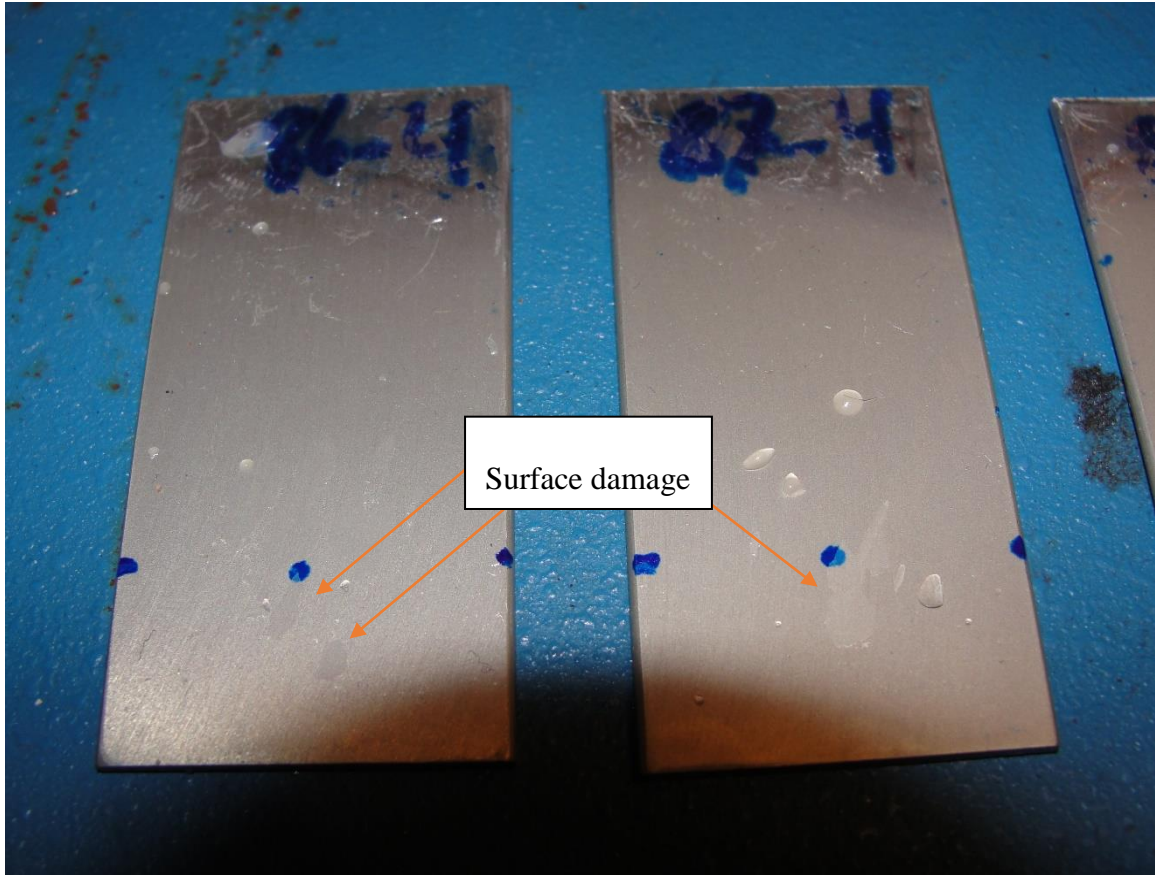


Figure A 5: Photographs of two oil+1360 SLIPS samples removed from testing after exhibiting an appreciable increase in ice adhesion strength. Visible removal of the cured oil+polymer coating was observed (around the area where ice growth occurred), between the 4th and 5th deicing cycle.

Appendix B: Supporting Information for Chapter 3

Notes on model fitting, SEMs of ablated surfaces, lacunarity analysis, and XPS spectra are available in the supplementary information of the original manuscript:

<https://doi.org/10.1016/j.apsusc.2019.03.296>

Appendix C: Supporting Information for Chapter 4

Table C 1: Contact angle and DSC data for prepared coatings. No trends were observed between ice adhesion and contact angles of materials. This is likely because the observed contact angles are affected by changes in surface roughness observed by SEM, and by the hydrophobicity of the coatings.

Formulation	θ_{adv} (deg)	θ_{rec} (deg)	θ_{hys} (deg)	T_g (°C)
EB1360	78 ± 1	43 ± 2	35	-58.4
5%LMA	50 ± 6	24 ± 3	25	-62.3
10%LMA	80 ± 2	38 ± 1	42	-57.2
25%LMA	89 ± 3	45 ± 4	44	-51.4
5%MMA	73 ± 1	33 ± 2	39	-63.2
10%MMA	81 ± 2	37 ± 1	43	-51.0
25%MMA	70 ± 1	32 ± 1	37	-44.6
5%Sty	77 ± 2	37 ± 4	40	-49.3
10%Sty	77 ± 1	37 ± 2	39	-64.5
25%Sty	69 ± 21	35 ± 3	34	-51.0

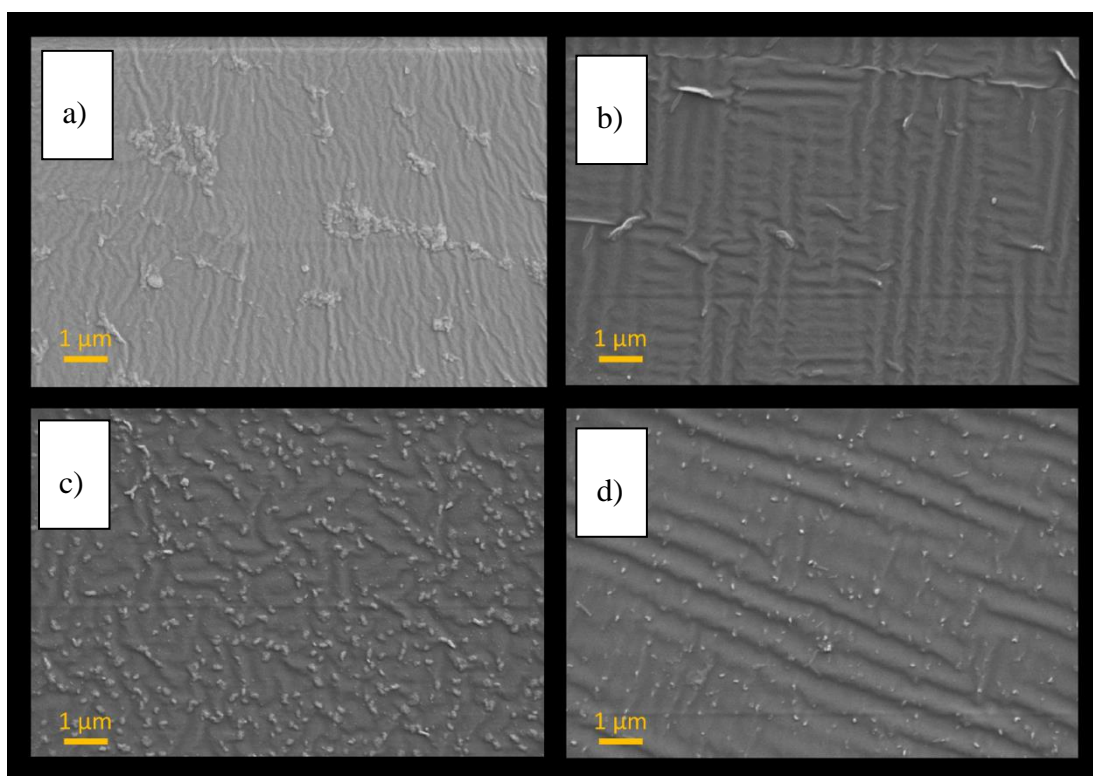


Figure C 1: SEM images showing topography of a) EB1360, b) 5% LMA, c) 10% LMA, and d) 25% LMA coatings.

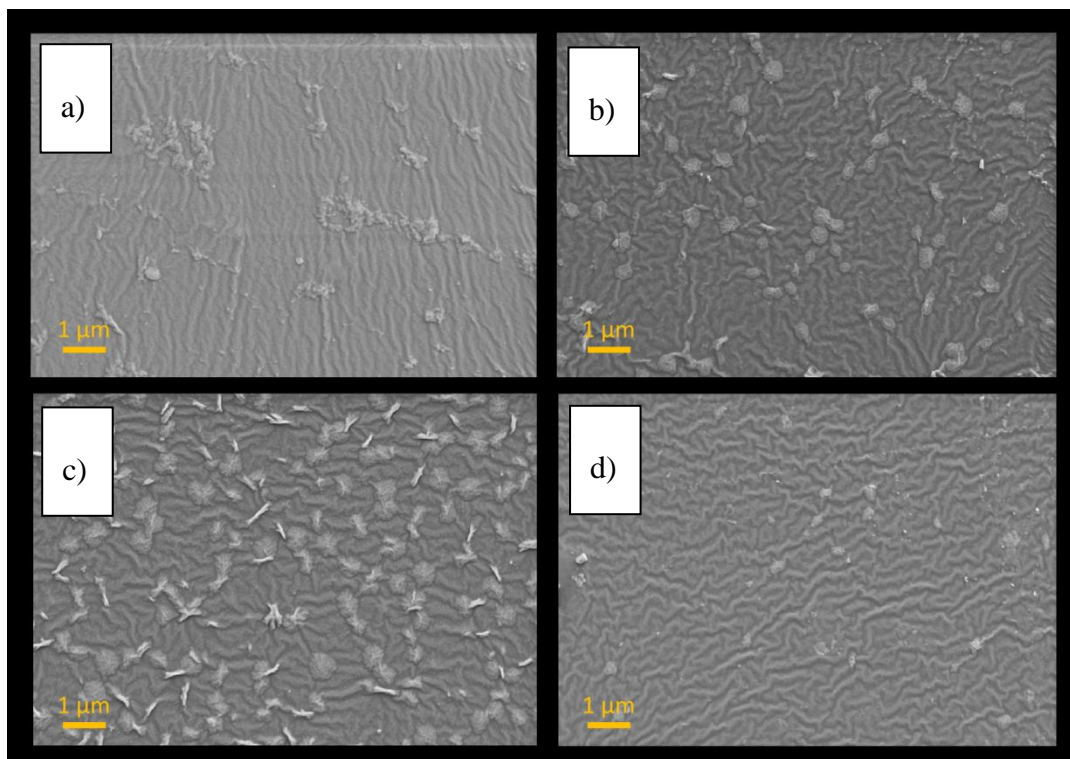


Figure C 2: SEM images showing topography of a) EB1360, b) 5% MMA, c) 10% MMA, and d) 25% MMA coatings.

Notes on Data Processing

Low-level data processing was used to improve the readability of the data collected. In the case of plots depicting ice adhesion over successive ice adhesion cycles, a trendline made using a simple moving average was used to smooth the average ice adhesion data series. The period selected for all these plots was 3. It was selected in a trial and error basis, because it smoothed the data significantly without altering any observed trends, or the meaning of the results.

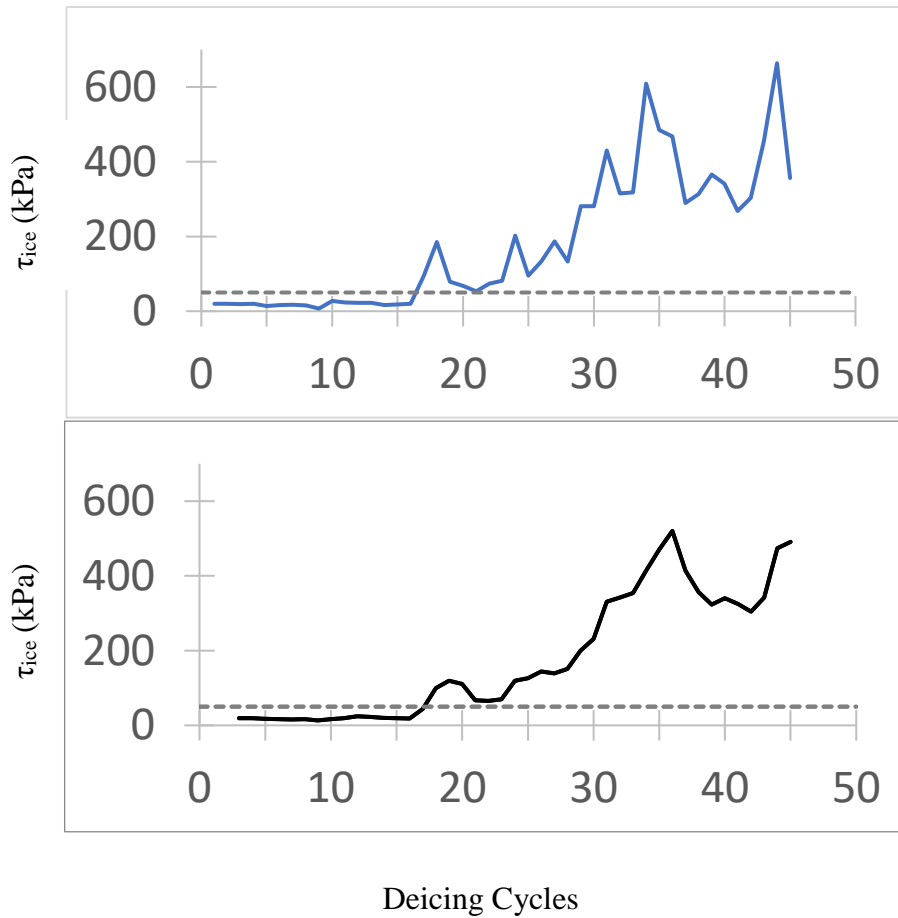


Figure C 3: Comparison of adhesion vs number of deicing cycles for a) EB1360 with no data smoothing, and b) EB1360 using moving average smoothing, P=3.

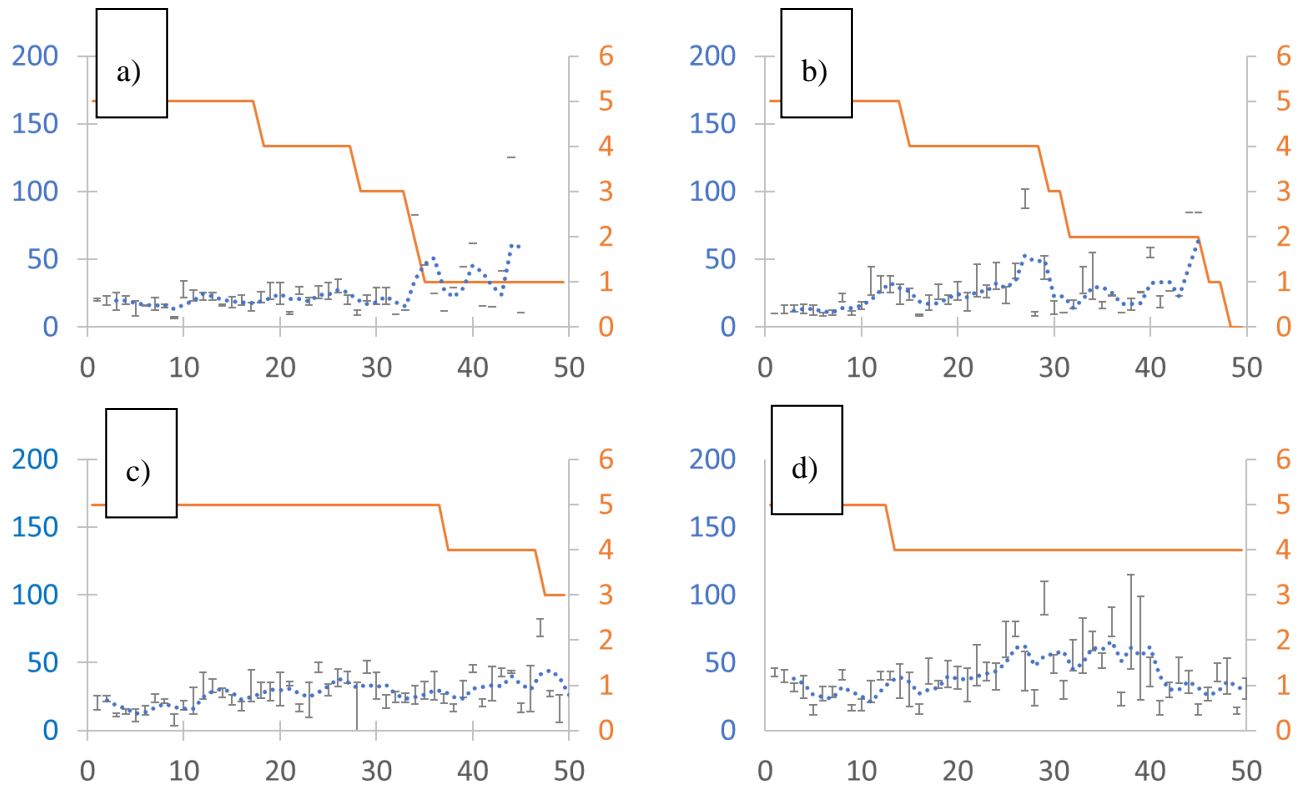


Figure C 4: Durability plots for a) EB1360, b) 5% MMA, c) 10% MMA, and d) 25% MMA. Note that damage caused to sample in 25% MMA was caused by apparatus failure, and not by ice removal.

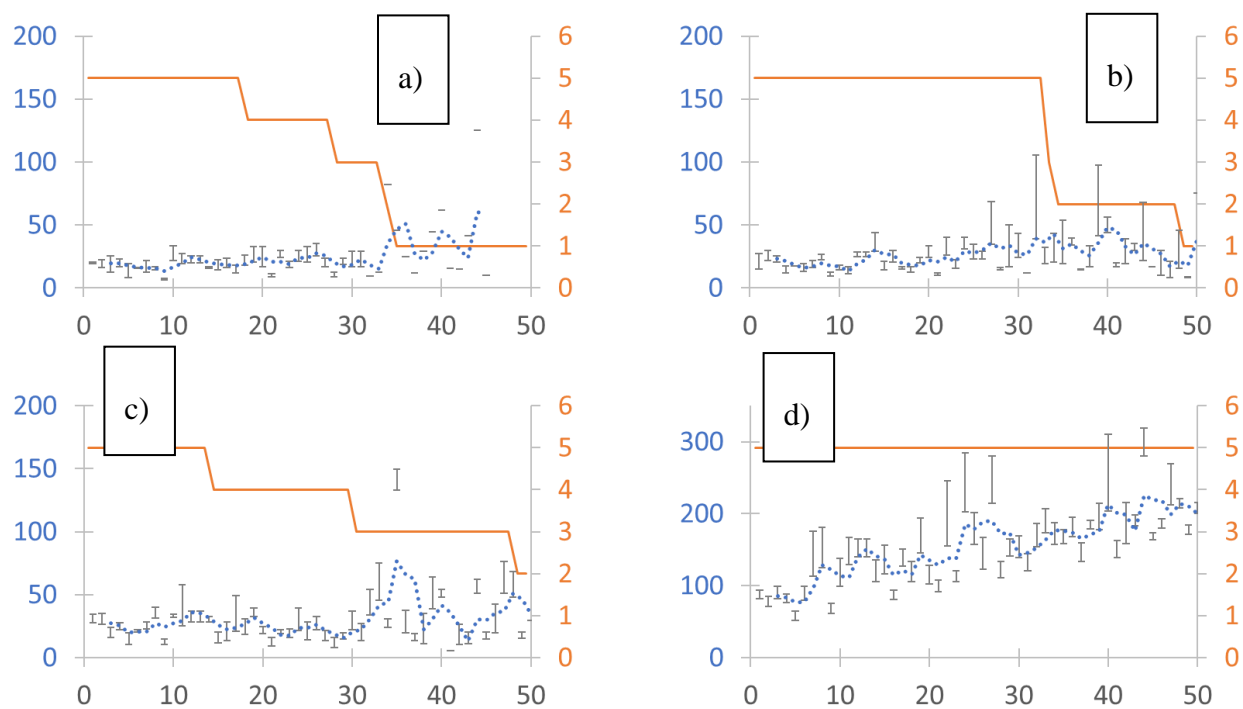


Figure C 5: Durability plots for a) EB1360, b) 5% styrene, c) 10% styrene, and d) 25% styrene.

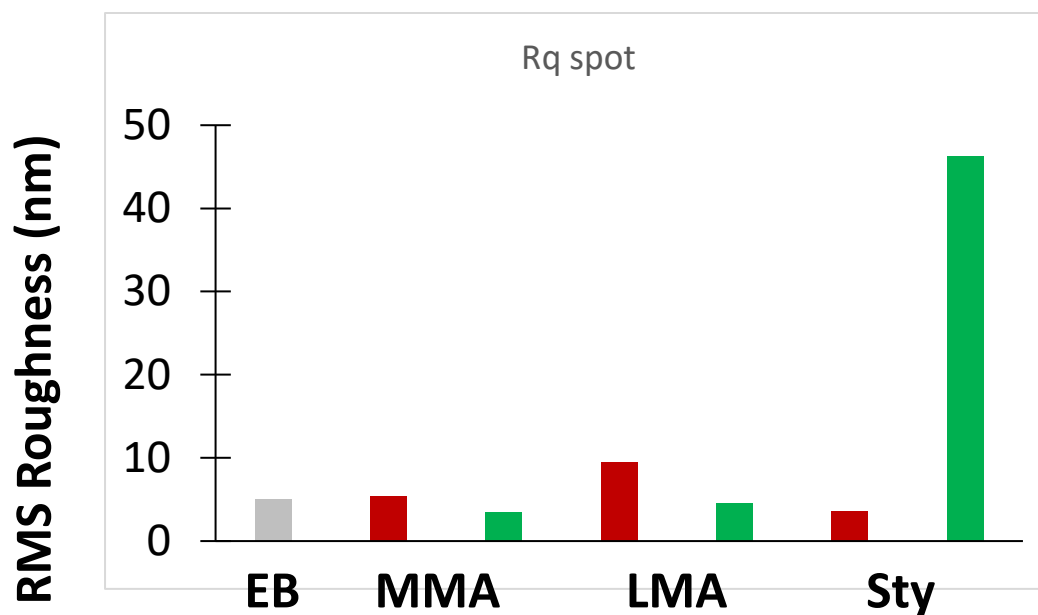


Figure C 6: RMS roughness for selected areas of 5% (red) and 25 % comonomer coatings. No obvious trend was observed, but the roughness of 25% styrene was much greater than all the others.

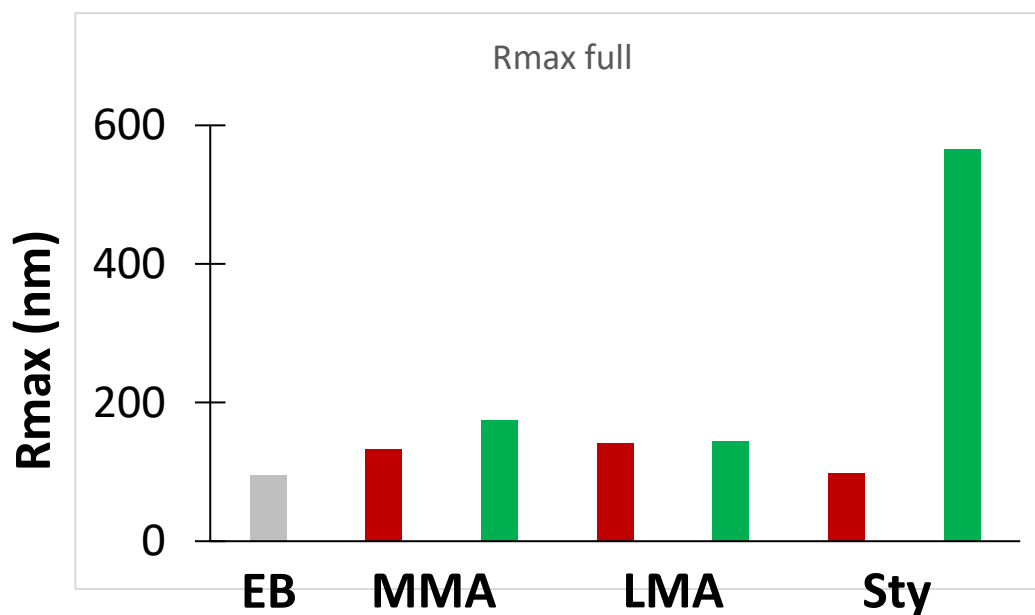


Figure C 7: Rmax roughness for full areas of 5% (red) and 25 % comonomer coatings. No obvious trend was observed, but the roughness of 25% styrene was much greater than all the others.

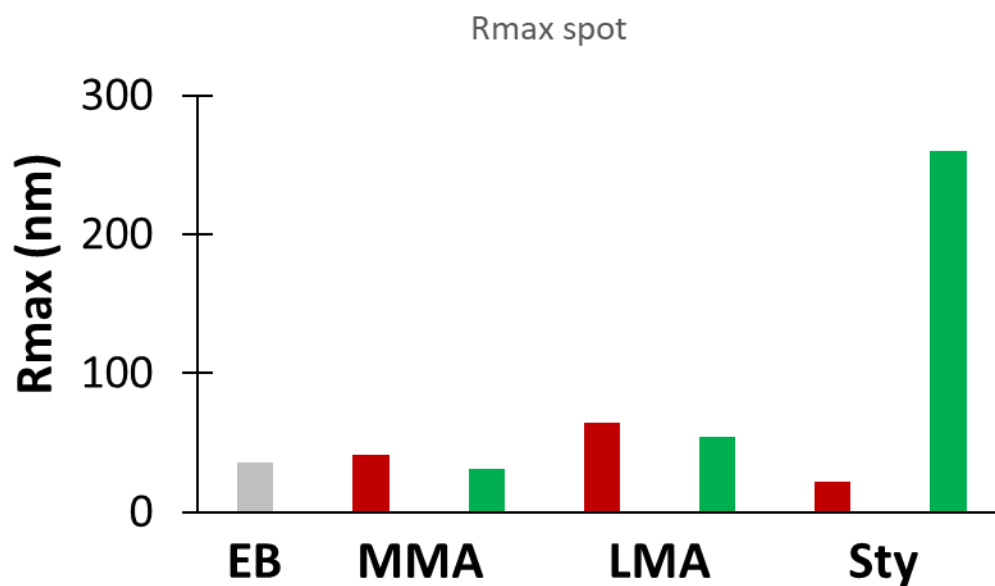


Figure C 8: Rmax roughness for selected areas of 5% (red) and 25 % comonomer coatings. No obvious trend was observed, but the roughness of 25% styrene was much greater than all the others.

Appendix D: Supporting Information for Chapter 5

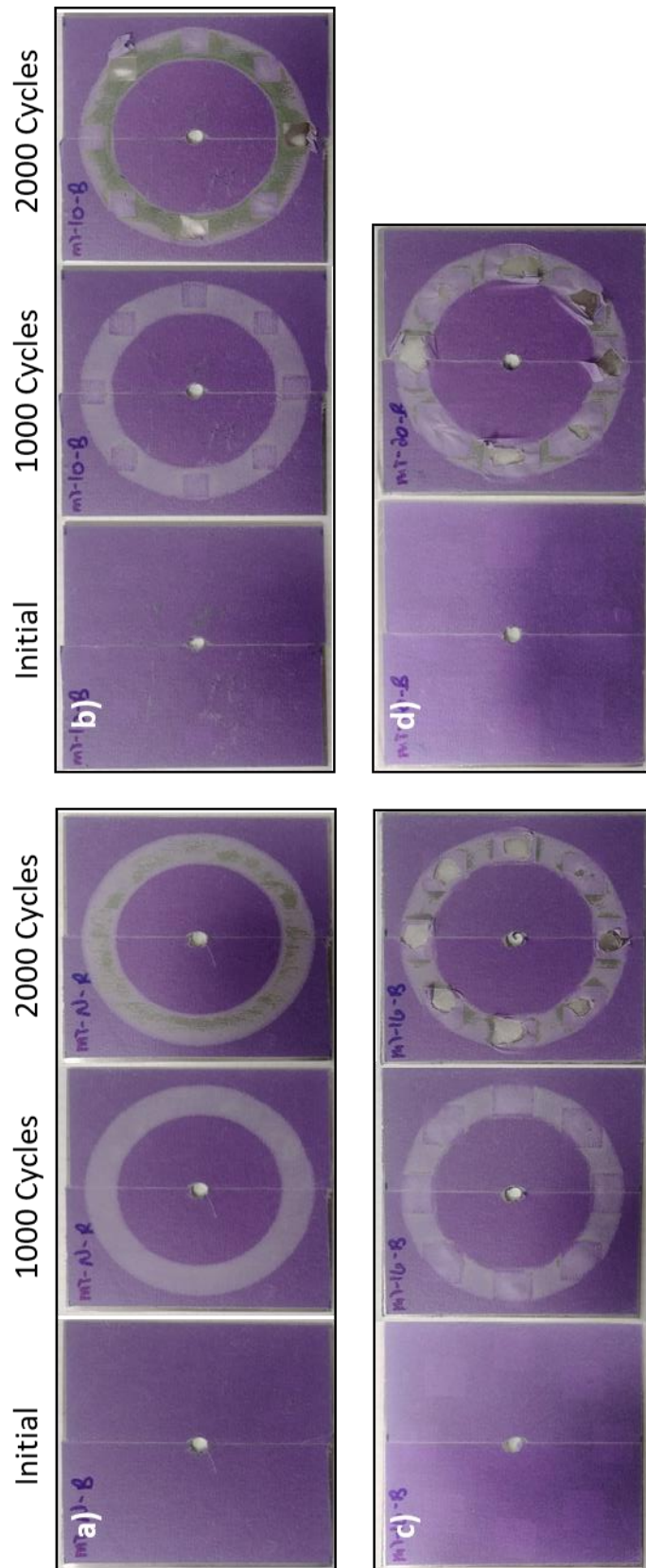


Figure D 1: Photos showing surface damage to a) normally attached masking tape, and films with b) 10 mm, c) 16 mm, and d) 20 mm detachments in the path of the abrasive wheels. Note: The second image in the 20 mm series underwent 1200 cycles.

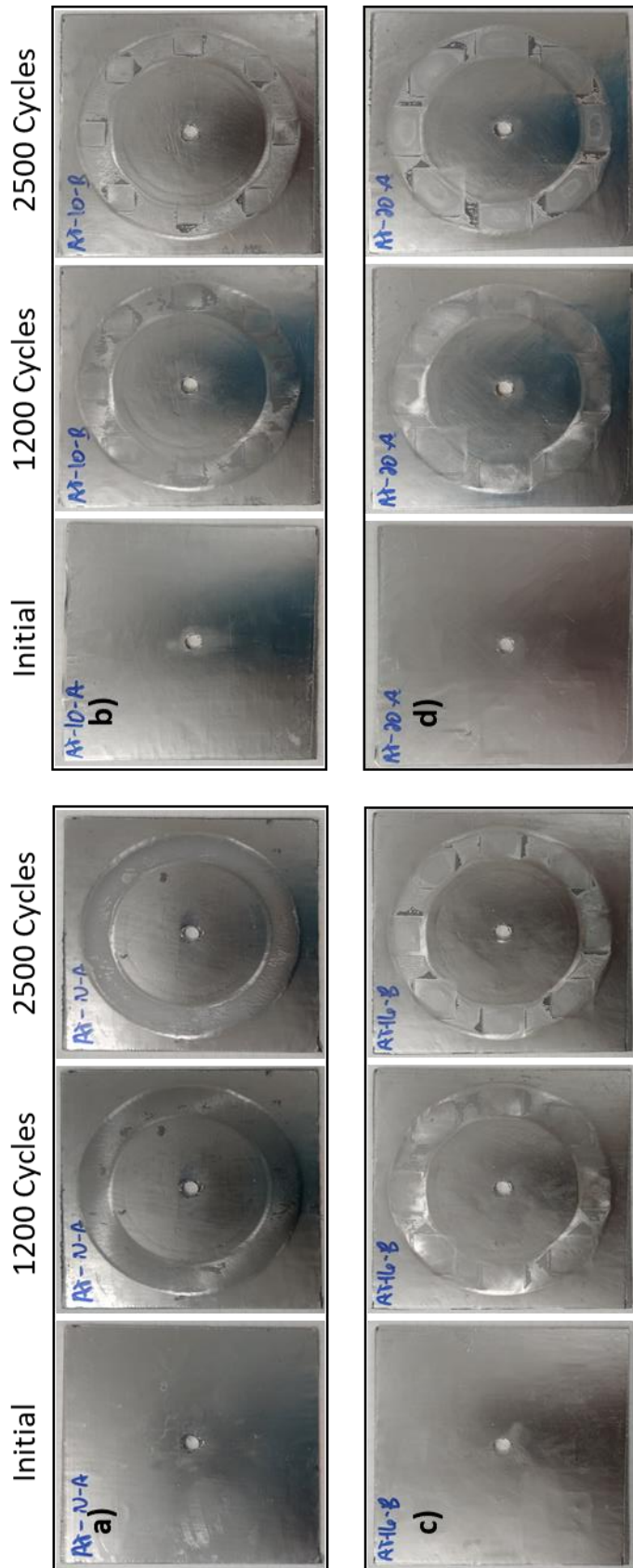


Figure D 2: Photos showing surface damage to a) normally attached shielding tape, and films with b) 10 mm, c) 16 mm, and d) 20 mm detachments in the path of the abrasive wheels.

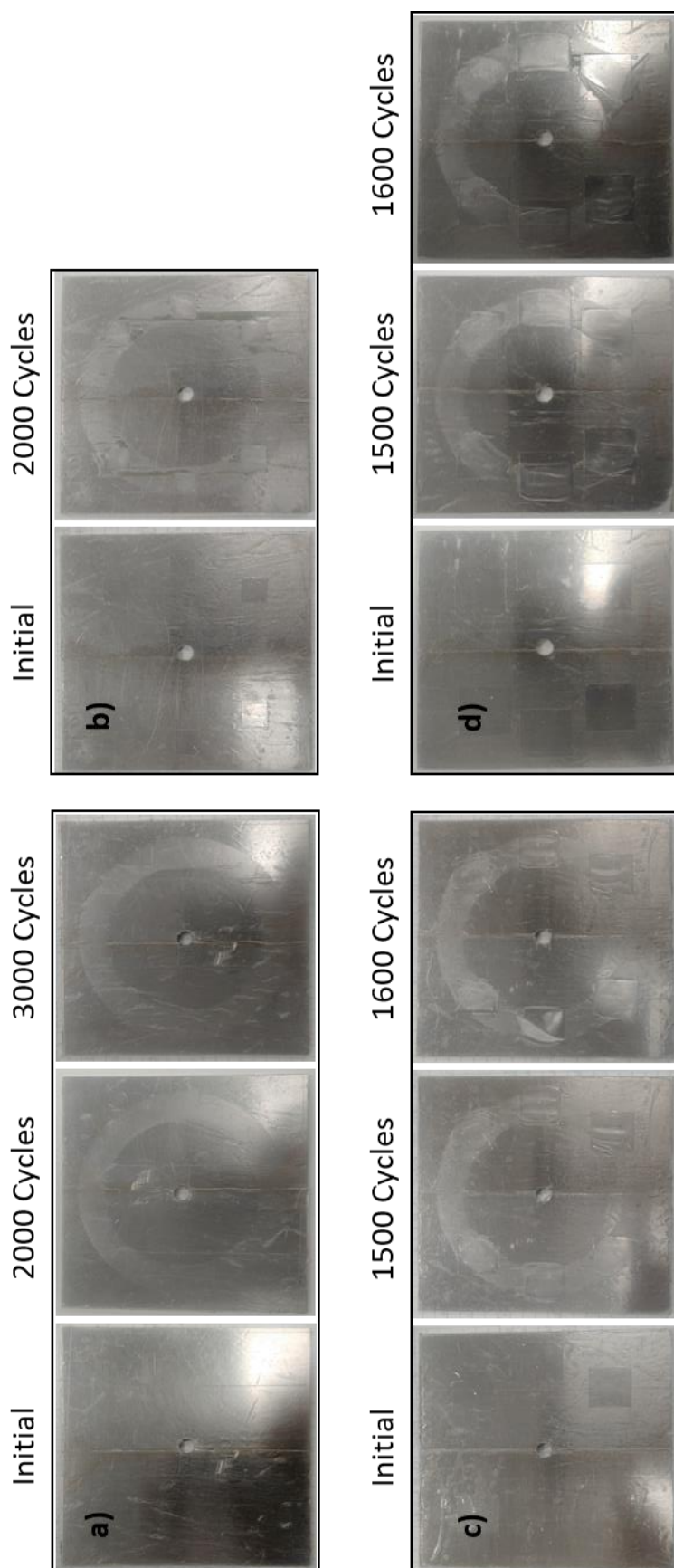


Figure D 3: Photos showing surface damage to a) normally attached PTFE skived film, and films with b) 10 mm, c) 16 mm, and d) 20 mm detachments in the path of the abrasive wheels. Note: the 10 mm series was not continued after 2000 cycles due to damage to the film.

Curriculum Vitae

Matthew J. Coady

Education

2015 – Present

PhD Candidate, Chemistry, The University of Western Ontario

2010 – 2015

BSc, Honours Specialization in Chemistry, The University of Western Ontario

Honours and Awards

Ontario Graduate Scholarship, \$15 000, 2018

NSERC Undergraduate Student Research Award (USRA), \$4 500 + contribution, 2015

Dean's Honour List, 2010-2015

Related Work Experience

Graduate Research Assistant, 2015 – Present, The University of Western Ontario

Graduate Teaching Assistant, 2015 – 2018, The University of Western Ontario

NSERC USRA Student, May – August 2015, The University of Western Ontario

Summer Research Student, July – September 2014, The University of Western Ontario

Chemistry Intern, May – December 2013, ARLANXEO Canada Inc.

Presentations

1. Matthew J. Coady*, Nuwansiri Getangama, Aria Khalili, Kent Nielsen, Paul Ragona. "UV-cured PDMS-based Copolymer Networks as Icephobic Coatings" (oral presentation). Presented at 102nd CCCE, Québec, QC. June 5th, 2019.

2. Matthew J. Coady*, Paul Ragona. "Progress Towards Passive Anti-icing OR: How We've Learned to Stop Ice Sticking to Stuff" (poster). Presented at 102nd CCCE, Québec, QC. June 5th, 2019.

3. Matthew J. Coady*. "3M Canada and Western University Collaborative Anti-Icing Research: Overview, Results and Outlook" (Invited, oral presentation). Presented at 3M Technical Forum. 3M Center, St. Paul, MN. May 6th, 2019.

4. Matthew J. Coady*, Gregory Q. Wallace, Michael Wood, Felipe Aristizabal, Anne-Marie Kietzig, Paul J. Ragona. Progress toward durable icephobic surfaces (poster). Presented at Surface Canada 2017, Concordia University (National).

5. Matthew J. Coady*, François Lagugné-Labarhet. Gold nanostructures fabricated by electron beam lithography for ultrasensitive spectroscopic measurements (oral presentation). Presented at SOUSCC 2015, University of Toronto Mississauga (Regional).

Publications

1. M.J. Coady, N. N. K. Getangama, A. Khalili, M. Wood, K.E. Nielsen, J.R. de Bruyn, R.J. Klassen, A.-M. Kietzig, P.J. Ragona. *Langmuir*. Submitted.

2. M.J. Wood, M. J. Coady, F. Aristizabal, K. Nielsen, P.J. Ragona, A. Kietzig. *Applied Surface Science*, **2019**, 483, 633.

3. M.J. Wood, F. Aristizabal, M. Coady, K. Nielsen, P.J. Ragona, A. Kietzig*. *Phys. Fluids* **2018**, 30, 027104.

4. M.J. Coady, M. Wood, G.Q. Wallace, K.E. Nielsen, A. Kietzig, F. Lagugné-Labarhet, P.J. Ragona. *ACS Applied Materials & Interfaces*, **2018**, 10, 2890.

5. V.A. Béland, M.A.S. Ross, M.J. Coady, R. Guterman, P.J. Ragona. *Chemistry of Materials*. **2017**, 29, 8884.

6. G.Q. Wallace, M. Tabatabaei, R. Hou, **M.J. Coady**, P.R. Norton, T.S. Simpson, S.M. Rosendahl, A. Merlen, François Lagugné-Labarhet. *ACS Photonics*, **2016**, 3, 1723.

3M Invention Disclosures

1. Matthew J. Coady, Paul J. Ragona, Anne-Marie Kietzig, Michael Wood. (2016) A composition including UV-curable resins to enhance the icephobicity and durability of Slippery Lubricant-Infused Porous Surfaces (SLIPS) Submission number: Submission number: **N058698**

2. Michael Wood, Anne-Marie Kietzig, Matthew J. Coady, Paul J. Ragona. (2017) Generation of Millimetric Liquid Droplets Using Extreme Anti-Wetting Surfaces. [Invention Submission with 3M Canada]. Submission number: **N060089**

3. Michael Wood, Matthew J. Coady, Anne-Marie Kietzig, Paul J. Ragona. (2016) Laser Ablation of UV-Curable Films to Produce Consistent Surface Topology. Submission number: **N058728**